Lightning Effects in the Payload Changeout Room

Garland Thomas, NASA, Kennedy Space Center, FL
Franklin Fisher, Lightning Technology, Inc.
Richard Collier, Electro Magnetic Applications, Inc.
Pedro Medelius, I-NET, Inc., Kennedy Space Center, FL

Technical Memorandum 112881

May 1997

This report is dedicated to the memory of James R. Stahmann, a pioneer lightning researcher, Kennedy Space Center's resident lightning expert for many years, and a co-developer of the concept and early planning of this study and collaborator in the modeling phase.

Funding for this study has been provided by a Research and Technology Objectives and Plans (RTOP) grant awarded by NASA Headquarters, Code Q. Peter J. Rutledge administered the grant. Additional funding was provided by the KSC Weather Office, administered by Jan A. Zysko and John Madura, with support by James Nicholson, PT.

Many people at Kennedy Space Center (KSC) contributed to this study, particularly the test. Among those who had the most important roles are Mark Gordon, NASA Test Director, Mark Paxton, Orbiter Test Conductor, Ron Bentti, Chairman of the KSC Lightning Safety Assessment Committee, Thomas Pentrack, Payload Changeout Room (PCR) Manager, John Gaudio and his crew of PCR Technicians, the I-NET simulator and data team, Joe E. Kashnic, of I-NET, who did many things to make the project successful, the RF Measurements Group, Carl Lennon and Mark Nurge, Randolf Myrsten, of Grumman, who provided data and other information from the Catenary Wire Lightning Instrumentation System, Diane Kent for her work in preparing the early drafts of this report, and Thomas Lundgren, for computer assistance in the report preparation.

This report was prepared by: Anthony J. Eckhoff, I-NET, Inc.
Richard S. Collier, Electro Magnetic Applications, Inc.
Franklin A. Fisher, Lightning Technologies, Inc.
Pedro J. Medelius, Ph.D., I-NET, Inc.
Garland L. Thomas, Ph.D., NASA

CONTENTS

TABLES

FIGURES

ACRONYMS

CCAS	Cape Canaveral Air Station
CWLIS	Catenary Wire Lightning Instrumentation System
EMA	Electro Magnetic Applications, Inc,
ET	External Tank
FDTD	Finite Difference, Time Domain
FSS	Fixed Service Structure
KSC	Kennedy Space Center
LIVIS	Lightning Induced Voltage Instrument System
LTI	Lightning Technologies, Inc.
NASA	National Aeronautics and Space Administration
OTV	Operational Television
PCR	Payload Changeout Room
PGHM	Payload Ground Handling Mechanism
PTCR	Pad Terminal Connection Room
RSS	Rotating Service Structure
SRB	Solid Rocket Booster
SRM	Solid Rocket Motor

1. EXECUTIVE SUMMARY

Analytical and empirical studies have been performed to provide better understanding of the electromagnetic environment inside the Payload Changeout Room (PCR) and Orbiter payload bay resulting from lightning strikes to the launch pad lightning protection system. There were four primary objectives: (1) Characterize the magnetic and electric fields and induced voltages in payload circuits in the PCR, (2) Evaluate safety rules regarding operations at the facility, (3) Determine appropriate facility modifications which would improve protection, and (4) Determine the optimum location for the Lightning Induced Voltage Instrumentation System (LIVIS) sensor inside the PCR.

The analytical studies consisted of physical and mathematical modeling of the pad structure and the PCR. Frank Fisher of Lightning Technologies, Inc. (LTI) developed a 1/24 scale physical model and used a previously developed mathematical model for evaluating currents, voltages, and magnetic fields in structural elements. When tested in a laboratory environment, there was good agreement between the physical and mathematical models. A relatively new analytical technique, the Finite Difference, Time Domain method, was used by Richard Collier of Electro Magnetic Applications (EMA).

Both mathematical models and the physical model verified the importance of using ground straps to electrically bond the Orbiter to the PCR.

Empirical testing was performed using a Lightning Simulator to simulate controlled (8 kA) lightning strikes to the catenary wire lightning protection system. The simulator connection replaced the ground connection at the north catenary wire terminal, and the south termination was left in its grounded state. Magnetic and electric field measurements were made at 13 locations inside the PCR and three locations outside. These data were used to evaluate the direct and induced electrical and magnetic effects of the simulated strike and the shielding characteristics of the PCR as well as to evaluate performance of the mathematical models. Loop antennas were used to evaluate potential locations for a new PCR LIVIS sensor inside the PCR and the feasibility of locating such sensors on the PCR roof. Values measured during the test were extrapolated to values expected from a NASA design stroke of 200 kA.

The test results indicated that the magnitude of the magnetic field inside the PCR resulting from the NASA design stroke varied somewhat with location but was not of major concern. Of more concern to payload owners is the rate of rise of the magnetic field, which is acceptable for properly shielded circuits.

In addition to the analyses and testing listed above, an analysis of the configuration with a vehicle present was conducted, in lieu of testing, by EMA using the Finite Difference, Time Domain method. This analysis indicated that the fields inside the PCR and the payload bay will be considerably higher when the PCR and Orbiter are mated than those in the PCR in the park position. This is believed to be due to the significant entry of

electromagnetic energy through the non-conducting environmental seal. (When the PCR is in the park position, the apertures around and between the doors provide a somewhat less severe entry source.)

In addition, this analysis showed that there can be a dangerous electrical potential across the interface between the vehicle and the Orbiter Access Arm (White Room) when its grounding cable is not installed. The bridge is ineffective in reducing the hazard as it is insulated at both ends. The interface potential can be reduced by shortening the cable and electrically bonding the bridge at both ends.

A number of other recommendations relative to procedures for personnel and hardware as well as equipment and subsystem upgrades resulted from the information gained from these studies. The background data, the analyses, and the recommendations are detailed in the report. Recommendations are listed in Section 8.8.

2. INTRODUCTION

This study was undertaken primarily to reduce the uncertainty regarding effects to payloads inside the Payload Changeout Room (PCR) from lightning which strikes the launch pad protective system. It had four specific objectives:

(1) Determine the magnetic and electric fields in the PCR and induced voltages in payload circuits in order to provide that information to payload organizations,

(2) Evaluate safety rules regarding operations at the facility,

(3) Determine any needed facility modifications,

(4) Determine the optimum location for the Lightning Induced Voltage Instrumentation System (LIVIS) sensor located in the PCR.

An additional objective, if circumstances allowed, was determination of effects inside the Orbiter payload bay when the vehicle is present and the payload bay and PCR doors are opened to each other.

The study consisted of three parts:

(1) Physical and mathematical modeling of the pad structure and PCR. This was done by Frank Fisher, of Lightning Technologies, Inc. (LTI) and Richard Collier, of Electro Magnetic Applications (EMA). Cuong Nguyen, DF-ELD, was Project Manager for this part of the LTI work.

(2) Experimental testing, using a lightning simulator, then on loan to KSC by Wright-Patterson Air Force Base, to apply pulses to the protective wire system (commonly referred to at KSC as the catenary wire system). The protective wire system consists of a 70 ft. insulating mast atop the fixed service structure with a steel cable running from the top of the mast to two ground points located 1000 ft. horizontally from the mast as shown in Figure 2-1. This protective wire system is the normal recipient of lightning strokes to the pad, so a pulse on the wire is the normal source of effects in the PCR and the Orbiter; and this is the situation considered in this study The pulse used in the test corresponded to that of a small lightning stroke to the wire (when corrected for the fact that the magnetic fields of the two wires added for the test but oppose each other in most instances of natural lightning).

The simulator was maintained and operated by I-NET, Inc. under the direction of Anthony Eckhoff.

Dr. Pedro Medelius, of I-NET, designed some of the electronics in the data system and was responsible for recording the external data and the internal data taken with the EG&G sensors (locations U, P,Q, and R, Figure 4-3).

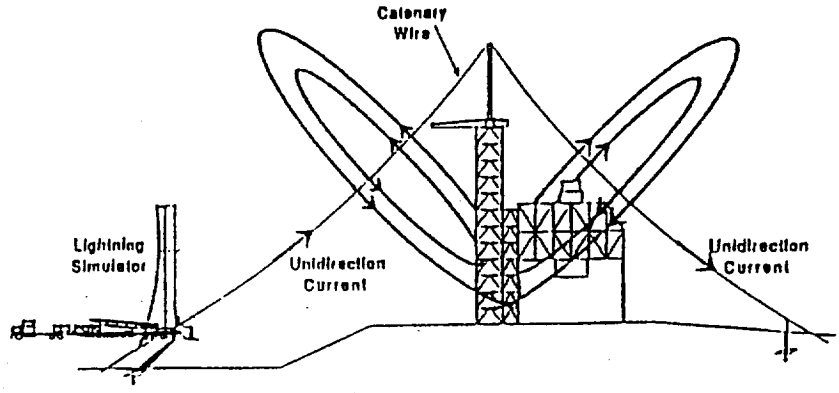

Figure 2-1
Test Configuration

Frank Fisher took the interior data using the sensors designed and built by him (locations C,D,E,F,G,H,I,J,L, and M).

(3) Circumstances did not permit conducting the test with the vehicle present, so the alternative was to conduct an analysis to predict the effects inside the PCR and the Orbiter payload bay when the vehicle is present. An analytical method developed by Electro Magnetic Applications, Inc. (EMA) and applied to this problem by Richard Collier of that company gave acceptable results and was used to evaluate the case with the vehicle present.

The modeling, analysis, and testing of this project were directed toward component A of the NASA standard design stroke because that is the component with greatest current and is most readily simulated in a test of full-scale hardware on the scale of the pad structure. Other components described in [13] are also of concern, especially the multiple bursts of component H. The effects of these other components (especially effects on electronic elements) are more amenable to laboratory study.

Discussion of a stroke which occurred recently to the Rotating Service Structure (RSS) is also included, as it produced some effects in the PCR.

The various parts of this report were written by the individuals responsible for the respective elements of the work. Editing was done by Dr. G. L. Thomas.

3. Modeling

3.1 Physical Modeling

The physical modeling done by LTI consisted of constructing a copper pipe model of the pad structure and PCR, applying current pulses, and making measurements of currents and fields. Results obtained in this way were compared to those obtained by the FILAMENT program, which computes currents and fields for a complex system of conductors. The methods and results will be summarized here; more details can be obtained from [14], which describes the modeling, and [13], which describes the FILAMENT program.

This study was similar in some ways to model studies that had been done previously, both to study lightning effects for Apollo, Skylab, and during design of the Shuttle launch facilities. Those models, however, were not aimed as much toward the magnetic fields in the PCR as was this one; and some of the conclusions reached in those earlier studies seem to have been in error with regard to the amplitude of the magnetic field.

The basic objective of the program was to study the payload environment, but a secondary objective was to provide data that would evaluate the abilities of the numerical techniques used in the study to predict lightning currents in a complex structure and the magnetic and electric fields produced. The previous model studies would not have been of much help in evaluating analytical procedures since they were made long before the advent of the more modern analytical procedures.

The results of the model study have been, in this report, scaled to component A of the NASA standard stroke for design purposes [19], which has a peak current of 200 kA and a maximum rise rate of 140 kA/μs.

3.1.1 Summary of Model Theory

Model theory and the laws of similitude are discussed in [14], but the essentials of the matter are that a small scale physical model of a large structure (the prototype) can be used to predict the lightning response of the prototype if several conditions are met:

Linearity: The first of these is that the systems, model, and prototype behave linearly; that is, that the response measured with an injection current of, say 100 A, be proportionately the same as if the injected current were 100,000 A. This condition will be met as long as the physical structure of the object under examination is not damaged by the lightning current and does not change with current. Since the launch facilities are very massive structures, this condition can be taken for granted. It can also be taken for granted on the model, since the currents used for testing the model are only a few tens of amperes and do not in any way change the model.

Time Scale: The second condition is that the ratio of the time scale used on the test to the time scale for the prototype be equal to the ratio of the physical dimensions of the model to the physical dimensions of the prototype. The model was built as 1/24 of full size; that is, one inch on the model corresponded to two feet on the prototype. The corresponding time scale should then be 24:1 but, for convenience, it was taken as 25:1. An event lasting 100 nanoseconds on the model would then correspond to an event lasting 2.5 microseconds on the prototype.

Materials: Ideally, a model structure should have a resistance that is scaled according to the length scale. This implies that the model should be built of material having a resistivity that is scaled by the same ratio as the length is scaled. For a 1/24 scale model, the resistivity of the material from which the model is made should be 1/24 of that from which the prototype is made. Generally, this requirement cannot be met in practice since one's choice of materials is limited. The question of materials can be rendered moot if the model is intended only to study general effects and is not built as an exact replica of the prototype. Such was the case in this study.

Current Amplitude and Scaling of Voltages and Currents: The model was tested with simulated lightning currents of about 44 A, but that amplitude was chosen only for convenience and compatibility with the test equipment, not because of any considerations of model scaling theory. Assuming linearity, a voltage or current measured on the model would be multiplied by a factor of 1000 to correspond to what would be produced on the prototype by 44 kA lightning stroke, or by about 4500 to correspond to a 200 kA stroke.

Scaling of Magnetic Fields: Two other quantities are of importance: magnetic field intensity, H, and mutual inductance, M. For equal currents in the model and prototype, the magnetic field intensity on the prototype will be 1/25 (1/24 to be precise) of that measured on the model; and, if the currents are not equal, the field intensity will scale directly with the current. A magnetic field intensity of 1 A/m measured on the 1:25 scale model into which a current of 44 A is injected will correspond to 1000/25 = 40 A/m on the prototype into which lightning injects 44,000 amperes. For a lightning current of 200 kA, the corresponding figure would be 182. Given all the uncertainties relating to the scale and detail of the model, it would probably be justifiable to say that a magnetic level of 1 A/m measured on the model would correspond to a 200 A/m level on the actual launch complex, assuming a lightning current of 200 kA. The 1 to 200 ratio will be used in subsequent discussions to evaluate the full scale significance of the calculations and measurements made on the model.

A mutual inductance measured on the model to be 1 nH would correspond to 24 nH on the prototype.

3.1.2 Description of Model

3.1.2.1 Construction of RSS, FSS, and PCR Models

No attempt was made to duplicate on the model all of the features of the actual launch complex, partly because the cost would be excessive, but mostly because it was felt unlikely that they would really influence the lightning behavior of the complex. Also, an intent of the program was to compare measured and calculated lightning performance; and the physical model needed to be simple enough that it could also be described by a mathematical model.

Since the basic structure of the RSS is made from pipes, the model was also made from pipes, copper tubing being used in place of steel pipes. Pipe diameters on the RSS vary from 18 inches to 36 inches; taking 24 inches as an average led to the choice of 1 inch copper tubing for the model of the RSS. One inch trade size copper tubing has an actual outside diameter of 1.13 inches.

The FSS was built from 1-1/4 inch diameter copper tubing, 1.31 inch actual diameter. No attempt was made to duplicate the finer detail of the FSS both because of the cost of doing so and because the focus of this study was the region around the PCR and the RSS. All joints on the model were clamped and soldered in order to eliminate any lingering concern as to joint resistance and its possible effect on the way current divides in the model.

While copper tube were used primarily for ease of fabrication, it might be noted that the considerations of material resistivity discussed in Section 3.1.1 favor the use of copper, which has a lower resistivity than does steel, a trend in the desired direction.

An important question about the PCR was the degree to which it provides effective shielding against electromagnetic fields produced by lightning. It is constructed of a grid of steel beams, some large, some small, onto which are fastened steel surfaced wall panels. Overall, the grid of steel beams can be approximated as a rectangular mesh averaging about two feet on a side. Taken by themselves, the steel members might justifiably be duplicated on the model by a wire mesh of one inch squares.

The wall panels of the PCR consist of a sandwich of two steel surfaces over an interior insulating material. These panels are then bolted to the steel supports, not welded. Presumably, all the panels make the electrical contact needed for effective electromagnetic shielding. Fasteners are spaced only as close together as needed to mechanically hold the panels in place, and all joints are well painted. The fact that the panels make electrical contact with each other and with the underlying structure was verified by making measurements of electrical bonding resistance.

Given these points, the decision was made to build the model PCR from 1/2 inch mesh galvanized hardware cloth with aluminum sheets for the floor and ceiling. The mesh size

was smaller than needed to duplicate the support mesh of the actual PCR and so provides some approximation of the additional shielding provided by the wall panels of the PCR.

Some tests were made with the mesh of the PCR model covered with aluminum foil, 0.0008 inch thick, so as to perhaps provide a better approximation of the magnetic field shielding properties of the walls of the PCR. The limited amount of testing done to compare the two treatments of the walls did not show much difference due to the foil.

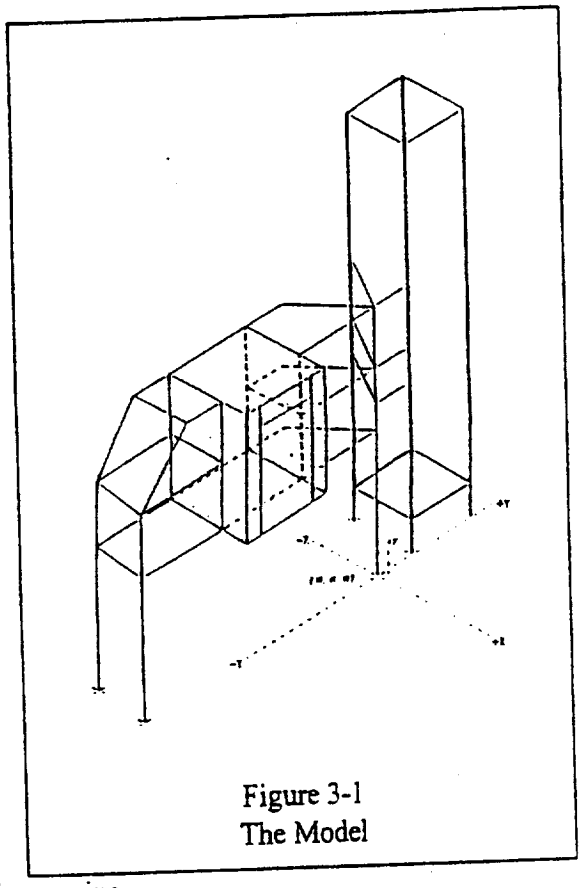

Figure 3-1
The Model

Figure 3-1 shows the model.

3.1.2.2 Modeling of the PGHM

No detailed modeling was done of the PGHM or work platforms of the PCR. A simple structure was built and installed in the PCR to check, in general terms, what the effect of the PGHM might be on the magnetic field; but it was not intended to be a model of the PGHM.

3.1.2.3 Modeling of the ET, SRM, Canister, and Orbiter

Only crude models of the ET and SRM were provided. The ET was modeled with 12 inch diameter steel stove pipe, while the SRMs were modeled by 6 inch diameter aluminum pipe.

The payload transport canister was built from 0.031 inch thick aluminum with welded seams.

No separate model was built of the Orbiter. Instead, since only the payload bay of the Orbiter was under study, the canister model was used as the Orbiter model.

3.1.2.4 Modeling of the Catenary Diversion Wires

Space in the laboratory precluded complete modeling of the catenary diversion wires. What was done was to model them as well as possible in the vicinity of the FSS but to terminate both wires at building beams instead of carrying them all the way to ground level. A sketch of the test setup, showing dimensions, is shown in Figure 3-2

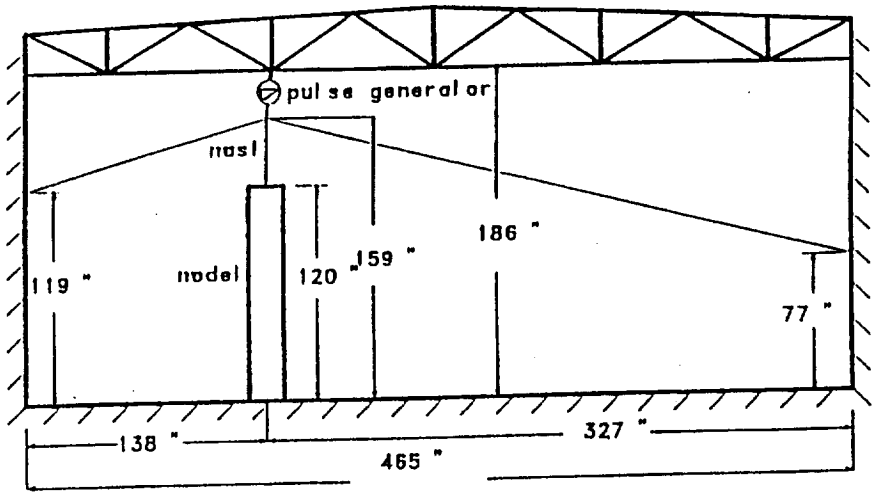

Figure 3-2
Arrangement of Model and Pulse Generator

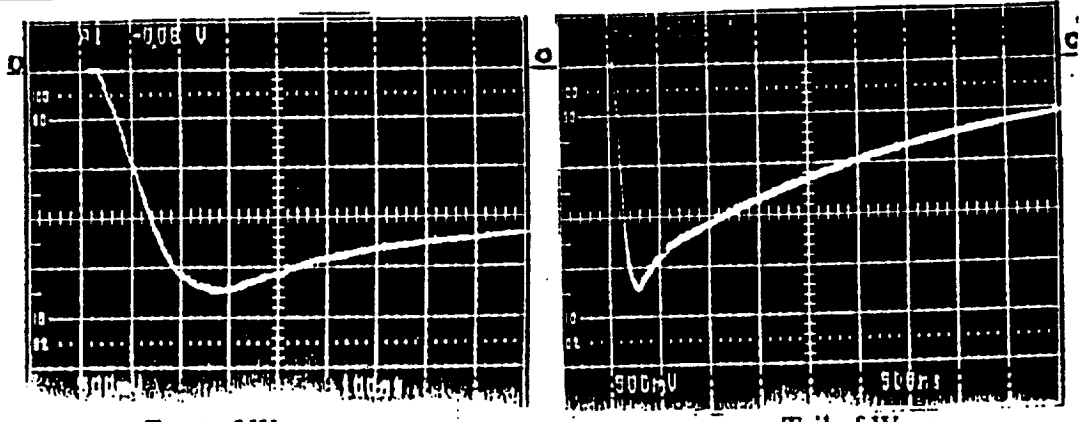

Front of Wave
100 ns/div

Tail of Wave
500 ns/div

Figure 3-3
Injected Pulse (Measured at Ground Level)

3.1.3 Pulse Generation

Details of the pulse generator circuit are given in [13]. It was enclosed in a metal case and mounted to a ceiling girder above the model. An oscillogram of the current pulse discharged into the model is shown in Figure 3-3. Peak amplitude was held between 43

and 44 A. The current had a front time of about 0.22 μs full scale. The waveform thus corresponded fairly well to the Component A waveform specified in [19].

3.1.4 Measurement Methods

Oscilloscope: Measurements were made with a Tektronix Model 2467 oscilloscope having a bandwidth of up to 250 MHz. To minimize high frequency interference, many measurements were made with the bandwidth limited to 20 MHz. Experience showed that such bandwidths were satisfactory for the waveforms encountered.

Current Measurements: The amplitude and waveshape of the current injected into the model were measured with a pulse current transformer built at Lightning Technologies. Its transient response and sensitivity were verified by comparing it to a Model SBNC-1-05 coaxial current shunt made by T&M Research Products.

Current in the members of the model was measured with a Pearson Model 3525 split core pulse current transformer which was verified to have a transient response adequate for the purpose.

Measurement of Magnetic Field: Considerable effort was made to develop suitable probes with which to measure the magnetic field in and around the PCR. The probe ultimately developed is sketched in Figure 3-4. It has a sensitivity of 31.1 volts output per A/m of magnetic field and has a response proportional to magnetic field, unlike

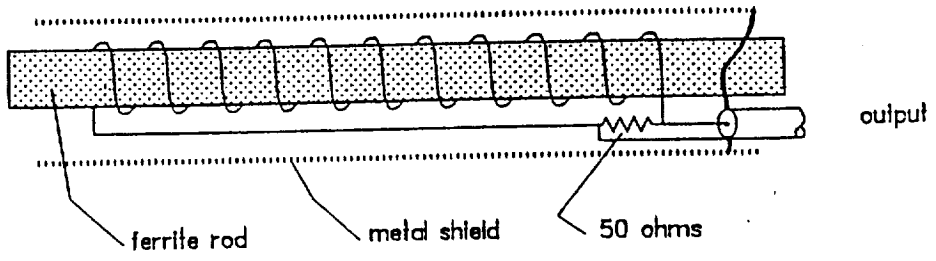

sensitivity = 31.1 A/m into high Z scope
= 62.2 A/m into 50 ohm scope

Figure 3-4
Magnetic Field Probe

some probes that are designed to respond to the derivative of the magnetic field. Its inductance was measured as 680 microhenries, which with the 50 ohm terminating resistor gave an L/R time constant of 13.6 μs, which is long compared to the duration of the pulse injected into the model.

Routing of Measurement Cables: Experience has shown that measurements of magnetic field are prone to interference by extraneous electrical noise introduced into the measurement cables connecting the probe to the oscilloscope. Experimentation showed that the most effective method of eliminating such interference was to run the measuring cable inside the copper tubes of the model. Measurements of noise pickup verified that pickup was negligible in comparison to the signal output from the probe.

Measurement of Voltage: Voltage was measured by direct connection to the 50 ohm input of the oscilloscope, the measurement cable being the one which was also used to connect the magnetic field probe to the oscilloscope.

3.2 FILAMENT

Filament, developed by LTI, is a transient analysis program that incorporates the ability to calculate the way current divides among a group of interconnected wires or filaments. To the degree that a solid surface can be approximated by filaments, it also allows one to calculate the distribution of current on that surface. One can also define the physical location of an electrical conductor and so calculate the voltage or current induced on that conductor. Since the program is basically a time domain transient analysis program for electrical circuits, the filaments can be connected to RLC branches to calculate the effects of load impedances.

Calculated values of currents on the various filaments can be directed to an output file, from which they may be read by an auxiliary program, FILAHMAG, which then calculates the magnetic field intensity at any point selected by the user. Other auxiliary programs include FILALIST, a program to read and make a hard copy printout of the contents of the input data file, and FILAVIEW, a program that makes an isometric sketch of nodes and filaments. These can be used to help debug data files.

FILAMENT is configured for the PC environment and has provisions for 240 physical nodes, 240 electrical nodes, and 180 branches, of which 120 may be mutually coupled filaments. A type of problem that can be treated directly by FILAMENT is that of a set of electrical conductors on a structure. FILAMENT provides a circuit-based approach to calculation of current division, as opposed to others that approach current division from time or frequency domain analyses of electromagnetic fields. In principle, problems treatable by FILAMENT could be treated by other circuit analysis programs, although the labor of calculating by hand the self and mutual inductances of all the defining filaments would present a serious problem.

The program is based on the principles outlined in many discussions of computer-aided analyses of electrical circuits such as [1], [2],[3], and, especially, [9] and [10]. It, like most other circuit analysis programs, treats circuits in terms of nodes and branches, a branch always being connected between two nodes, one of which may be a reference node or "ground." Examples of the node and branch notation system are given in Figures 3-5 and 3-6. Details of the program are given in [13].

3.3 Magnetic Field Behavior

Some aspects of magnetic field behavior, and the behavior of shielding systems, will be described in this section in order to avoid repetition when discussing test results.

3.3.1 Division of Current

The time at which the current in a particular branch reaches its peak depends upon the inductance and resistance of the branch, as well as the time at which the current injected into the structure reaches its peak. To a first approximation, the inductance of a conductor depends on its length and cross sectional area. On this model, all branches of the RSS were built from the same type of tubing; accordingly, the L/R time constant was about the same for each of the members. Thus, the currents all reach their peak at about the same time.

3.3.2 Field Penetration through a Conducting Surface

A changing magnetic field penetrates through a metal surface only with difficulty. As sketched in Figure 3-7, a magnetic field in the vicinity of a conducting surface can be resolved into two components: one component, H_n, normal to the surface and another component, H_t, tangential. The normal component tends to be suppressed; the tangential does not. The normal component is suppressed because any magnetic field line changing with time that attempts to penetrate a conducting surface sets up circulating eddy currents. These eddy currents produce a magnetic field of their own with a direction opposite to the original field. As a result, the total field penetrating the surface is reduced from what it would be without the conducting surface being present. As the eddy currents die away, the field penetrates the surface.

3.3.3 Penetration through Apertures

Magnetic fields penetrate more easily through openings. The degree of penetration depends on the orientation of the field relative to the opening as well as the size of the opening.

The most important apertures in the PCR are between the doors when the doors are closed and, when the vehicle is present, the environmental seals around the Orbiter.

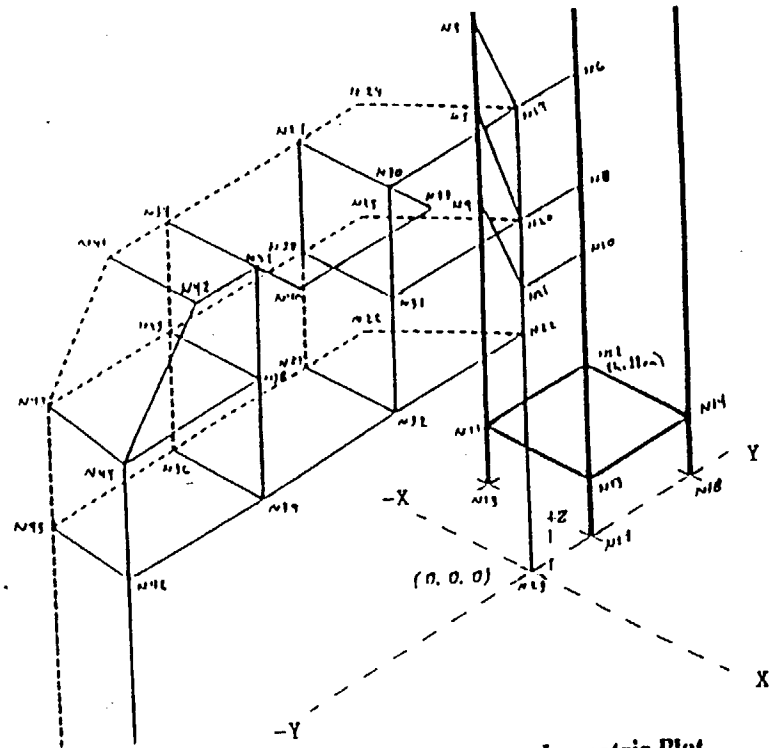

Figure 3-5: Node Designations on an Isometric Plot (Configured for Case 1)

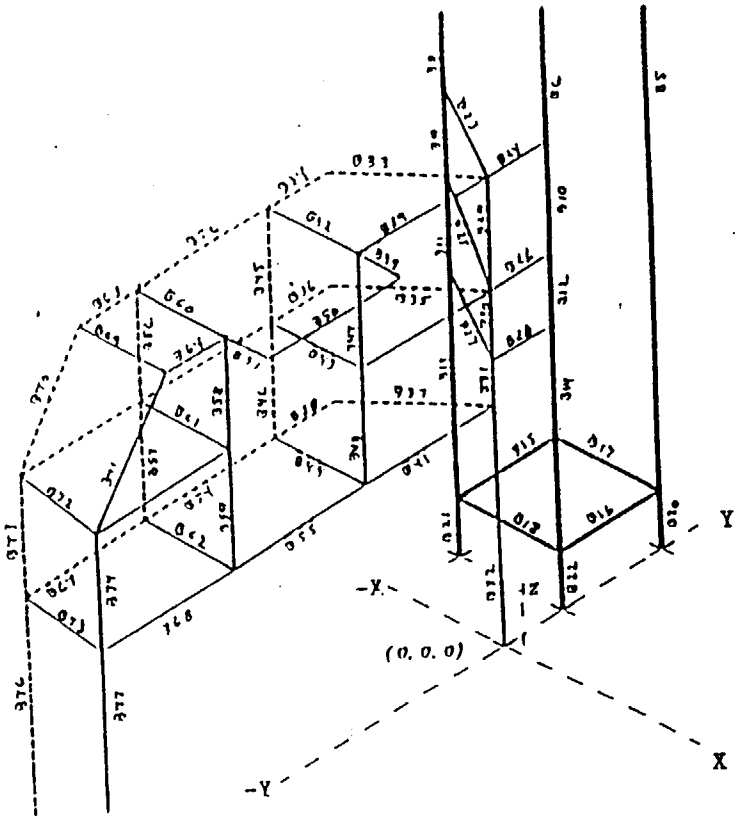

Figure 3-6: Branch Designations on an Isometric Plot (Configured for Case 1)

These seals are closed by non-conducting materials. The aperture around and between the doors is approximately 1-1/2 inches; the environmental seal around the Orbiter is about 10 inches. There also is a significant aperture at the floor of the PCR when the Orbiter is present.

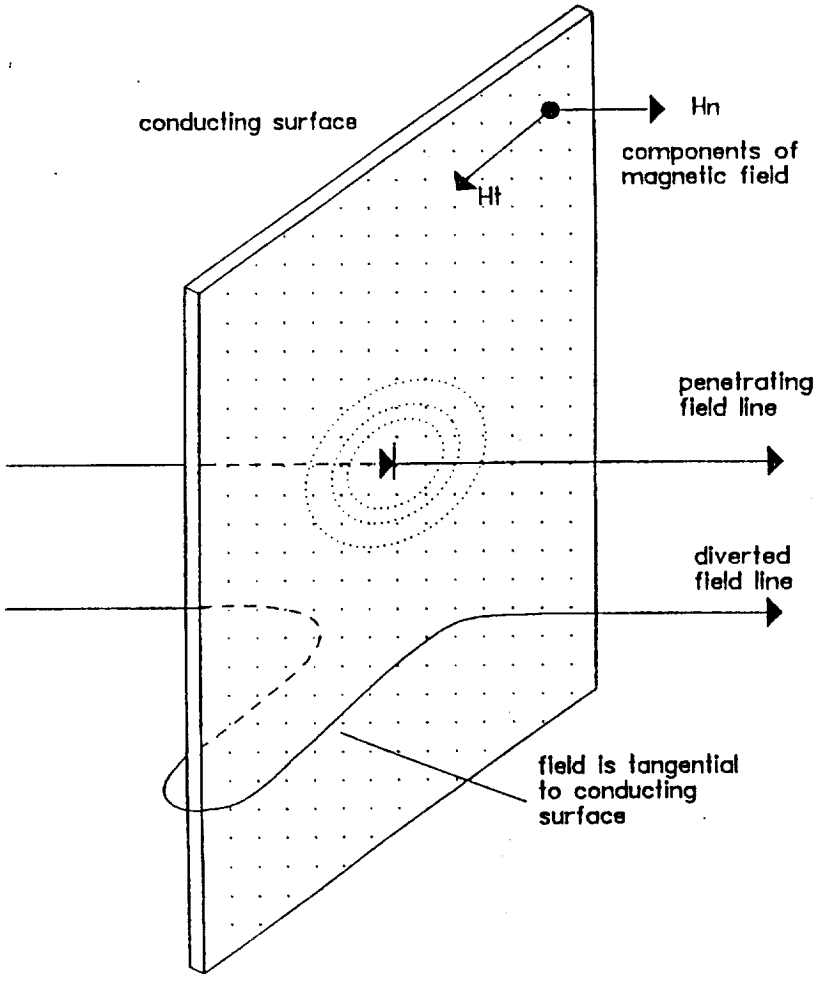

Figure 3-7
Magnetic Field Line Penetrating a Conducting Surface

3.3.4 Waveshape of Internal Fields

Penetration through metal surfaces is frequency dependent: low frequencies penetrate more easily than high frequencies. As a result, the magnetic field penetrating to the inside of a shielded structure will have a slower rise time and a longer decay time than the external field.

Penetration through openings is also frequency dependent: high frequencies penetrate more easily than low frequencies. Magnetic fields that penetrate through openings *tend* to have the same waveshape as that of the external field, but may have superimposed higher frequency components or oscillations due to the internal structural features of the enclosure.

3.4 Configurations Studied

Tests and calculations have been carried out for the following cases:

Case 1 Stroke to FSS with RSS in park position

Case 2 Stroke to FSS with RSS in mate position

Case 3 Stroke to diversion wires with RSS in park position

Case 4 Stroke to diversion wires with RSS in mate position

Case 5 Artificial surge test with current injected at ground level into one end of the diversion wires

Case 6 Study of PCR by itself, including study of effect of the Payload Ground Handling Mechanism (PGHM)

Cases 3 and 6 are the ones of the most immediate interest in this study. Cases 1 and 2 are representative of what could happen if a lightning strike were to bypass the catenary wire and terminate on the FSS.

3.4.1 Results of Measurements and Calculations

Measurements were made on the model; and calculations using the FILAMENT program were made for the model for the above cases as indicated in Table 1, which summarizes the results as extrapolated to a 200 kA stroke.

The following material describes some of the results of the modeling tests and FILAMENT calculations performed by LTI. More complete information is contained in [14].

3.4.1.1 Cases 1 and 2 - Strokes to the FSS

These cases developed basic information relative to the problem and considered the worst situation: a direct strike to the top of the FSS.

TABLE 3-1

Summary of Voltages, Currents, and Magnetic Field Levels

LTI data except where designated as EMA

Values are for a 200 kA stroke.

Type of measurement or calculation	Stroke to FSS		Stroke to Mast				Stroke to one end
	Case 1	Case 2	Case 3	Case 4a	Case 4b	Case 4c	Case 5
	Park position	Mate position	Park position	Mate position			Park position
Structure currents							
calculated	yes	no	Figure 3-8	yes	Figure 3-11	Figure 3-13	yes
measured	yes	no	no	no	Figure 3-11	Figures 3-13,3-24	no
Magnetic fields (A/m) without PCR model in place							
in front of location for PCR doors -- calculated	500	500	120-160	30 - 40	60	80	500
in front of location for PCR doors -- measured	540	---	---	---	---	68	---
Measured magnetic fields (A/m) with PCR model in place							
in front of PCR doors - doors open	546	500	---	---	---	---	---
in plane of PCR doors - doors open	400	---	62	---	---	---	---
at center of PCR - no canister - doors open	124	---		---	---	---	---
at center of PCR - no canister - doors closed	74	---	12 0.5-1.6 (EMA calc.)	---	---	---	---
at center of PCR - with canister - no ground wires	126	---	---	---	---	---	---
at center of PCR-with canister-with four ground wires	96	---	---	---	---	10	---
Measured shielding effectiveness of PCR							
	7.3:1	---	5:1	---			---

Measured potential between PCR and canister (volts)							
with no ground wires	8800	---	---	---			---
with four ground wires	2500	---	---	---			---
Measured potential between PCR and Orbiter (volts)							
with no ground wires	---	---	---		20,000		---
with four ground wires	---	---	---		800		---
with only top two ground wires	---	---	---		3,200		---
with only bottom two ground wires	---	---	---		900		---
Calculated electric fields (EMA)							
external			6 kV/m				
PCR internal			0.2-0.3 V/m				

3.4.1.2 Case 3 - Stroke to Diversion Wires with RSS in Park Position

This is the case with direct application to the test with the actual PCR.

3.4.1.2.1 Results of Calculations

Currents are shown in Figure 3-8. Magnetic fields calculated at various locations are listed in Table 2. Fields at the face of the PCR (more exactly, where the face of the PCR would be) were in the range of 0.6 - 0.8 A/m, figures that would scale to 120 - 160 A/m if the lightning current were 200 kA.

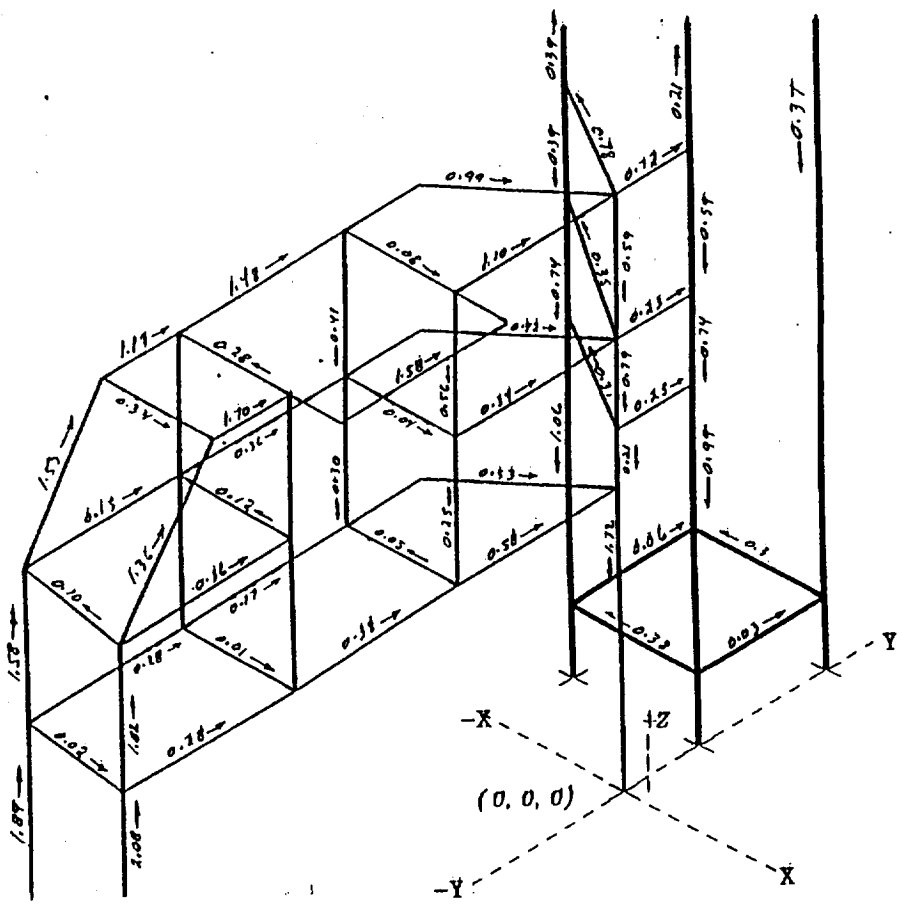

Figure 3-8
Calculated Currents for Case 3

3.4.1.2.2 Results of Measurements

Magnetic Field Levels External to PCR: Measurements of the magnetic field levels at the face of the PCR doors, with the doors open, are shown in Figure 3-9. Horizontal and

TABLE 3-2

CASE 3

This set of data pertains to 79 filaments
Time = 2.979998E-07 S

LOCATION			CALCULATED MAGNETIC FIELDS		
X	Y	Z	magnitude A/m (Hx)	latitude degrees (Hy)	longitude degrees (Hz)
-3.900E+01	-8.000E+00	+5.000E.01	+6.404E-01	-4.127E+01	+1.681E+02
-3.900E+01	-8.000E+00	+5.500E.01	+7.522E-01	-3.924E+01	+1.577E+02
-3.900E+01	-8.000E+00	+6.000E.01	+8.724E-01	-3.602E+01	+1.508E+02
-3.900E+01	-8.000E+00	+7.000E.01	+1.157E+00	-1.458E+01	+1.64E+02
-3.900E+01	-8.000E+00	+7.500E.01	+1.939E+00	+3.512E+01	+1.261E+02
-3.900E+01	-8.000E+00	+8.000E.01	+8.739E+00	-7.100E+01	+1.123E+02
-3.900E+01	-8.000E+00	+8.500E.01	+4.261E+00	-5.938E+01	+1.260E+02

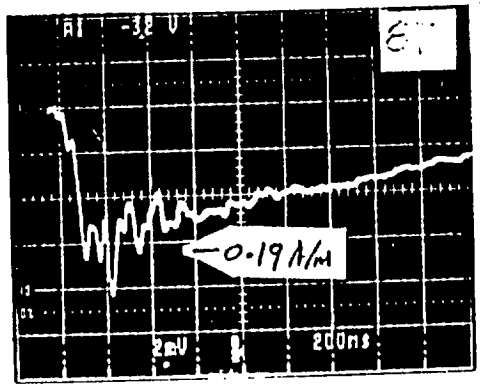

Vertical field at face of open door

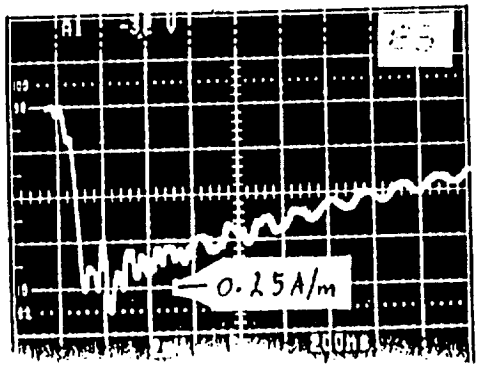

Horizontal field at face of open door

total = 0.31 A/m

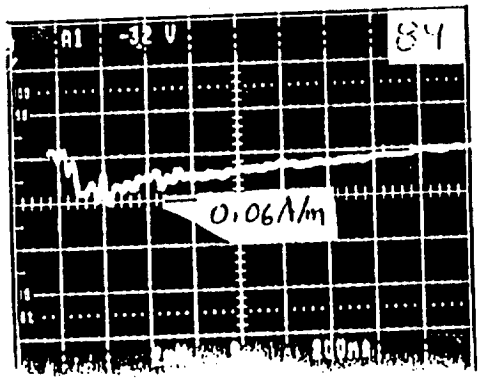

Vertical field at center of PCR

doors closed

0.062 a/m per div
200 ns/div

Figure 3-9
Magnetic Fields - Case 3

vertical components of the field were roughly equal; and the total field was about 0.31 A/m, a figure that scales to 62 A/m for a lightning current of 200 kA. The field farther away from the open doors would be somewhat higher, but no measurements were made during Case 3. Results of Case 1 indicate that it might be higher by factor of 1.35.

Magnetic Field Internal to PCR: The vertical field at the center of the PCR with the doors closed was about 0.06 A/am, a figure that scales to 12 A/m for a 200 kA stroke. (Figure 3-9)

Voltage on Sense Wire (for LIVIS sensor Purposes): Voltages induced on a horizontal sense wire 12 inches long and spaced 1 inch away from the wall (2 ft. full scale) were 0.006 - 0.008 volts, figures that scale to 30-37 volts for a lightning current of 200 kA.

Magnetic Effectiveness of Catenary Diversion Wires: Comparing the 2.02 A/m of Case1 with the 0.31 of Figure 3-9 suggests that having a stroke hit the apex of the diversion wires reduces the magnetic field by about a factor of 6.5 compared to what it would be if the stroke were to hit the FSS.

3.4.1.3 Case 4 - Stroke to Diversion Wires with the RSS in the Mate Position

This test relates to analysis presented later in this chapter and to the actual case of primary interest.

Case 4a: For this set, the ET, SRMs, and Orbiter were not represented in any way. Results of this test are given in [14].

Case 4b: For this set, the ET, SRMs, and Orbiter were represented by cylinders, as indicated in Figure 3-10. A metal cylinder was provided to represent the hydrogen vent arm, and four wires were represented as connecting from the top and bottom of the ET cylinder to the four corners of the RSS adjacent to where the model of the PCR would sit. These were intended to represent the four ground wires used to connect the Orbiter to the PCR.

As discussed earlier, space in the laboratory precluded installation of model diversion wires of a length proportional to those at KSC. This set of calculations was made with the catenary diversion wires terminated at points equivalent to those used on the physical model. The diversion wires were, however, represented as having a high resistance so that the calculated current was the same in each diversion wire. Case 4c, which follows, perhaps treats the wires more properly.

The calculated currents are shown in Figure 3-11, with some measured values also shown. The currents in the RSS showed a general swirl in a clockwise direction, which should produce a magnetic field with a strong vertical component. The calculated magnetic fields were larger than calculated for case 4a. Overall, the magnetic field in the

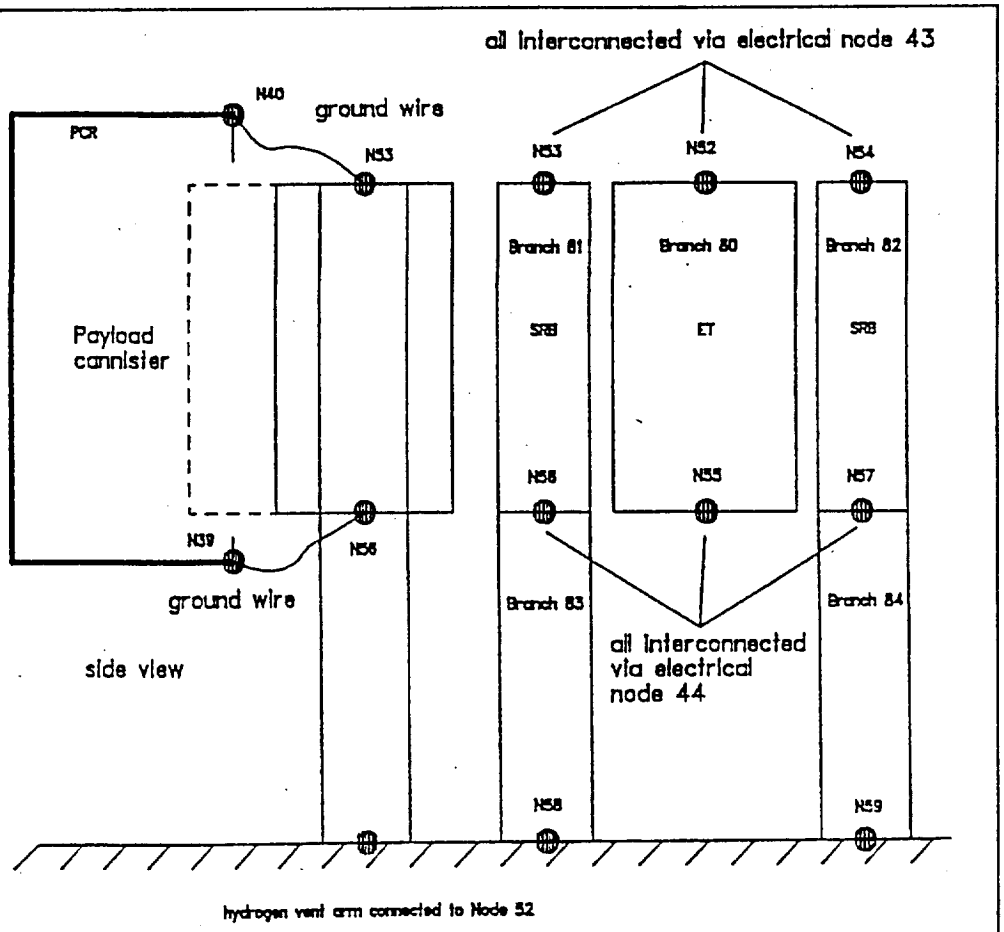

Figure 3-10
PCR, ET and Orbiter Representation

PCR doors was about 0.3 A/m, corresponding to about 60 A/m for a 200 kA stroke.

Case 4c: Physically, this case was identical to Case 4b; but the resistance of the diversion wires was reduced to a low value so that the division of current betwen the two wires was determined by the inductance of the wires. Computed, and some measured, values of the currents are shown in Figure 3-12; and calculated magnetic field values are show in Figure 3-13. The field is around 0.4 A/m at the face of the PCR, corresponding to about 80 A/.m full scale, and is predominantly in the vertical direction.

Probably this is the case for which the calculations most closely match the measurements.

3.4.1.3.1 Results of Measurements, Case 4c

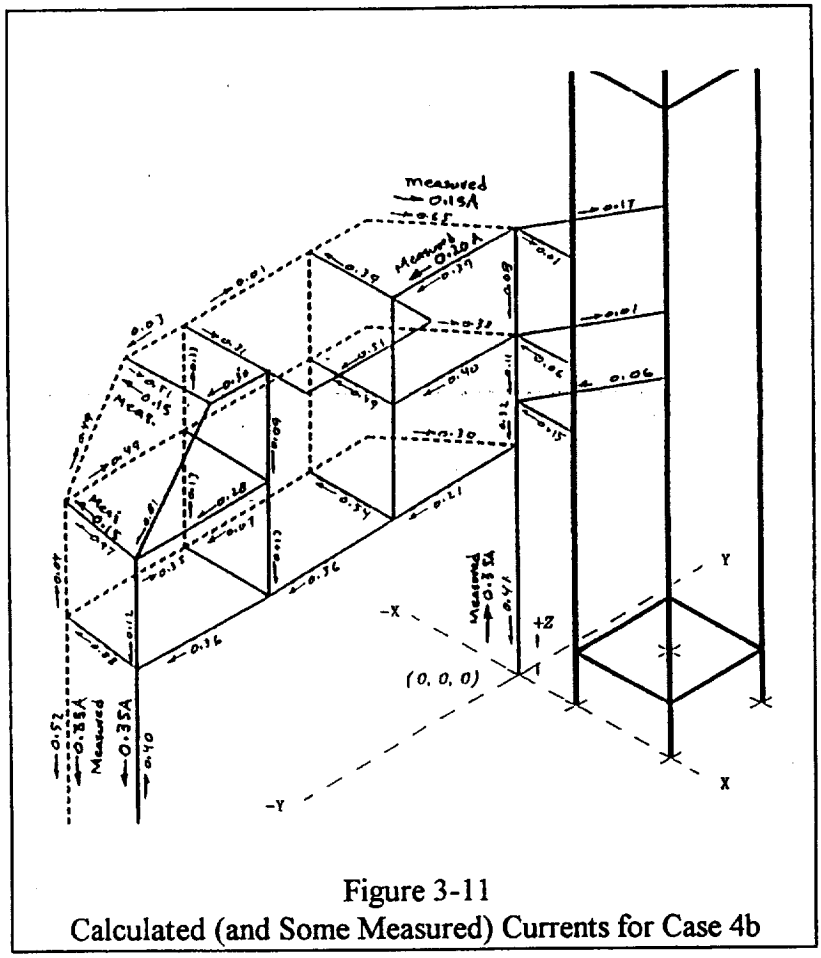

Figure 3-11
Calculated (and Some Measured) Currents for Case 4b

All of the measurements for this case were made with the ET and SRM models in place. The model canister was mounted to the ET so as to simulate the Orbiter. For these tests, the walls of the model PCR were covered with 0.8 mil thick aluminum foil in order, it was hoped, to better model the shielding provided by the wall panels of the PCR.

Model Lightning Current: The distributed transmission line nature of the catenary diversion wires had some effect on the waveshape, but since the pulse generator was designed to produce a wave with a relatively long front, the effect was minor. An oscillogram of the injected current is shown in Figure 3-14. Comparison with Figure 3-3 shows that the catenary diversion wires introduced some small degree of oscillation into the current. The oscillations would have been more pronounced had the front time of the current been less.

How the catenary diversion wires would respond to an actual lightning current of short front time is not completely amenable to calculation. Shorter front time currents would introduce more oscillation, but in nature the oscillations would be damped by several factors: non-linear effects of ground impedance where the wires are grounded, radiation losses from the wires, non-linear effects of the corona that forms around conductors when they are elevated to high voltage, and the degree to which oscillations are damped by the dynamic resistance of the lightning channel.

Current in Grounding Cables: There are four cables used to electrically bond the Orbiter to the PCR: two at the top and two at the bottom of the doors. Current was measured in one of the bottom cables, with the results shown in Figure 3-15. With all the cables in place, the injected lightning current of 43 amperes caused a peak current of

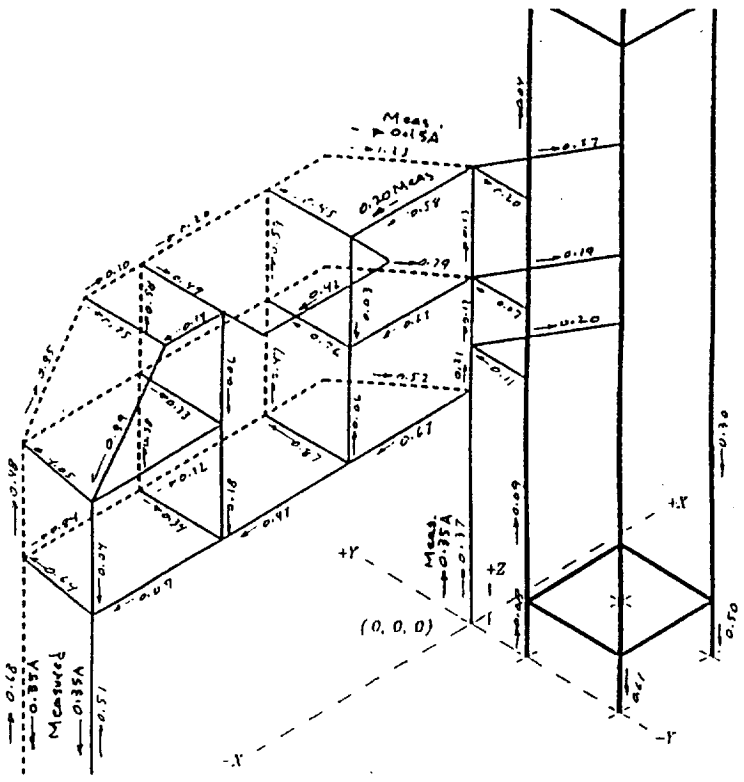

Figure 3-12
Calculated (and Some Measured) Currents for Case 4c

about 0.16 amperes in the grounding cable, a figure that would scale to 740 amperes if the lightning current were 200 kA. Disconnecting the other three ground straps caused the current to increase to 0.40 amperes, or 1,860 amperes for 200 kA of lightning current. Some of the current results from the connection between the FSS and the ET provided by the hydrogen vent arm, but eliminating that connection on the model reduced the current only slightly.

A significant point is that the waveshape of current in the ground cable was basically the same as that of the incident lightning current. It did not show any strong evidence of localized oscillations.

Voltage Between Orbiter and PCR: Voltage between the Orbiter and the PCR was measured on the model. With all four ground cables in place, the voltage on the model was 0.18 volts, a figure that scales to 800 volts for a 200 kA lightning stroke.

Effects of Removing Ground Wires: Removing all ground wires would allow the voltage to go to 20,000 volts. Installing only the top wires would result in a voltage of GG3,200 volts, and installing only the bottom wires would result in a voltage of 900 volts.

Leakage Path for Magnetic Fields: The primary path by which magnetic fields leak into the PCR when mated to the Orbiter appears to be through the environmental seal between the PCR and the surface of the Orbiter. Site inspections have shown the gap to be of the order of 10 inches, or on the order of one foot when including the thermal protective covering of the Orbiter (Figure 3-16). On the model, this would scale to about 0.5 inch.

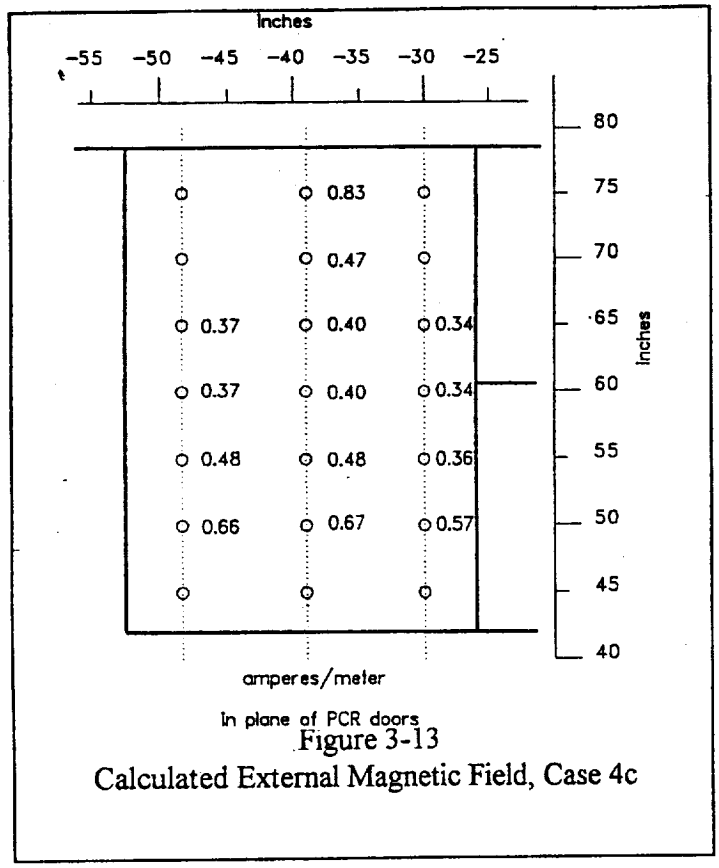

Figure 3-13
Calculated External Magnetic Field, Case 4c

For tests, the gap between the model of the PCR and the Orbiter was covered with aluminum foil with a gap of about 0.5 inch left between the edge of the foil and the model of the Orbiter.

External Magnetic Field: A measure of the field available to leak into the PCR would appear to be that on the outside of the PCR. One measurement was made of this field, as shown in Figure 3-17. Only the vertical component of field is shown, but measurements were made which showed the horizontal component to be negligible around the seal.

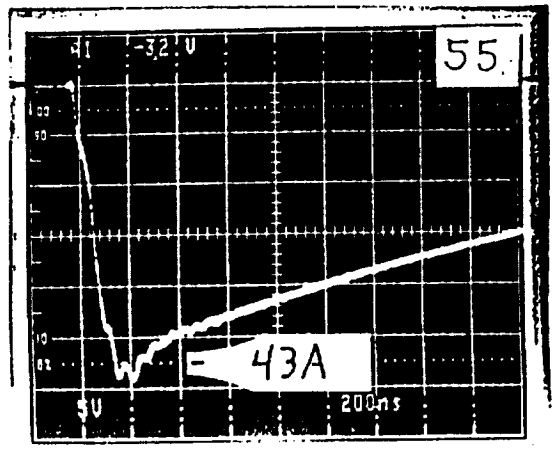

8 A/div

200 ns/div

Figure 3-14
Current Injected into Apex of Diversion Wires

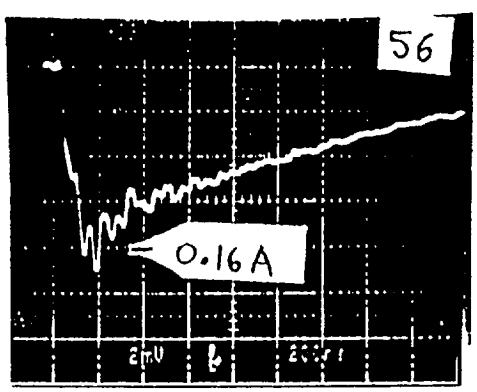

All ground straps in place

ET vent arm in place

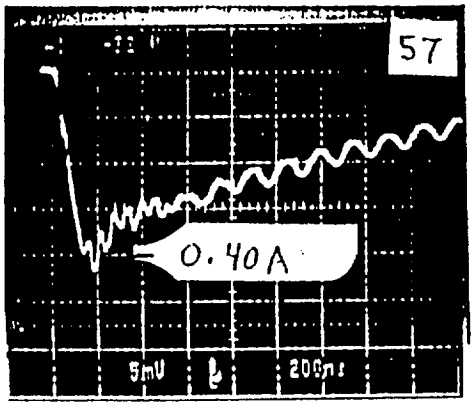

All other straps removed

ET vent arm in place

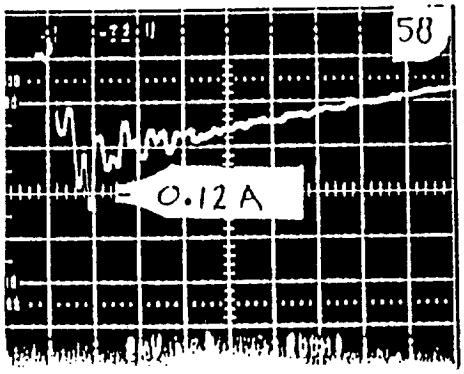

All ground straps in place

Vent arm removed

Figure 3-15
Current in One Ground Wire
(43 A injected into catenary diversion wires)
(Measured with 0.050 ohm shunt)

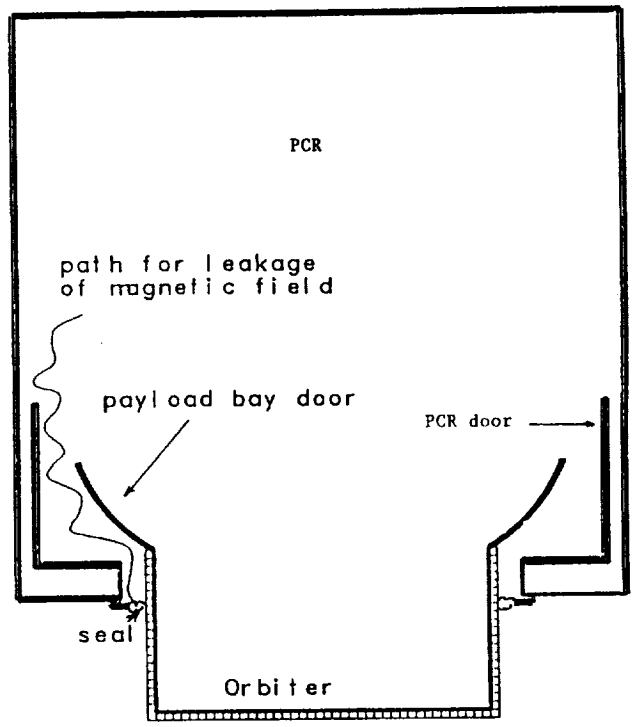

Figure 3-16
Magnetic Field Penetrating an Environmental Seal

The overall magnitude of the vertical component was found to be 0.34 A/m, a figure in line with that calculated by FILAMENT. Using the scaling factor of 200:1 discussed in Section 3.1.1 gives a field level of 68 A/m for a 200 kA lightning current. The waveshape of the field was predominantly that of the injected current.

Internal Magnetic Field: Fields internal to the PCR are shown in Figures 3-18 and 3-19. The field was predominantly oriented vertically and had a peak magnitude in the model of about 0.05 A/m, a figure that scales to about 10 A/m for a lightning current of 200 kA. Checks were made on the magnitude of the horizontal components; and at all locations, the horizontal field was much less than the vertical field. This vertical orientation of the field is in line with the fact that the openings into the model are predominantly vertical, as the significant aperture at the bottom of the doors is not included in the model. (In the simulator test, horizontal and vertical field components were of comparable magnitude except near the floor of the PCR- 135 foot level - where the horizontal components were larger.)

Field levels varied somewhat with location within the PCR model, but the variation did not seem to be more than 2:1 for any of the cases studied.

Influence of Seal Spacing: The most effective way to improve the magnetic shielding would be to provide a continuous metal contact between the PCR and the body of the Orbiter. Figure 3-20 shows that doing so would reduce the field levels inside the PCR by about 40%, but providing such a metal contact probably is not practical.

Waveshape of the Internal Field: Voltages induced by a changing magnetic field are proportional to the rate of change of the field. The waveshape of the field inside the PCR

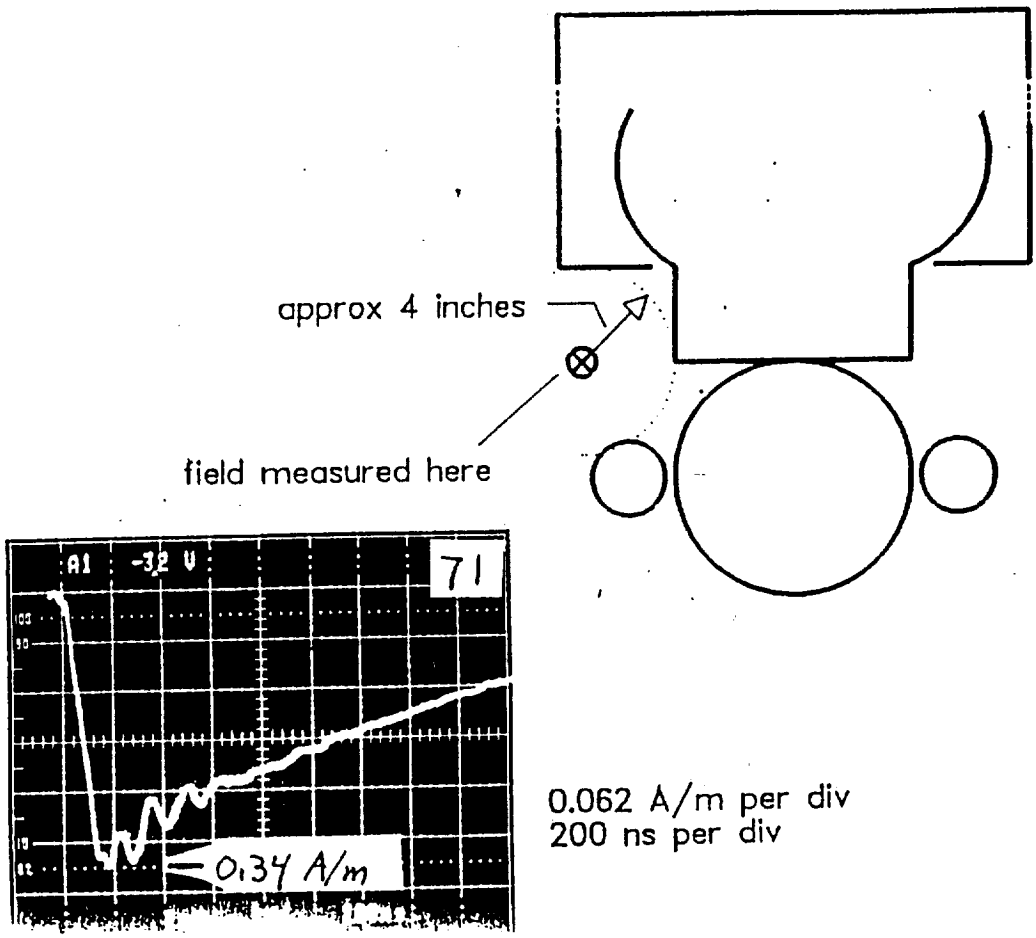

Figure 3-17
Vertical Magnetic Field External to PCR
(43 A injected into catenary diversion wires)

is thus of as much importance as the peak magnitude. On this model, the fields appear to have a shape similar to that of the external field, with the front neither significantly stretched by diffusion through the PCR walls nor the shape significantly contaminated by high frequencies brought on by resonant coupling through apertures.

Voltage Induced on Sense Wires: One purpose of this study was to determine the optimum location in the PCR for a magnetic field-sensing coil for the Lightning Induced Voltage Instrumentation System (LIVIS) system. The fact that the internal field appeared to be predominantly vertical suggests that preferred orientation of a sense wire would be horizontal rather than vertical. A short series of tests was made to determine what voltages would be picked up by various sense wires. Orientation of the various wires is shown in Figure 3-21 and resulting induced voltages in Figure 3-22. The best orientation did appear to be horizontal, but the difference between horizontal and vertical was not great.

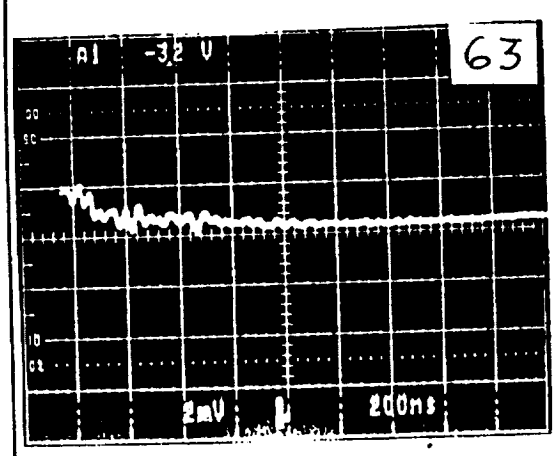

Field at center of PCR

9 inches from face of PCR

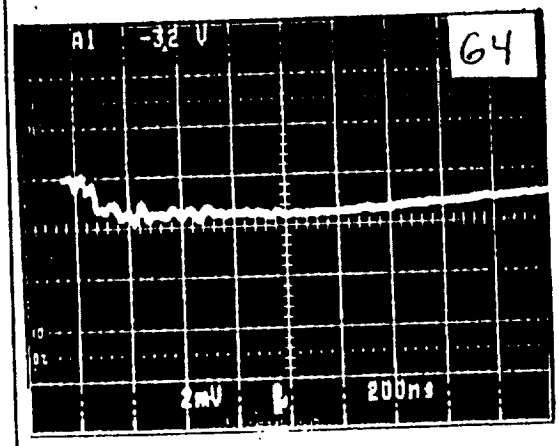

Field at face of cargo bay

Field inside cargo bay of Orbiter is aboul the same as this

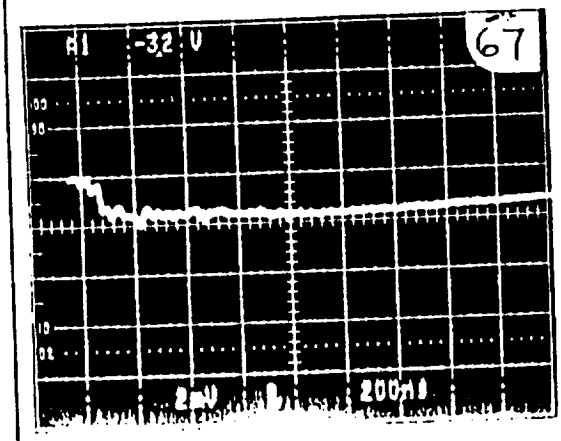

Field along side wall

4 inches from wall
9 inches from face of PCR

0.062 A/m per div
200 ns per div

Figure 3-18
Vertical Magnetic Field 15 Inches from Floor of PCR
(43 A injected into catenary diversion wires - doors closed)

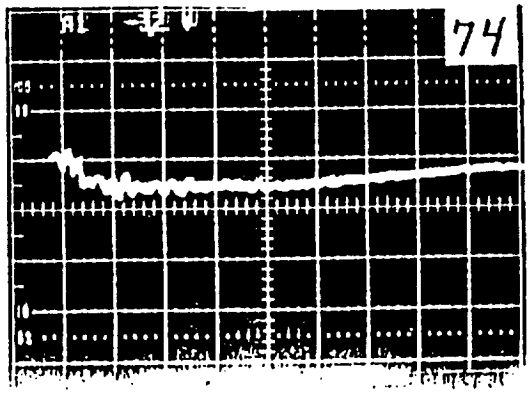

Field 20 inches from floor

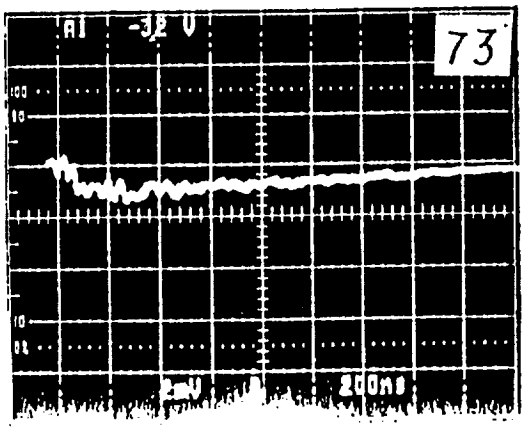

Field 12.5 inches from floor

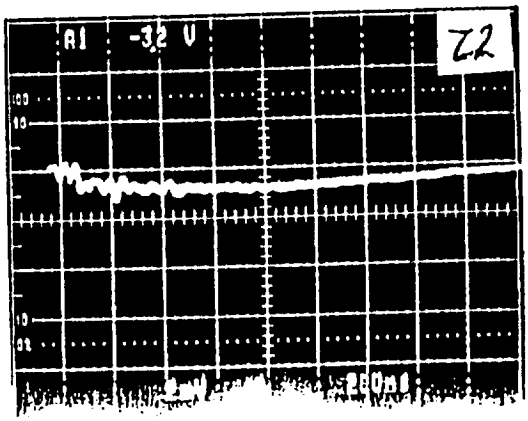

Field 5 inches from floor

Centerline of PCR 6 inches from front face

0.062 A/m per div
200 ns per div

Figure 3-19
Vertical Magnetic Field vs Distance from PCR Floor
(43 A injected into catenary diversion wires)

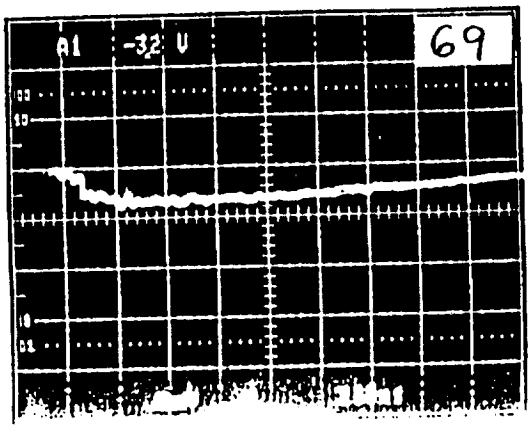

1/2 inch opening around Orbiter
base case

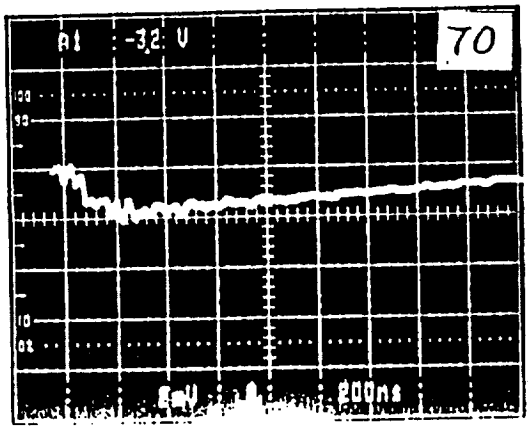

Seals removed -- 2 inch opening
worst case

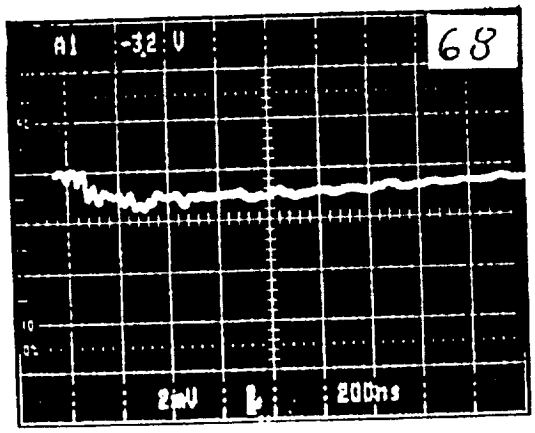

Metallic contact with Orbiter
best case, but not practical

0.062 A/m per div
200 ns per div

Figure 3-20
Impact of Seal Opening around Orbiter
(43 A injected into catenary diversion wires)

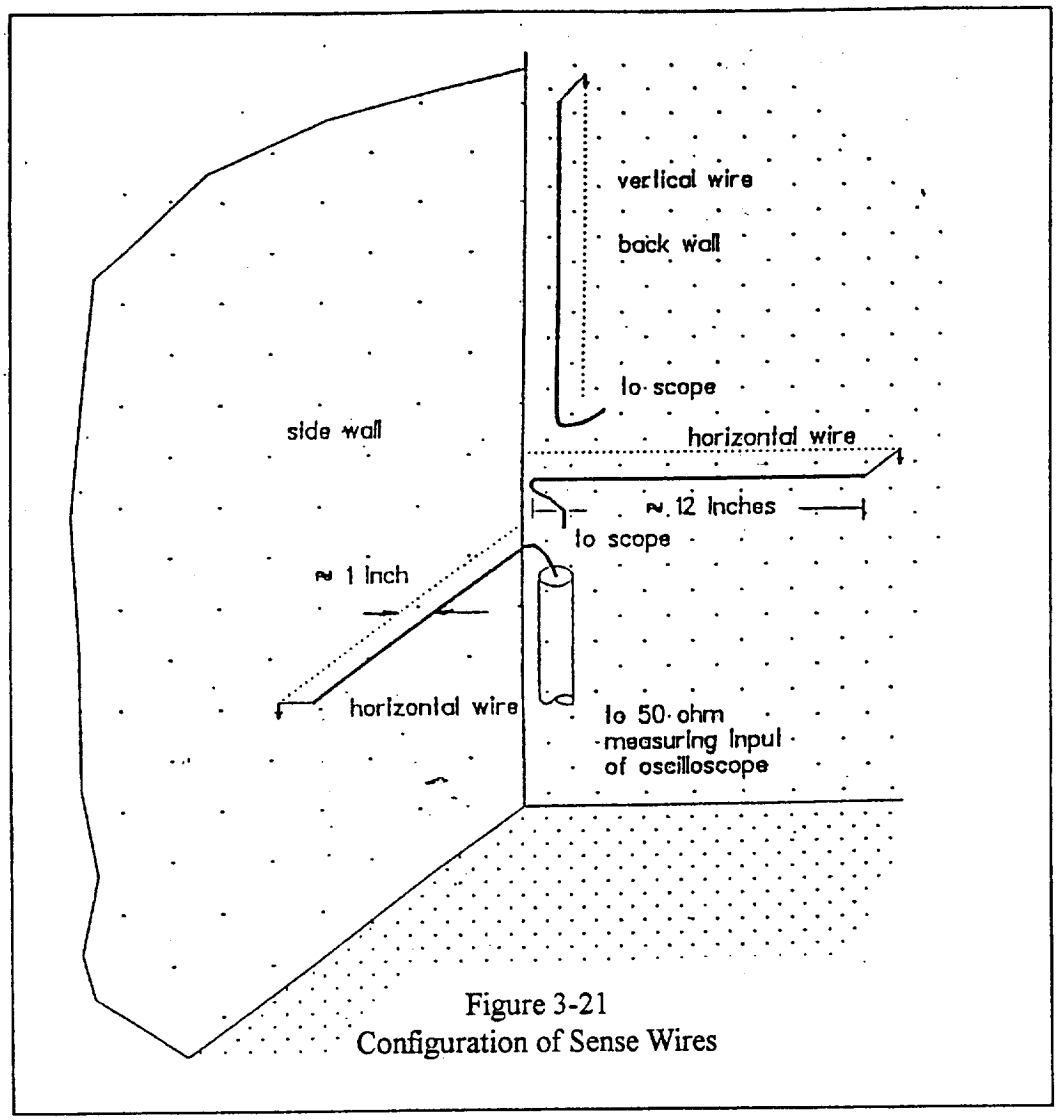

Figure 3-21
Configuration of Sense Wires

Peak magnitudes on the model were in the range 0.004 - 0.005 volts, values that would scale to 18 - 23 volts for a 200 kA lightning stroke.

Current in Structural Members: A few measurements were made of current in structural members of the RSS, with oscillograms shown in Figure 3-23. Those currents are predominantly unidirectionial with some superimposed oscillations. Those oscillations should be viewed with suspicion, and undue significance should not be ascribed to them. Some of them are very characteristic of the spurious noise signals induced on measuring cables although care was taken to use the measuring techniques shown by experience to be most effective in controlling noise. The 0.35 A values shown correspond to 1,600 A for the full scale lightning stroke.

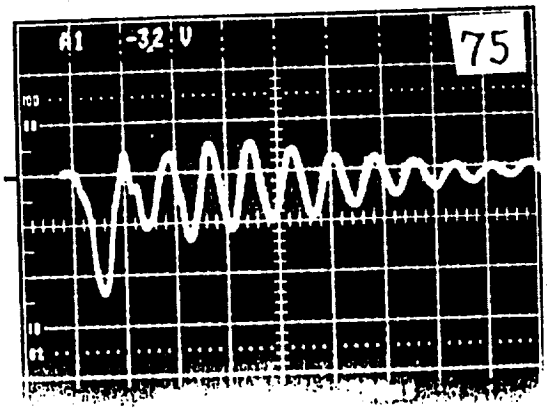

Wire along side wall
Horizontal wire

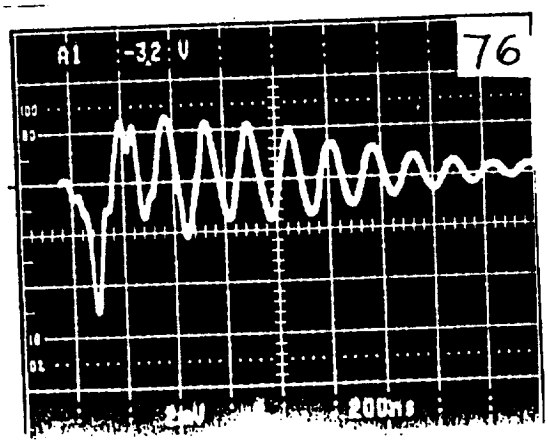

Wire along back wall
Horizontal wire

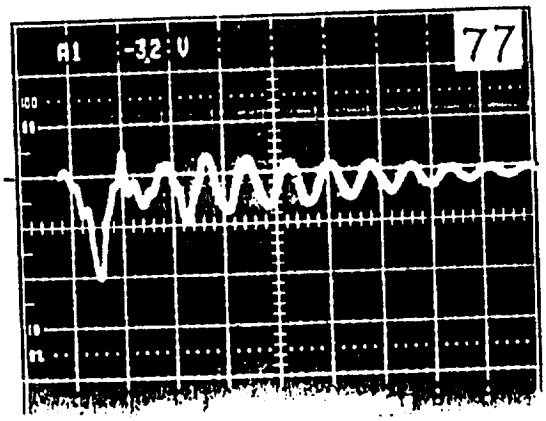

Vertical wire in corner

200 ns/div

Figure 3-22
Voltage Induced on Sense Wires
(43 A injected into catenary diversion wires)

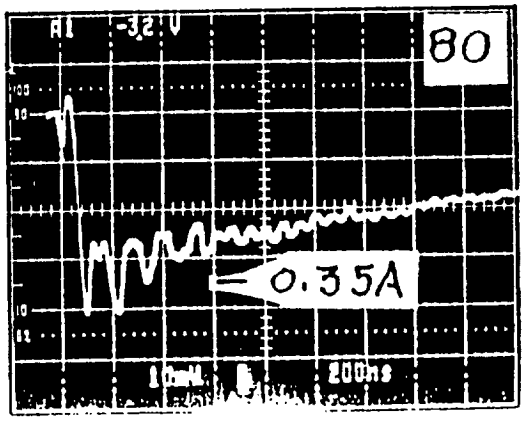

Current in Branch 76

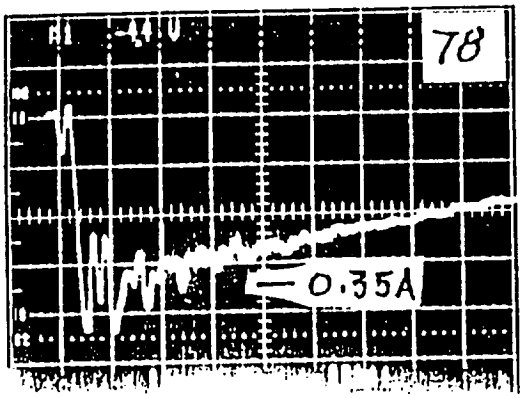

Current in Branch 77

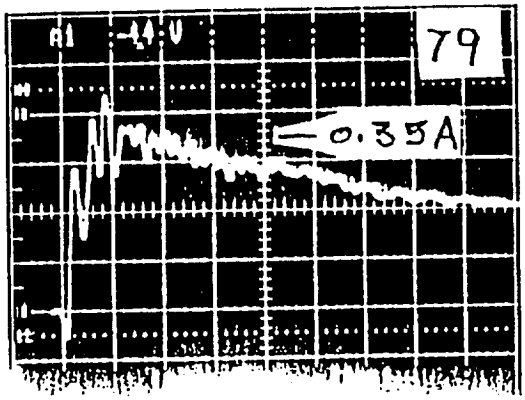

Current in Branch 32

0.1 A per div

Current of negative polarity flowing in assigned direction of branch would result in a negative going measured signal from the transformer.

Figure 3-23
Current in Various RSS Branches
(43 A injected into catenary diversion wires)

A direct comparison of measured and calculated values is difficult since the measurements were made with the physical model of the PCR in place while the calculations did not allow for the PCR. Overall, the amplitudes compare, at best, moderately well with those calculated. Measured and calculated polarities do not always agree, but the measurements at least indicate that currents in nearby members may well be flowing in opposite directions, as was predicted by the calculations.

3.4.1.4 Case 5 - Current Injection into One End of Catenary Diversion Wires

To estimate effects of the planned test using a lightning simulator at the launch pad, FILAMENT calculations were made for the test configuration. Calculated magnitudes were about 2.5 A/m, a value that scales to 500 A/m for a 200 kA stroke. Injecting a given current into one end of the catenary wire produces magnetic fields that are greater than those produced by a similar current injected into the mast, but the ratio does depend upon the location of the point for which the calculations are made. That is because the fields from the two sections add for injection at the end rather than subtract as they do for injections at the mast (Figure 2-1). For this geometry, the ratio at the PCR location was calculated to be 2.2.

Injecting current into one of the wire terminals does produce a field with more of a horizontal orientation than does injecting current into the mast, but the vertical component of the field is still greater than produced by injecting into the mast.

3.4.1.5 Test of the PCR by Itself

The magnetic fields produced by injecting current into the diversion wires were so small inside the model of the PCR as to be at the limits of sensitivity of the measuring equipment. The test had, however, shown that the internal fields were proportional to the magnitude of the external field, however it might be produced. This suggested that effects inside the PCR could be studied by creating an external field using a current-carrying wire stretched along the front of the PCR to produce a large magnetic field outside the PCR.

The test geometry is shown in Figure 3-24, along with the waveshape of the injected current. The current amplitude was somewhat larger than used for other tests, and modifications to the scaling factors must be made. The appropriate factors are 4,167 to scale current or voltage to 200 kA and 174 to scale magnetic field amplitude to 200 kA.

Leakage of magnetic field into the PCR when in the park position is primarily through the gaps between the two doors, at the door folds, and at the top and bottom of the doors. If those gaps were bridged by conductors, the field would be reduced. Bridging by a piece of aluminum foil taped across the center joint reduced the magnetic field at the center of the PCR to 0.67 A/m. Such a connection not only reduces the magnitude of the field, it

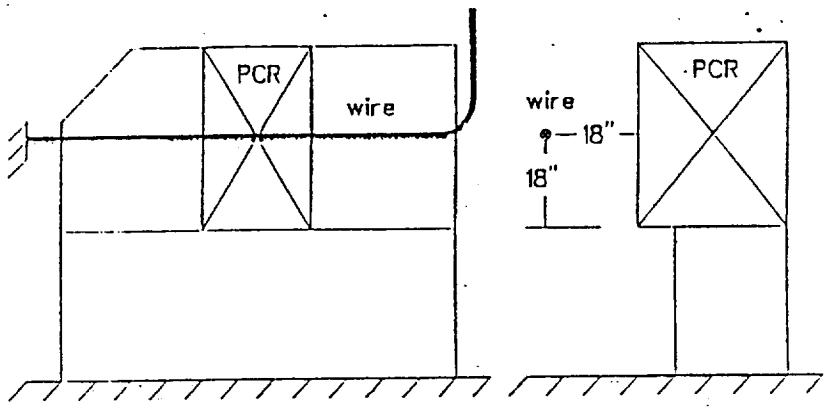

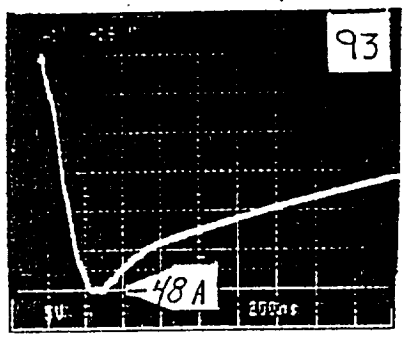

8 A/div

200 ns/div

Figure 3-24
Configuration for PCR by Itself and Applied Current

increases the front and fall times as well and, accordingly, causes the rate of change of field to be reduced by more than the reduction in peak magnitude.

Actually making such a connection on the doors of the PCR would present many practical difficulties, and this test should not be taken as a recommendation for doing so.

Influence of PGHM on Magnetic Field: No tests were made using a detailed model of the PGHM, but the expected influence of the PGHM was checked using the model structure shown in Figure 3-25. It was two feet high, one foot square in plan view, made from one inch aluminum angle, and built so the magnetic probe could be placed at a certain point inside the empty PCR and then the structure placed over the probe.

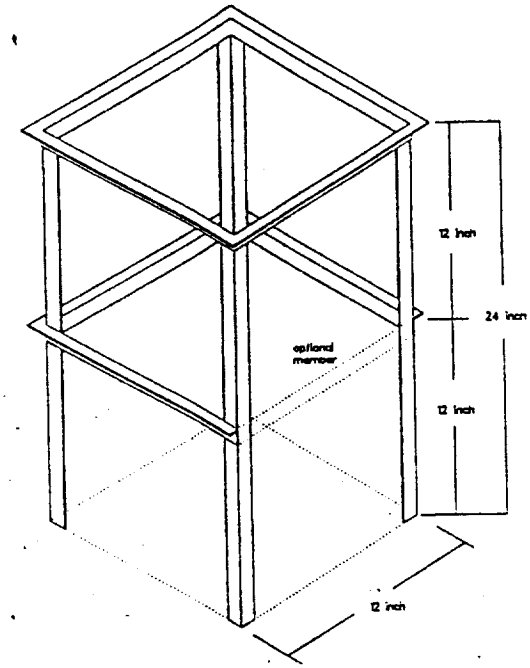

Figure 3-25
Structure Used to Evaluate Effects of PGHM

In this way, "before" and "after" measurements could be made and the effect of the structure evaluated. Results are shown by Figure 3-26.

Probe at Center of Structure: For the structure to have much effect on the magnetic field, it must provide a short-circuited loop into which the changing magnetic field can induce a circulating current. Such a loop is provided by the closed ring at the top of the structure, but that loop should have little effect at remote points. Measurements at the center of the structure, shown in Figure 3-26, where there was no such loop, showed that the magnetic field was reduced by only about 15%.

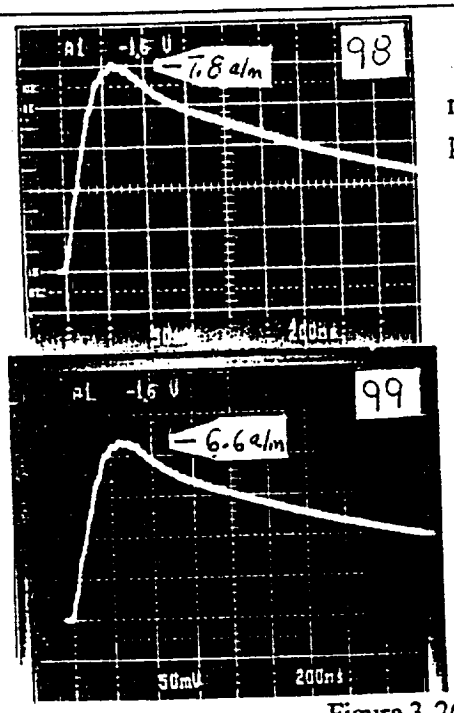

no PGHM
probe at center of PCR

PGHM centered on probe

1.56 A/m per div
200 ns/div

Field 10 inches from plane of open doors

Figure 3-26
Influence of PGHM on Magnetic Field

Completing the loop by connecting a metal bar as indicated by the dotted lines caused the field to be reduced by 45% over what it was without the structure. (Figure 3-27)

Probe at Top of Structure: A probe at the top of the structure was surrounded by a conducting loop, and there the structure did reduce the field amplitude as shown in Figure 3-28.

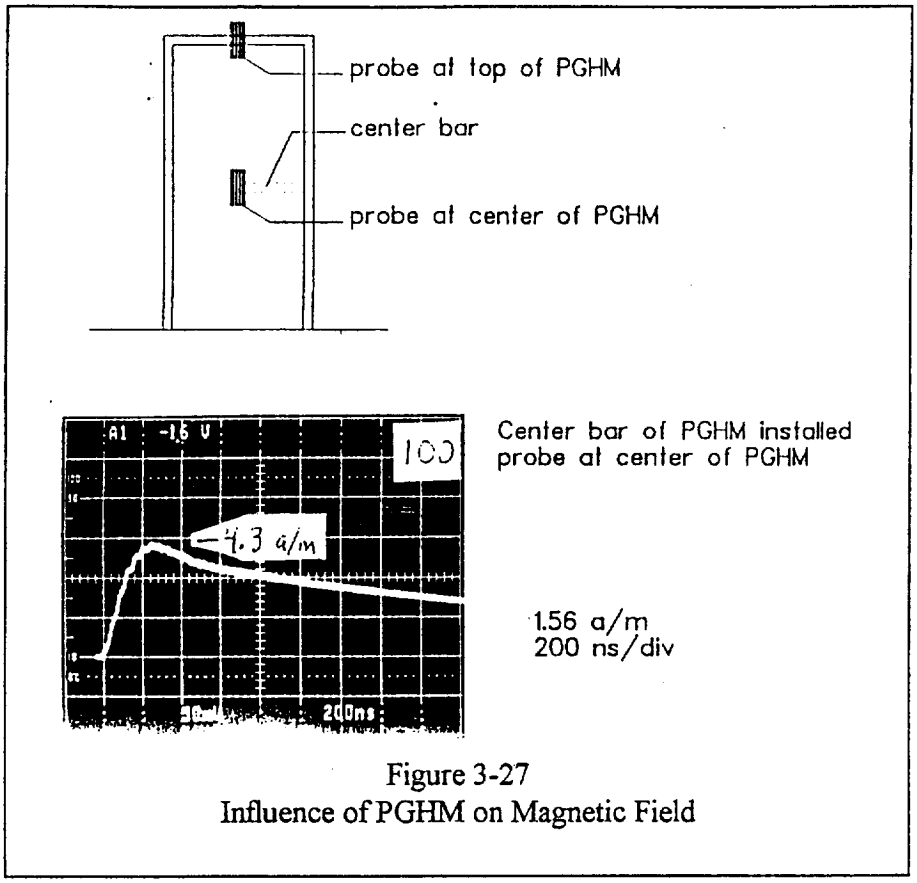

Figure 3-27
Influence of PGHM on Magnetic Field

Applicability of Results to PGHM at KSC: At KSC, the PGHM surrounds the payload on only three sides and does not provide short-circuited structure needed to make substantial reduction in the vertical magnetic field. Accordingly, it appears best to use the magnetic field in the empty PCR as the best measure of the field that might pose a threat to payloads.

3.5 Finite Difference, Time Domain (FDTD) Analysis

The physical model and FILAMENT did not provide information on electric fields, so the FDTD method of EMA was applied for that purpose. A summary of that work follows; more details are given in [7].

3.5.1 The FDTD Method

The method is based upon a finite difference, time domain solution of Maxwell's equations. The solution technique is explicit and accurate to second order in the time and spatial increments, which in these models corresponds to the three dimensional Cartesian coordinate increments as obtained by Merewether and Fisher [17].

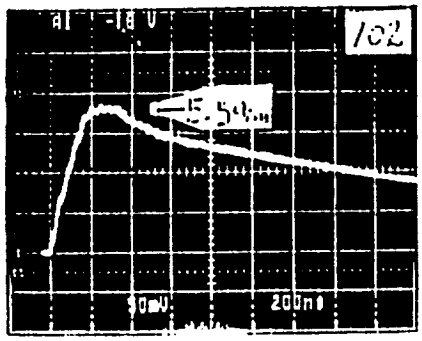

no PGHM

probe at top of PCR

1.56 A/m
200 ns/div

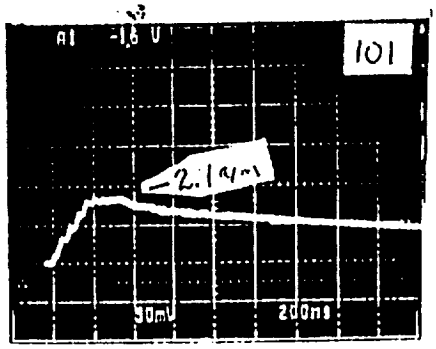

with PGHM centered on probe

1.56 A/m
200 ns/div

Field 10 inches from plane of open doors

Figure 3-28
Influence of PGHM on Magnetic Field

A finite problem space containing and surrounding the launch pad environment is broken up into rectangular cells. The fields calculated by Maxwell's Equations are equivalent to the average value of the electric and magnetic fields which occupy the cell. The number and size of the cells are determined by the size of the problem space, the available computer memory and speed of the computer, and the desired frequency bandwidth of the solution, which for lightning problems should be on the order of 20 MHz or somewhat greater. The cell size also dictates the time increment for time stepping the solution for the entire problem space. The time increment gets shorter for smaller cell sizes, hence there is a practical computational limit as to how small the cells can be made. The solutions described herein are obtained using a CRAY II computer. For these problems there are typically .1 to 1 million cells in the problem space. The cell sizes range from .25 to 1 meter, and the solutions as obtained by the CRAY II computer give about 1 microsecond of calculated lightning response for each approximately 10 to 30 minutes of CPU computing time. The fields, currents, and voltages are calculated for each cell in the problem space as functions of time for time steps on the order of 2 nanoseconds or somewhat less. Fields, currents, and voltages are saved at desired test point locations and written to computer files for use in display and analysis of data.

3.5.2 The Staggered Spatial Grid for Electric and Magnetic Fields

Each cell has a staggered spatial grid composed of the vector components of E and H, as shown in Figure 3-29. There are approximately one million cells in this case. The cell dimensions Δx, Δy, and Δz are 1 meter for the external launch pad coupling problem and 0.5 meter and 0.25 meter for the internal PCR coupling problem. The division into cells is shown in Figure 7-1, except that figure is for the case with the vehicle present and in this chapter we are considering the case with the PCR in the park position and no vehicle present. The field components in each cell are calculated numerically via the finite difference form of Maxwell's equations [7].

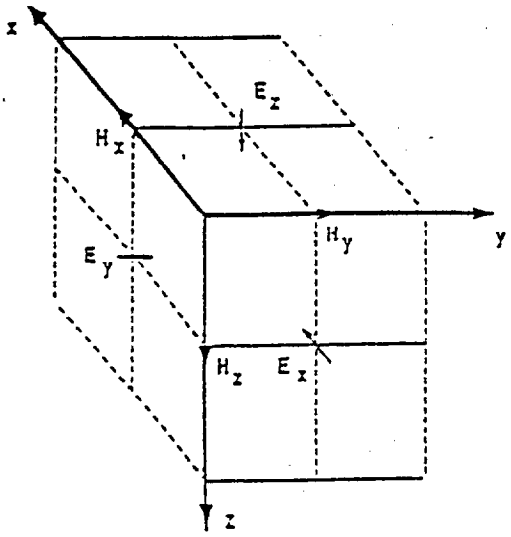

Figure 3-29
Staggered Spatial Grid

MAXWELL'S EQUATIONS

$$\mu\frac{\partial H}{\partial t} + \nabla\times E = M \qquad (3.1)$$

$$\epsilon\frac{\partial E}{\partial t} + \sigma E - \nabla\times H = -J \qquad (3.2)$$

$$\nabla\cdot E = \frac{\rho}{\epsilon} \qquad (3.3)$$

$$\nabla\cdot H = 0 \qquad (3.4)$$

The time step (increment) for this finite difference solution of Maxwell's equations is determined by the Courant criterion, which may be viewed as requiring that the speed of numerical propagation be greater than the fastest physical wave speed, in this case, the speed of light in air. Specifically, the Courant condition is:

$$\Delta t \le \frac{1}{c\sqrt{\frac{1}{\Delta x^2} + \frac{1}{\Delta y^2} + \frac{1}{\Delta z^2}}} \qquad (3.5)$$

where Δt is the time step, Δx, Δy, and Δz are the three Cartesian spatial increments and c is the speed of light in the air. For the external coupling problem, Δt is 1.8×10^{-9} sec; andfor the internal cycling problems, Δt is 0.45 to 0.9×10^{-9} sec. The smallest spatial increments control the time step, but the largest spatial increments determine the

bandwidth of the solution. The rule of thumb used is that the upper frequency limit of the solution, f_{max}, is given by

$$f_{max} = \frac{c}{8 \max(\Delta x, \Delta y, \Delta z)}. \tag{3.6}$$

For the launch pad model discussed here, this corresponds to an f_{max} of about 37 MHz, which is more than sufficient to describe the worst case lightning environment scenario.

Maxwell's curl equations (3.1), (3.2) form a system of hyperbolic partial differential equations which not only require initial conditions at all spatial locations, but also the boundary values of the electromagnetic field components (or their normal derivatives) at all times to obtain a well posed solution. These values must be supplied at the boundaries of the computational volume by an appropriate termination condition. The boundary condition employed was derived by Mur [18] and is essentially a first order integration along outgoing (with respect to the interior of the computational volume) characteristics. That is, the characteristic direction is chosen to be causal in time and along the outward normal to the bounding surface, which is a two dimensional Cartesian coordinate plane. Boundary conditions also must be imposed on metallic surfaces such as the door, interior wall, and metal equipment. The boundary condition on metal surfaces at least as large as a cell face is that the tangential electric fields at the surfaces of the metallic objects are set equal to zero each time step. Although this is correct only for perfect electrical conductors, on the time scale of interest it is an excellent approximation.

If the Maxwell divergence equations (3.3), (3.4) are satisfied at the original step, then the finite difference time development of the curl equations automatically satisfies the divergence equations at each time step. Thus, the static solution in the problem space satisfying (3.3) and (3.4) is tantamount to specifying the initial conditions for the problem. The simplest initial condition is to set $E = H = \rho = 0$ throughout the problem space. However, physically, a lightning discharge is normally a dynamic release of a static field buildup ("pre-polarization") between the cloud and ground. The launch pad structure will cause local static field enhancements from the pre-polarization between cloud and ground. The air dielectric breakdown will then usually occur at the point of highest electric field, e.g., the catenary cable mast or protrusion of the structure.

Thus, it is sometimes necessary to obtain the initial static solution for the facility under high pre-polarization field conditions in order to faithfully track the fields and currents of the resulting lightning strike. At other times, it may be sufficient to realize that under linear conditions and a given lightning or experimental current injection waveform, the final solution is the superposition of the initial static solution and a dynamic solution with the initial fields and charge density set at zero. This report will be primarily concerned with the dynamic part of the solution under zero initial conditions.

In addition to the appropriate boundary and initial conditions, the material properties at each cell location must be specified. These are the magnetic permeability, μ, in equation (3.1), the conductivity, σ, in equation (3.2), and the dielectric constant, ε, in equations

(3.2) and (3.3). If the material is homogeneous within the cell (for example, volumes of air, soil, concrete, etc.), then the appropriate values of μ, σ, and ε are included in the time advance equations for the cell in question.

If the material properties are inhomogeneous in each cell (detailed structure, etc.), then a decision must be made on how to represent the properties in each cell. In some cases, average properties are sufficient; and in other cases they are not. Special considerations are available for treating apertures in metal walls and also for pipes and thin wires (radii much smaller than cell dimensions) which may run throughout the problem space. These pipes and wires can be carriers of high current. Most facilities of interest, including the launch pad structure and PCR interior, have a large number of "thin wire" situations in the form of signal and power lines, rebar in reinforced concrete, pipes, plumbing, metal poles, lightning protection cables, underground return paths, etc. Methods for inserting "small" objects (e.g., wires, apertures) into the finite difference problem space are described in Section 3.5.4.

3.5.3 Lightning Excitation and Input Waveforms

The Maxwell Equations are driven by the current density, J, in equation (3.2), by including J in the cells which are assumed to contain the lightning channel. The location of the lightning channel and attach point to the catenary cable are inputs to the numerical problem. The time dependent waveform for J may be taken from measured catenary currents due to natural lightning events or from lightning simulation experiments. Theoretical statistical bounds to investigate upper limits for the lightning threat at given test point locations may be obtained from the NSTS standard waveforms [19]. Those waveforms, which are typically double exponential time dependent waveforms may be inserted directly for J in equation (3.2) and its numerical counterpart for an assumed lightning channel and attach point. The channel and attach points for natural lightning could be taken from video images of the lightning event coupled with current measurements from the CWLIS system to complete the description of lightning input excitation.

3.5.4 Thin Wires and Apertures

Thin wires and apertures can have strong influence on local fields and currents but have one or more physical dimensions which are much less than the established size of the underlying finite difference cell. In most of these instances, if the cell size were decreased to accommodate the size of these objects, extremely large numbers of cells would be necessary to fill the problem space, resulting in extreme, if not impossible use of computer time and memory. It is sometimes useful to use limited subgrids (smaller cell sizes) in some regions of the problem space in connection with these objects; however, this also increases the number of needed time steps for the total problem. In other cases described in this chapter, self-consistent approximation techniques are utilized which embed these smaller wires and apertures into the normal finite difference grid.

3.5.4.1 Thin Wires

The thin wires, cables, and rods are implemented in a self-consistent fashion by making use of the telegrapher's transmission line equations. Those equations , (3.6) and (3.7), are a one dimensional solution of Maxwell's equations in terms of currents, I_w, and voltages, V_w, on the wires, which are required to have diameters less than cell size (spatial increment). The per unit length inductances and capacitances are defined (3.8), (3.9) with respect to the cell size and the wire diameter, 2a.

One dimensional transmission line equations:

$$\frac{\partial V_w}{\partial Z} = -L_w \frac{\partial I_w(K)}{\partial t} - I_w R_w + Ez(i_w, j_w, k) \tag{3.6}$$

$$\frac{\partial I_w}{\partial Z} = -C_w \frac{\partial V_w}{\partial t} - G_w V_w \tag{3.7}$$

where L_w and C_w are the in-cell inductance and capacitance of the wire per unit length.

$$L_w = \frac{\mu l}{2\pi} \ln\left(\frac{\Delta y}{2a}\right) \tag{3.8}$$

$$C_w = \frac{2\pi a \epsilon E_r(a)}{V_w} = \frac{2\pi\epsilon}{\ln\left(\frac{\Delta y}{2a}\right)} \tag{3.9}$$

G_w is the in-cell conductance from the wire to the surrounding conductive medium

$$G_w = \frac{\sigma}{\epsilon} C_w \tag{3.10}$$

The wire resistance per unit length, R_w, is obtained by considering the surface conduction of the metal in question using the skin depth obtained for a frequency of 1 MHz. The resistance for pipes, iron rebar, etc., is normally on the order of 10^{-3} ohms/meter. In practice, the major results at early time seem to be relatively insensitive to variations of the resistance.

In the computer code, the wires and pipes are embedded into the staggered grid and are driven by the electric field component (see equation (3.6)) calculated by the three dimensional solution of Maxwell's equations. In order to maintain electrical charge conservation, this wire current must also be injected back into the driving electrical field component as a source current via Maxwell's equation (3.2). At the interconnections,

which are voltage nodes, Kirchoff's law is invoked. At locations where the wires are situated in the soil or concrete, the wires are in electrical contact with the soil or concrete with in-cell conductance given by G_w in equation (3.10). This is also true of the ground wires which are in contact with the soil.

Complex networks of thin wires (e.g., metal rebar mesh embedded in conducting concrete) are included in the model by a vectorized extension of the transmission line formalism. Vectorized average wire currents coincide with the electric field vectors in each cell and a corresponding average inductance and resistance is associated with each wire current vector.

At the boundaries of the problem space, some termination condition must be applied to both cable extensions and the power and signal lines and metal pipes entering the problem space. The boundary condition is applied at current nodes and is the equivalent of the Mur boundary condition applied to the magnetic fields.[18]

3.5.4.2 Apertures

The electromagnetic coupling through apertures is calculated using the method of algorithms for including the aperture polarizabilities into the framework of finite difference calculations using the Maxwell equations. According to Dalke, external electric and magnetic fields at an aperture generate electric and magnetic dipole currents at the center of the aperture. These currents are proportional to the electric and magnetic polarizabilities and, to a first approximation, the time derivatives of the electric and magnetic fields, respectively. They are converted into electro and magnetic current densities for the cell. The resulting currents are then the source currents which drive Maxwell's equations (3.1) and (3.2) being solved numerically for the interior space coupled by the aperture to the exterior lightning environment. The aperture is normally considered to be totally absorbing; that is, the generated fields are considered to have negligible effect on the magnitudes and waveforms of the external fields. Thus, the external fields act as drivers for the internal fields.

The polarizabilities depend on the vector components of the external field and the size and shape of the aperture. Values are calculated explicitly for the various applications and used to calculate the coupling. Results show the strongest magnetic coupling to be due to magnetic fields which are parallel to the long length of the slit. This may be viewed heuristically as parallel magnetic field lines "squeezing" through the slit. Another point of view is that the parallel magnetic field at the surface represents a linear surface current density which is normal to the long dimension of the slit. The normal current is then driven into the interior through the discontinuity of the slit. Visualization of these concepts is shown in Figure 3-30, and applicability to the PCR case is discussed in Section 3.3.3.

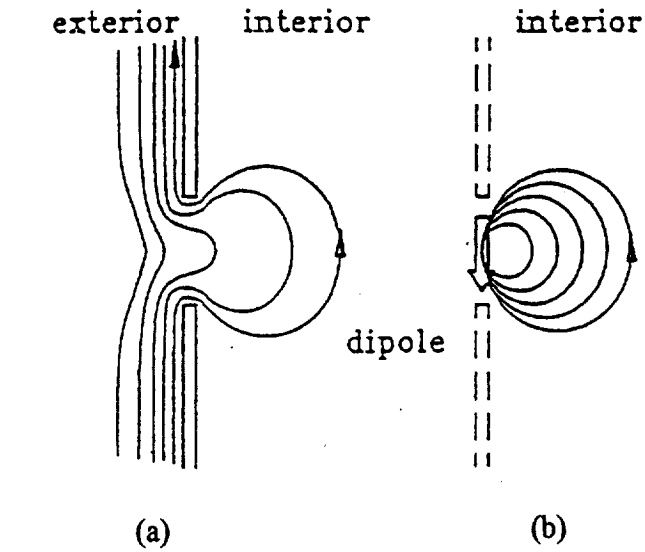

Figure 3-30
Development of Equivalent Magnetic Field Dipole [3]
(a) Actual magnetic field
(b) Equivalent dipole

3.5.5 FDTD Model of Case 1 - Scale Model Experiment

In order to compare results from an FDTD calculation and LTI results, the methods described above were used to construct a computer model of the scale model described in Section 3.1.2. Specifically, the computer model was related to Case 1 of the LTI study.

This case simulated a strike to the top of the FSS with the RSS rotated back 90 degrees from the launch pad toward the park position. The computer grid size is 1.66 inches in the x, y, and z directions. The time step is 0.075 nsec. The copper tubing representing the structural members of the launch pad structure was modeled assuming a perfect conductor for each of these members with metal ground planes at the floor, walls, and ceiling of the building as shown in Figure 3-2.

An effort was made to model the LTI Case 1 study as closely as possible in the context of the vectorized three dimensional finite difference solutions of Maxwell's equations.

A waveform designated as Waveform 1 (Figure 3-31) was intended to approximate the experimental waveform used in the LTI Case 1 study. The magnetic fields computed for the location of the PCR doors are shown in Figure 3-32 alongside the measured values from the physical model and the values computed by FILAMENT. The total FDTD calculated peak field is 2.2 A/m, which is about 15% less than the experimental and theoretical values obtained. Also, the amplitude of the computed superimposed oscillations (Figure 3-32) is smaller than found experimentally. Both of the above effects

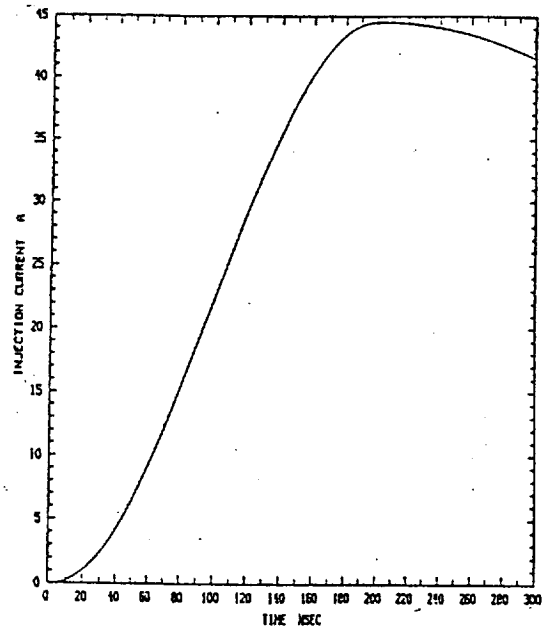

Figure 3-31
Waveform 1

are due to the fact that Waveform 1 is smoother than the experimental waveform and, even though the rise time is about the same, the experimental waveform appears to have some higher frequency content.

3.5.5.1 Effect of Waveform

The extent of oscillations in the results, both computed and experimental, is a function of the rise rate of the injected pulse. This is illustrated by applying three other waveforms , in addition to Waveform 1, in this computational method. These waveforms are shown in Figure 3-33, along with the resulting magnetic fields. The leading edge of waveforms 1, 2, and 3 is a sine squared waveshape having zero derivative at zero and peak times. Each waveform had a peak amplitude of 44.5 amperes. Rise times were 200,82, and 41 nsec, respectively. Waveform 1A is a double exponential waveform with the same zero to peak rise time as Waveform 1. It will be noted from these curves that an increasing rise rate results in an increasing magnitude of oscillations and, thereby, an increasing magnitude of the peak magnetic field. Two frequencies are evident in the FDTD results: 7.7 MHz and 14 MHz, the second perhaps being just a harmonic of the first. Both frequencies are evident in the experimental traces. Differences in the amplitudes of these two frequencies between calculation and experiment may be due to: (1) the input waveform, (2) the modeling details, (3) the dynamic response of the field sensor, or perhaps some combination of those factors.

The rate of change of magnetic field and the electric field also increase with increasing rise rate of the input signal as shown by Figure 3-34.

3.5.6 The Full Scale Case

3.5.6.1 External

The maximum magnetic field outside the PCR doors for the NSTS 07636 stroke (component A) is calculated to be 140 A/m.

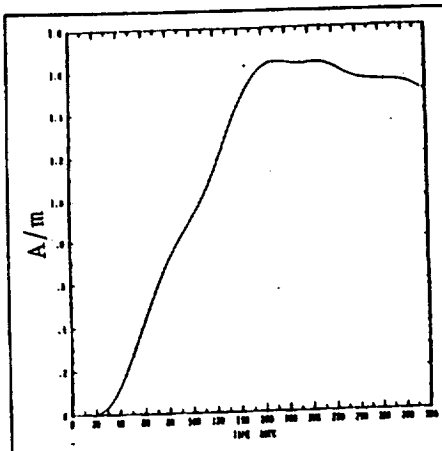

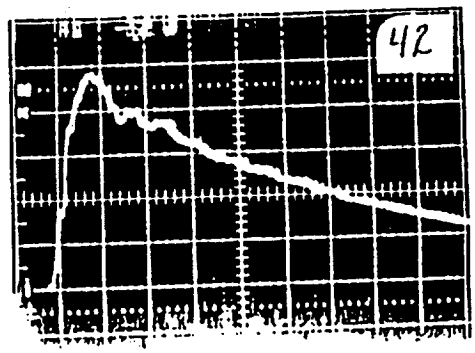

Field left to right, H_y

LTI:
1.49 A/m (meas)
1.82 A/m (calc)

EMA: 1.63 A/m

200 ns/div

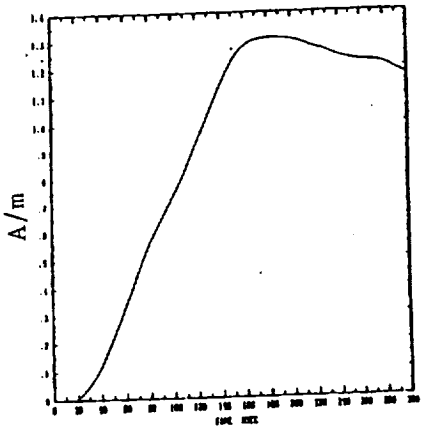

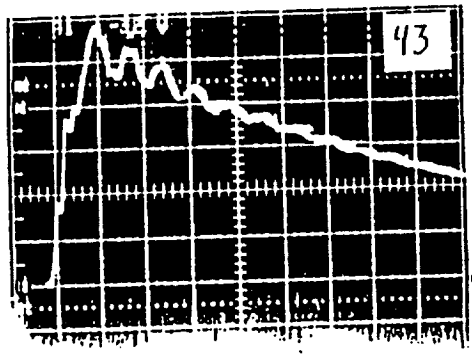

Field top to bottom, H_z

LTI:
1.74 A/m (meas)
1.36 A/m (calc)

EMA: 1.30 A/m

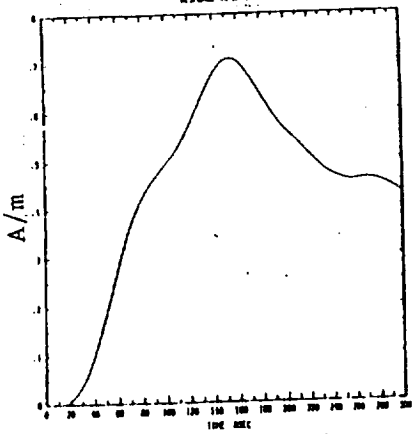

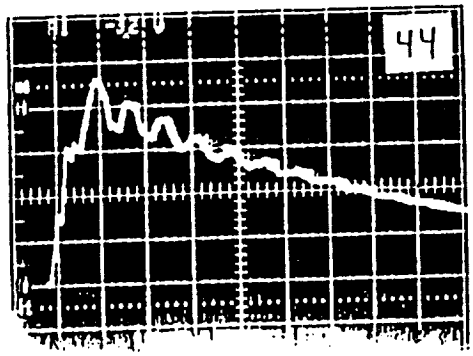

Field front to back, H_x

LTI:
1.40 A/m (meas)
1.08 A/m (calc)

EMA: 0.71 A/m

LTI:
Total = 2.68 A/m (meas)
Total = 2.52 A/m (calc)
EMA:
Total: 2.20 A/m

EMA LTI

Figure 3-32
Magnetic Field at Location of PCR Doors
(PCR not installed)

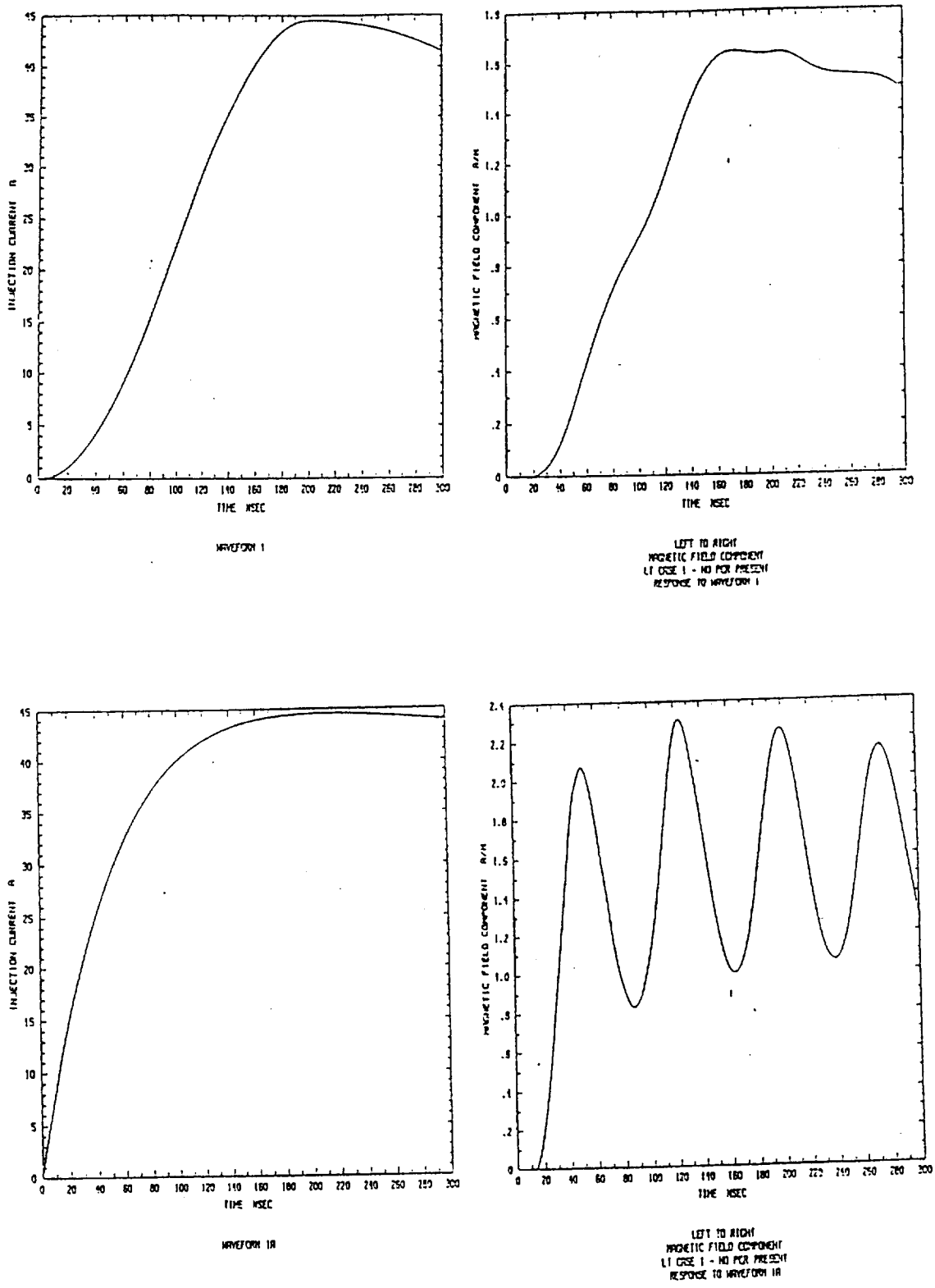

Figure 3-33
Effect of Rise Rate

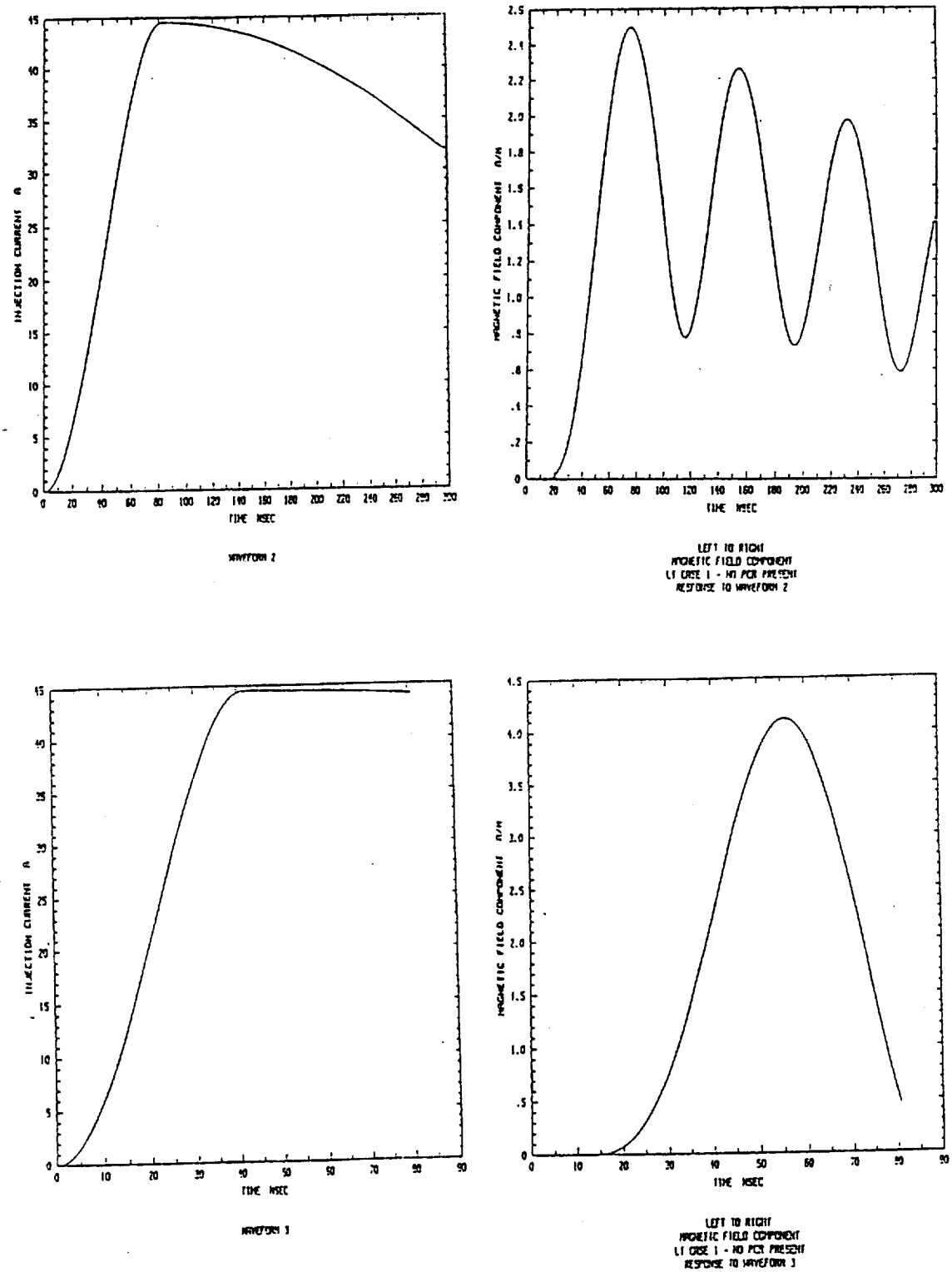

Figure 3-33 (Continued)
Effect of Rise Rate

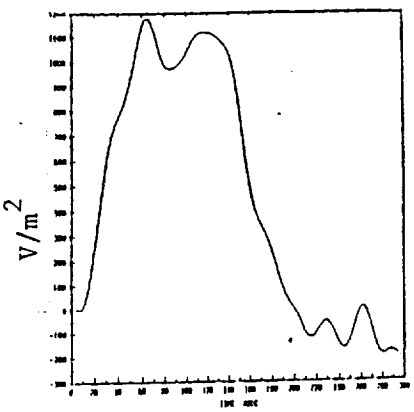

$\dot{B}_Y$
Response to Waveform 1

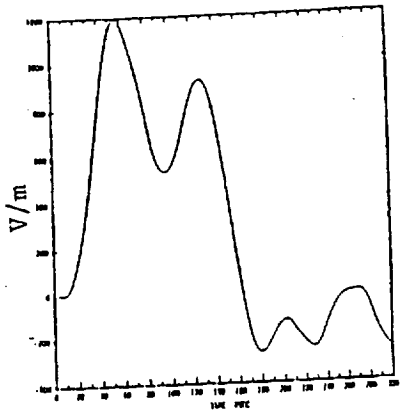

E_X
Response to Waveform 1

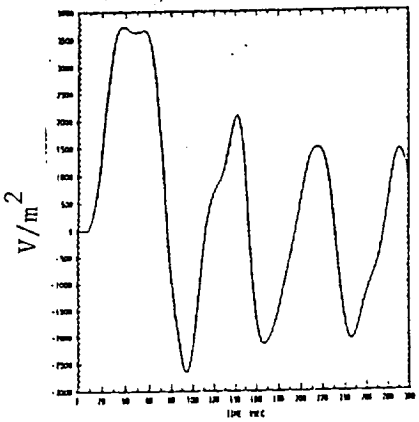

$\dot{B}_Y$
Response to Waveform 2

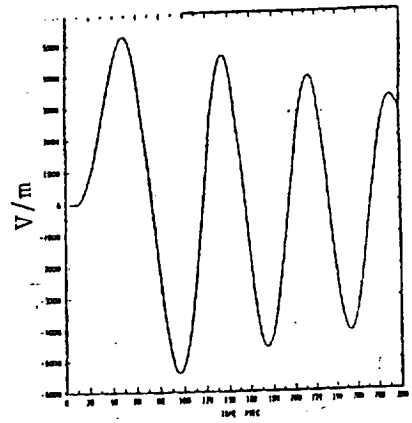

E_X
Response to Waveform 2

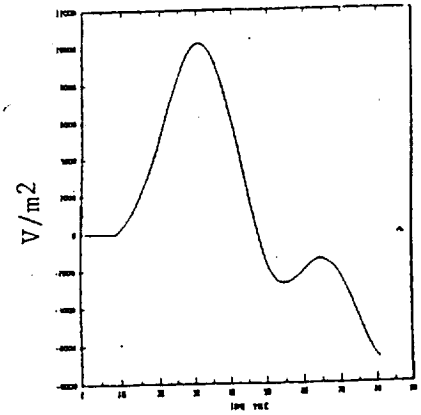

$\dot{B}_Y$
Response to Waveform 3

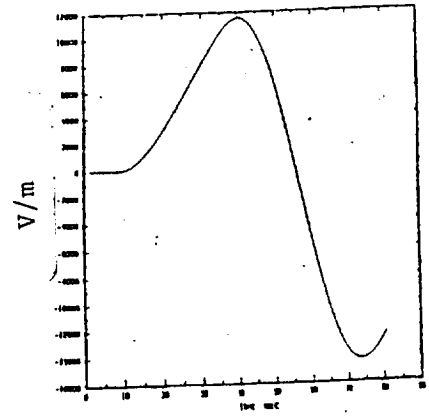

E_X
Response to Waveform 3

Figure 3-34
Effect of Rise Rate
60 m (200ft) level
LTI Case 1, PCR not present

For higher rise rates, the values of H and E are higher.

3.6 Conclusions

When field values are quoted in this section, they are the values scaled to a 200 KA lightning stroke as specified in [19]. A summary of voltages, currents, and magnetic field levels for various cases is given in Table 3-1. It will be noted that more attention is given in this document to magnetic fields than to electric fields; that is because electric fields are more easily shielded and, therefore, do not present as serious a problem as do magnetic fields.

3.6.1 Accuracy and Utility of the Computer Programs

The FILAMENT program seems to predict currents and magnetic fields around the model reasonably well. It is useful in predicting the magnetic field outside the PCR but is not well adapted to determining the field internal to a shielded room such as the PCR.

The FDTD program, when considering the configuration corresponding to the LTI Case 1, gave results consistent with the measured values and the FILAMENT values. More will be seen about FDTD results later in this report.

3.6.2 Magnetic Fields

External to the PCR: The magnetic fields external to the PCR have been calculated and measured on the model by LTI to be in the neighborhood of 500 A/m for a stroke to the FSS and 120 - 160 A/m calculated, 60 A/m measured, for a stroke to the mast. EMA calculated 140 A/m for a stroke to the mast.

Internal to the PCR: LTI extrapolation of model-measured values gives 12 A/m. EMA calculation gives 0.5 - 1.6 A/m.

It should be pointed out that magnetic field gradients are large near metal surfaces. Factors of two in the magnetic field can occur over relatively small distances.

Orientation and Waveshape: The magnetic field in the PCR seems to be predominantly vertical. The waveshape seems to be about the same as that of the external lightning current.

3.6.3 Importance of Ground Wires between PCR and Orbiter

The ground wires of most importance would be those closest to people likely to be in contact with both the PCR and the Orbiter. Connecting only the bottom ground wire would appear acceptable. Eliminating all the ground connections would not be advisable.

As long as there are ground wires between the PCR and the Orbiter, it is unlikely that a lightning flash to the catenary wire would cause enough voltage to present a hazard to personnel inside the PCR (as contrasted with those at the PCR - Orbiter interface). There could be enough induced voltage to cause a hazard to electrical and electronic equipment, either PCR or payload equipment. Methods of controlling such voltages (shields on wires, surge protectors, interconnecting ground wires) are available, but a study and discussion of such protection is beyond the scope of this study.

3.6.4 Shielding Effectiveness of the PCR

Table 4-3 indicates a shielding effectiveness of 36-40 dB for magnetic fields (external/internal). This is within the range of values found earlier for radio signals, when the shielding was found to vary strongly with frequency [16].

3.6.5 PCR LIVIS Sensor

An effective sensor for monitoring magnetic fields could be built from a length of wire, either stretched vertically along a corner or stretched horizontally along a wall. One end would be grounded to the wall of the PCR and the other end connected to recording instruments. The tests did not show a clear advantage on one orientation over the other, although the horizontal wire would seem, on theoretical grounds, to be preferable.

4. THE SIMULATOR TEST

4.1 The Configuration

The second phase of the study was a full-geometry test using a lightning simulator[1] to apply reduced-magnitude lightning-type pulses to the pad protective system. The test configuration is shown in Figure 2-1. The Rotating Service Structure (RSS) was in the Park position.

Normally, each ground terminal of the catenary wires is connected directly to ground and the current to ground is measured by a pulse current transformer (Pearson coil). The current values and waveform data are conducted to recording instruments in a room (PTCR) beneath the launch pad. This system is known as the Catenary Wire Lightning Instrumentation System (CWLIS) and is used to record data on lightning strikes to the catenary wire system. For this test, the CWLIS connection at the north ground terminal was replaced by the simulator output lead (Figure 4-1).

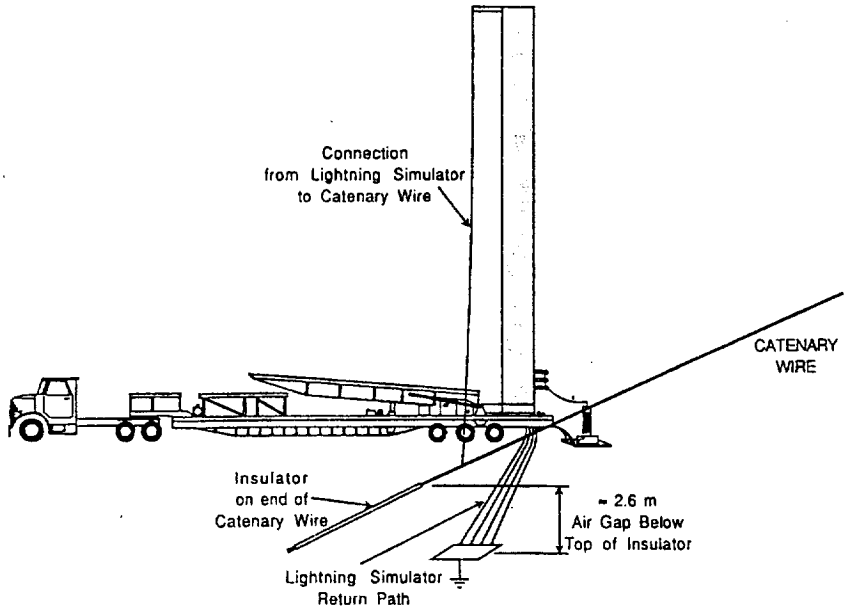

Figure 4-1. Simulator--Catenary Wire Configuration

4.2 The Simulator[1]

The simulator is a Marx generator consisting of two banks of 76 capacitors each (Figure 4-2). In a Marx generator, the capacitors are charged in parallel and discharged in series. The discharge is produced by using a trigger generator (a small Marx generator) to fire the three low gaps in each column.

[1]On loan from Wright-Patterson Air Force Base

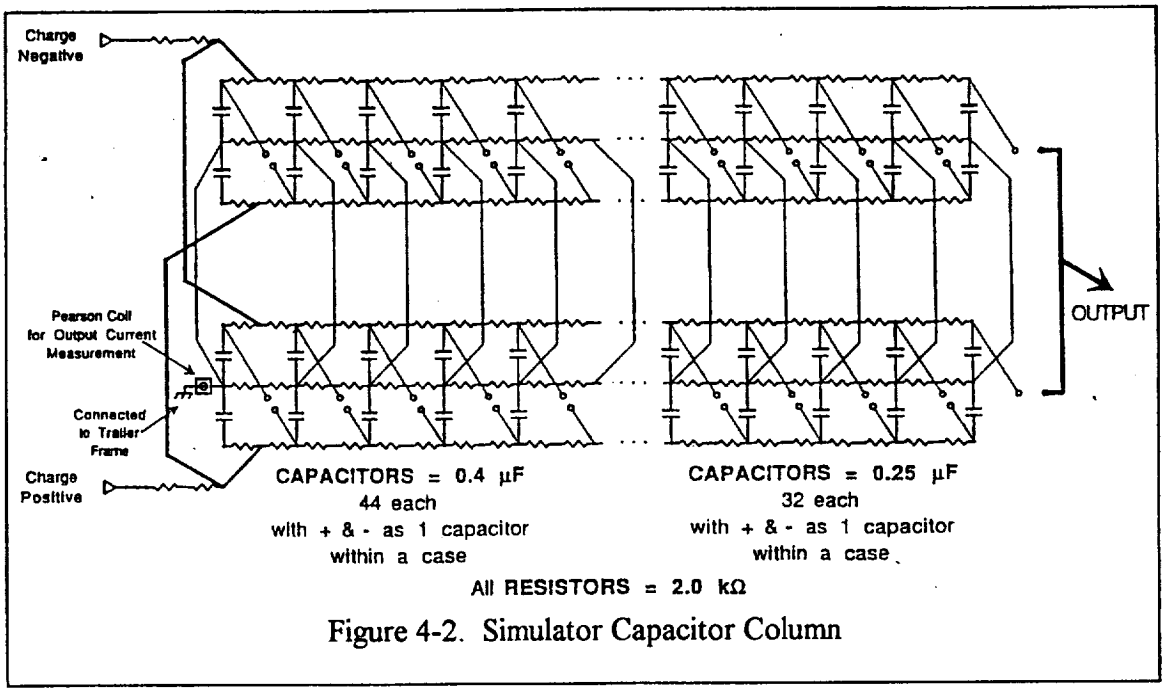

Figure 4-2. Simulator Capacitor Column

Each capacitor was charged to 67 kV, giving an output potential for the simulator of 4.7 MV. The simulator has been measured to have an inductance of 143 μH, and the inductance of the catenary wires was taken as 650 μH (based on 1 μH/m), giving a circuit inductance of 793 μH. This predicts a current pulse of 16.6 kA.

4.3 The Measurement System

4.3.1 Catenary Wire Current

Catenary wire current was measured at two points: (1) a Pearson coil on the input from ground to the simulator (Figure 4-2) and (2) a Pearson coil in the CWLIS system at the south terminal of the catenary wire.

4.3.2 Magnetic Fields

Magnetic fields were measured at several locations external and internal to the PCR, as shown in Figure 4-3, and on the roof of the PCR.

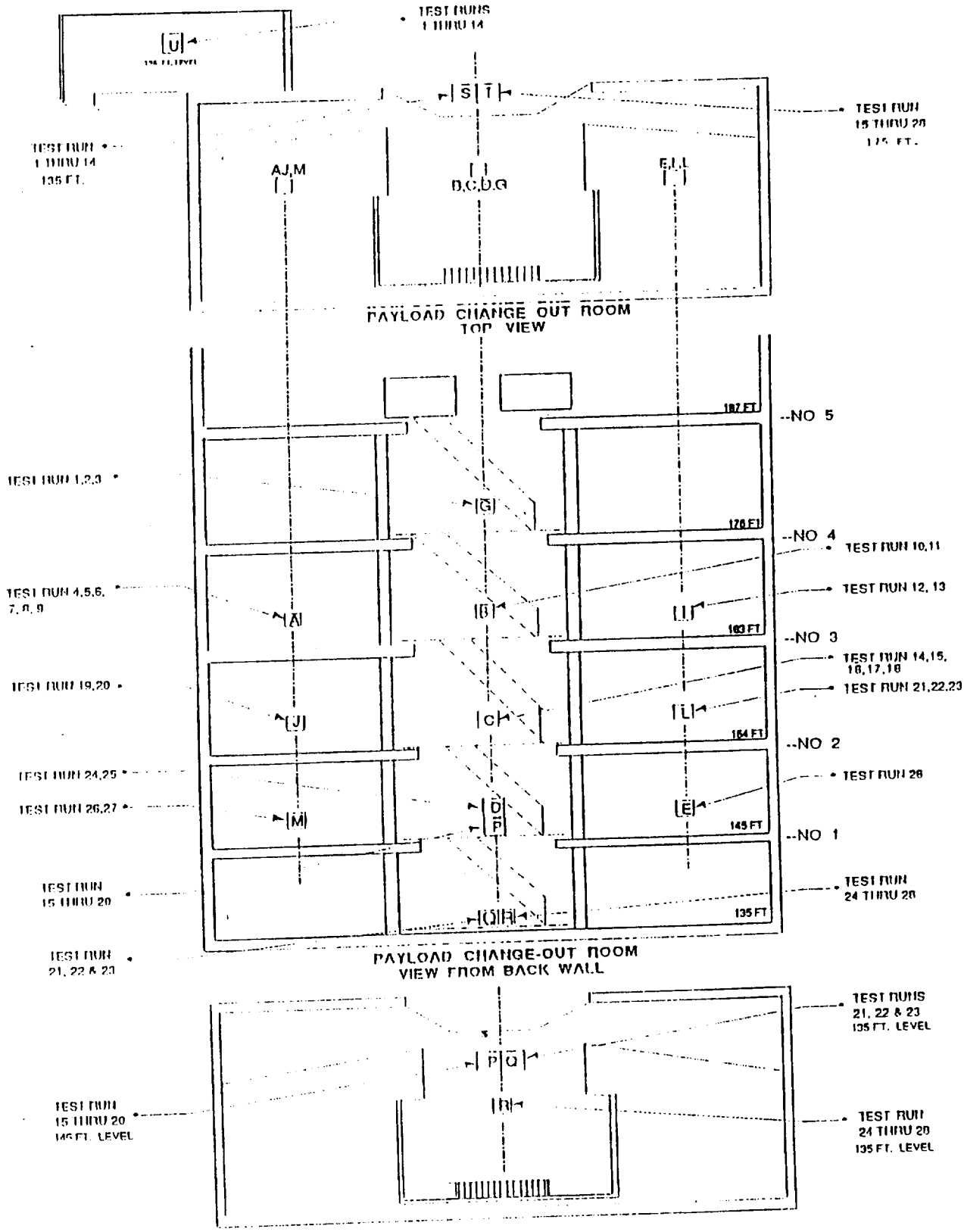

Figure 4-3. Measurement Locations

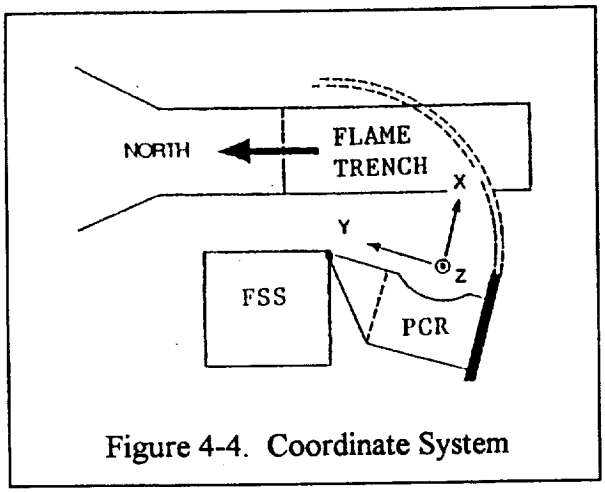

Figure 4-4. Coordinate System

Where field directions are given in terms of coordinate directions, the coordinate system shown in Figure 4-4 applies. The coordinates are different for the two RSS locations--park and mate--but the coordinate system remains constant with respect to the PCR.

4.3.2.1. EG&G Sensors

The sensors used at locations U, P,Q, and R were manufactured by the EG&G Corporation. They consisted of three Model MGL-2a sensors measuring dH/dt with a frequency response (to -3 db) > 300 MHz.

4.3.2.2 LTI Sensors

The sensors used at locations S, T, and the remaining interior locations were designed and constructed by Lightning Technologies, Inc. (LTI). At locations S and T, the sensors were suspended from a facility hoist so that they were located in front of the closed PCR doors at the levels indicated in Figure 4-3, where the elevations are listed relative to sea level, the pad apron being at an elevation of 48 feet. At the interior locations, the sensors were moved from location to location, as shown in Figure 4-3.

The LTI magnetic field sensors were shielded loop antennas having an output proportional more or less to the rate of change of magnetic field. They were used in conjunction with an electronic integrator to get an overall response proportional to the magnetic field. Two outputs were provided: one described as a dH/dt, or H-dot response, and one described as the H-field response. The whole system was optimized, however, to the measurement of magnetic field; and, intentionally, the antennas themselves were made partially self-integrating. As a consequence, the dH/dt response was only approximate.

The sensors were six-turn shielded loops enclosing an area of 0.153 square meters and having a self inductance of 46.7 μH. The outputs were connected to the processing amplifier through shielded twisted pair cables having an inductance of 5.7 μH and terminated in 102 ohms. The physical configuration of the LTI antennas is shown in Figure 4-5.

Derivative response: By virtue of the inductance of the antennas and connecting cables, 52.7 μH total, and the102 ohm terminating resistor, the voltage developed at the input to the processing amplifier was partially self-integrated with a L/R time constant of 0.51 μs.

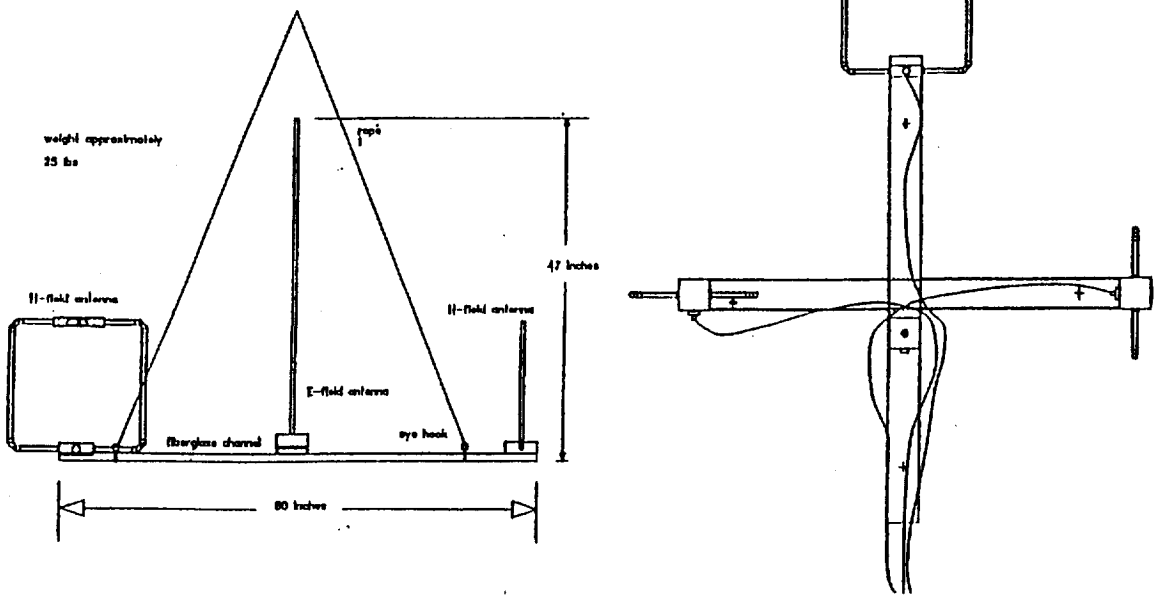

Side View Plan View

Figure 4-5. Antenna Assembly

As a consequence, the derivative response was only approximate. Transient magnetic fields having a duration small compared to 0.51 μs produced an output proportional to the magnetic field, not the derivative field. Only for transient fields having a duration long compared to 0.51 μs were the outputs proportional to dH/dt. The break frequency corresponding to 0.51 μs is 1.96×10^6 radians/second or 312 kHz. For frequencies substantially above 312 kHz, the output from the antennas would be proportional to H. For frequencies substantially below 312 kHz, the output would be proportional to dH/dt. This self-integrating feature of the antennas was provided intentionally, since the primary aim was to measure the magnetic field, not its derivative.

Magnetic field response: The outputs from the loop antennas were integrated in an electronic integrator compensated for the partial self-integration provided by the inductance and resistance of the antennas and connecting cable (Figure 4-6). The result is that the magnetic field response did faithfully track the incident magnetic field.

Circuit and calibration details are given in [14]. Performance as a function of frequency is shown in Figure 4-7.

4.3.2.3 LIVIS

Loop antennas were constructed and used by Kennedy Space Center (KSC) personnel [19] to provide data to be used in determining an appropriate location for a new PCR

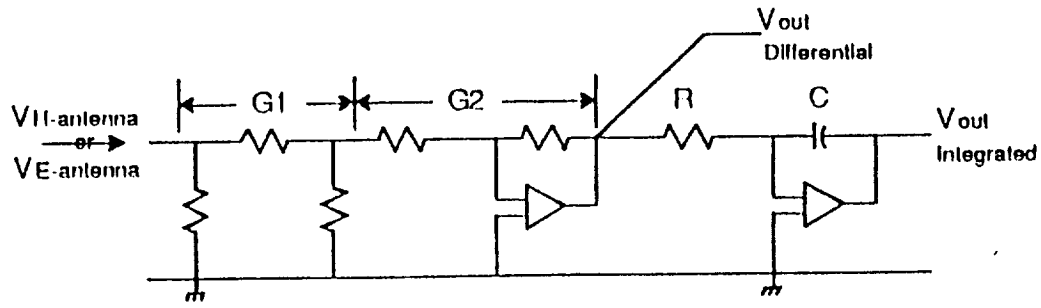

Figure 4-6
Basic Circuit for Differential and Integral Output

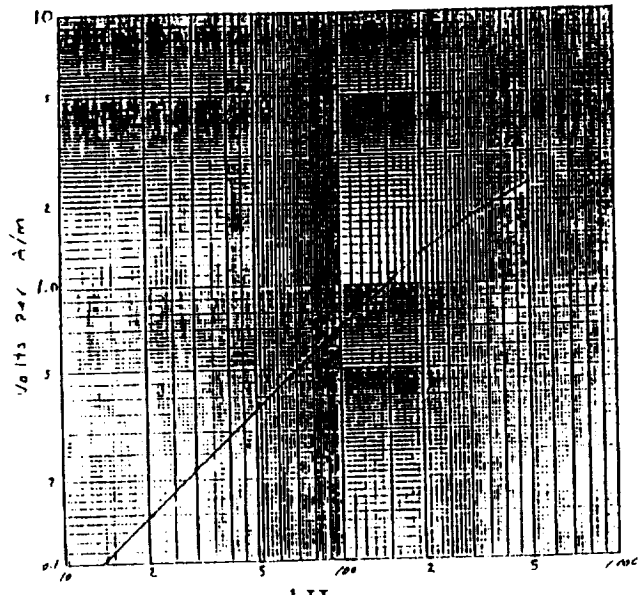

Figure 4-7
Measured Response of H-Field Antenna vs Frequency

sensor which is part of the Lightning Induced Voltage Instrumentation System (LIVIS), a system designed to measure lightning effects on the Orbiter. This antenna is shown in Figure 4-8. The loop antennas were composed of a single turn of 16 gauge copper wire held in the form of a 36" diameter loop by an aluminum frame. The frame was fabricated from aluminum tubing welded to an aluminum box which was in turn welded to an aluminum base plate. A phenolic spacer separated the two frame halves to prevent the frame from acting as a loop and generating its own field. The copper antenna was terminated in a threaded twin-ax connector.

External: Three of these antennas were on the PCR roof measuring the three components of the magnetic field.

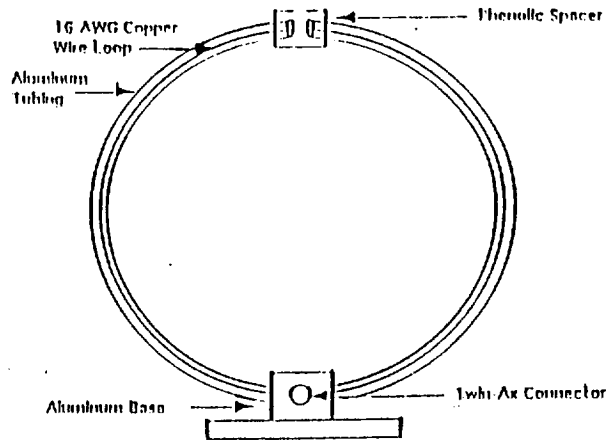

Figure 4-8
Rooftop Antenna

Internal: Two of the three interior antennas were also of the type shown in Figure 4-8. Measurements were made at locations A, B, D, G, J, and a point 30 feet directly above A (Figure 45-3).

A "longwire antenna" was suspended with tie wraps wherever it was convenient to do so. The antenna was a 16 AWG stranded copper wire of the type commonly used to wire industrial control circuits. One end was connected to a ground bus on the 5th level platform, and the other was tied to a conduit near the floor of the room, giving a length of approximately 40 feet. The impedance between the conduit and the ground bus was found to be negligible; thus the structural members of the PCR formed one side of a roughly rectangular loop.

4.3.3 Electric Fields

4.3.3.1 EG&G Sensors

Two EG&G electric field sensors were available. They are model HSD-2R, hollow spherical dipole sensor which measures dE/dt and has a frequency response (-3 dB point) 45 MHz with a 10% to 90% output rise time of less than 7.4 nsec.

4.3.3.2 LTI Sensors

Along with each group of three LTI magnetic field sensors, there was a single rod type electric field antenna, constructed as sketched in Figure 4-9. The antenna can be viewed as a capacitive voltage divider having a high voltage arm composed of a 37 pF capacitor and a low voltage arm composed of a 4,340 pF capacitor loaded with a terminating resistor of 51 ohms, giving a time constant of about 0.22 μs. The equivalent circuit is shown in Figure 4-10. The antenna thus operated as a sensor of rate of change of electric field for transients having a duration substantially greater than 0.22 μs and as a sensor of electric field for transients having a duration substantially shorter than 0.22 μs. The antenna was connected to a differential amplifier and a compensated integrator. Measured performance is shown by Figure 4-11. As it turned out, there was no evidence of any long duration electric field in the PCR; and the output from the integrator was never used

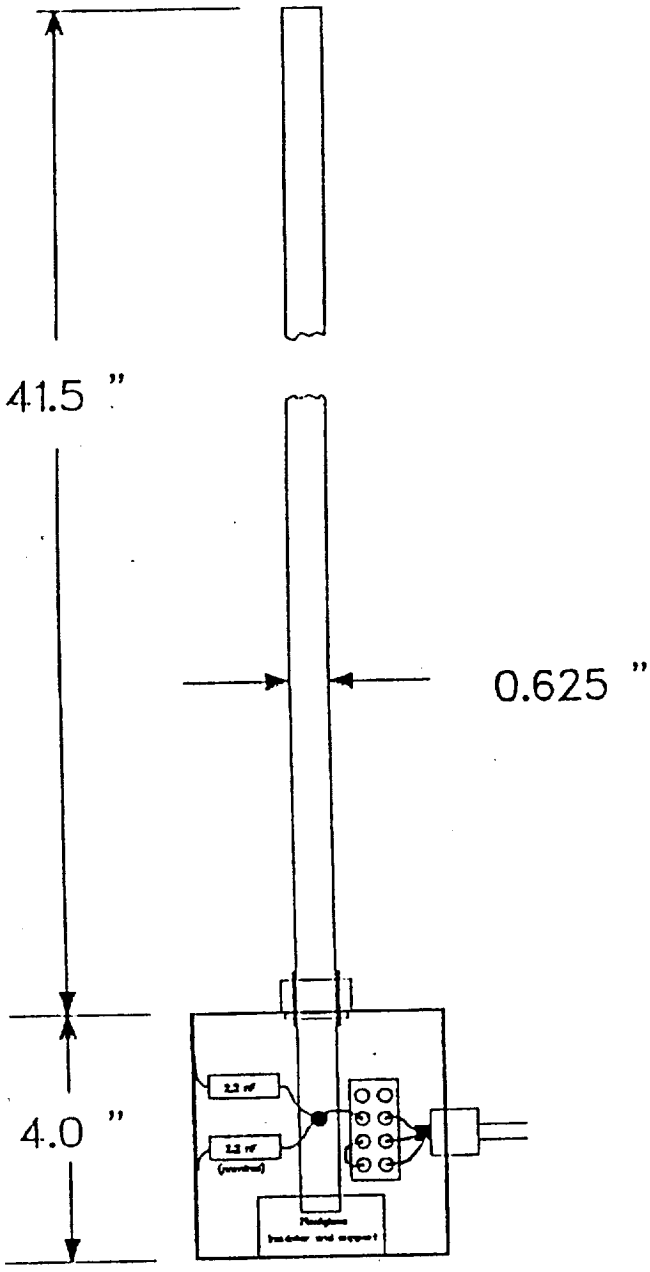

Figure 4-9
Construction Details of E-Field Antenna

4.3.3.3 LIVIS

The LIVIS group did not measure electric fields.

4.3.4 Data Acquisition and Processing

4.3.4.1 I-NET Data Acquisition and Processing

Data from the EG&G sensors and the external LTI sensors were transmitted by optical fibers to the instrumentation van on the pad apron, where they were digitized and recorded for further processing (integration, frequency spectra plotting, waveform plotting) in the laboratory. This system was assembled and operated by I-NET personnel.

Two different types of waveform digitizing and recording systems were utilized for the test; and measurements were recorded at rates of either 20 or 100 megasamples per second, depending upon the system used. All measurements were transferred from the sensors to the data acquistion system by means of fiber optic cables, with a 150 MHz bandwidth, to avoid coupling of electromagnetic fields into the analog data of interest. A NanoFast fiber optic transmitter and receiver combination transferred the analog sensor outputs to optical signals for transmission to the data acquisition trailer. The signal was then converted back to an electrical signal for input to the digitizers. The fiber optic receivers also allowed for various attenuations and gains to be applied to the resulting signals in order to apply an

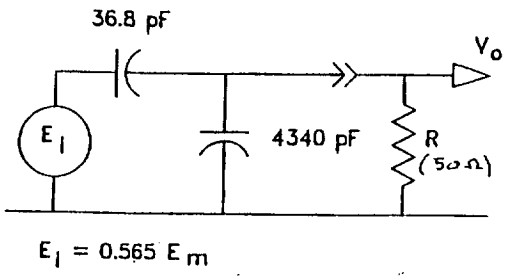

Figure 4-10
Equivalent Circuit for E-Field Antenna

appropriate signal level to the digitizers. Eight channels were recorded at 20 megasamples per second by a Hewlett Packard 70000 Digitizing System with Model 70700A digitizer plug-in modules. The remaining two channels were recorded at 100 megasamples per second by a Tektronix RTD Digitizing Waveform Recorder. A diagram of the system is shown by Figure 4-12. Both digitizing systems were controlled by a National Instruments labVIEW software program operated on a MacIntosh computer. The program and computer allowed for quick set-ups and configuration changes of all digitizers and allowed for large amounts of data to be stored for later analysis. As seen in the block diagram, communication between the computer and the digitizers was by way of an IEEE-488 bus. To synchronize the recording of measurements, each digitizer was triggered by the current pulse at the simulator.

4.3.4.2 LTI Data Recording

Data taken by LTI in the PCR were recorded on a Tektronix TDS460 digital sampling oscilloscope. This instrument provides for four separate inputs, each of which can be sampled as fast as 100 times per μs with 8-bit resolution. The instrument has an analog bandwidth of up to 350 MHz, though during all these tests the input bandwidth was limited to 20 MHz. The instrument provides the capability of storing as many as 15,000 points for each channel, though during these tests only 5000 points were normally stored. It also provides pre-trigger capability, as do most modern digital storage oscilloscopes.

For most of the tests, the instrument was triggered on the output from the electric field antenna. After some learning as to the best sensitivities for data and trigger, the instrument performed quite reliably.

In operation, the recording process consisted of first acquiring the four channels of data, then storing the data from each channel in a memory. After that, each record was plotted out on appropriate time and amplitude scales. Generally, plots to several time scales were made of each record.

The instrument has the capability of downloading the stored data through a GPIB interface to a controlling computer, but that capability was not used during these tests.

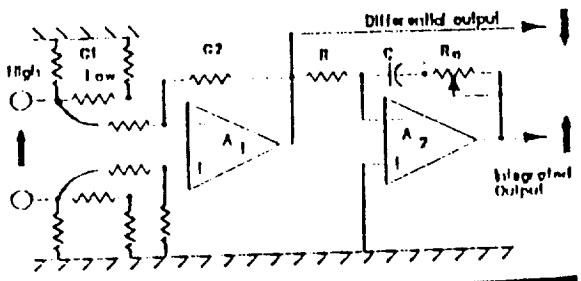

Configuration

G1 = 1.0
G2 = 1.0

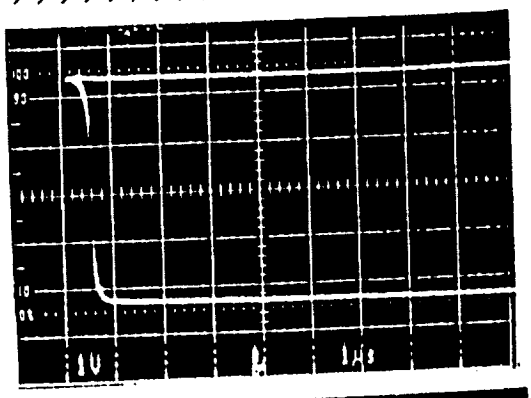

Injected Voltage

100 V/div
1.0 us/div

465 Volts peak

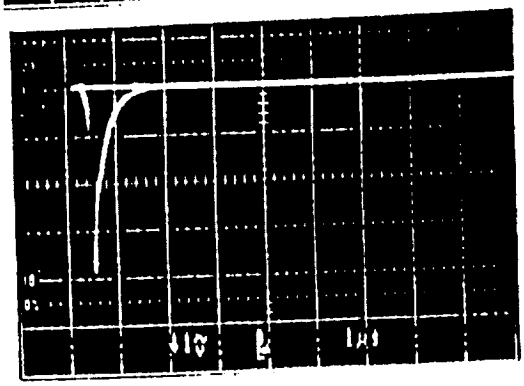

Differential Output

1.0 V/div
1.0 us/div

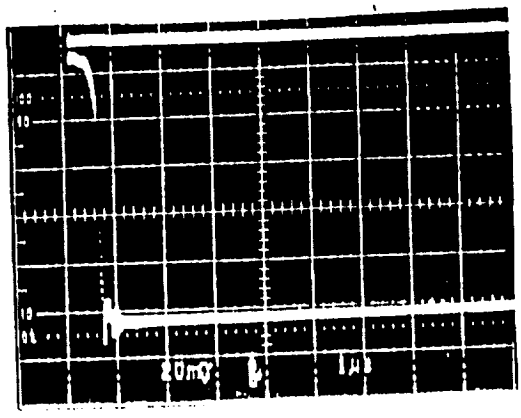

Integrated Output

0.02 V/div
1.0 us/div

Figure 4-11.
Response of E-Field Antenna to Voltage Input
(High sensitivity on input amplifier - 50 pF coupling capacitor)

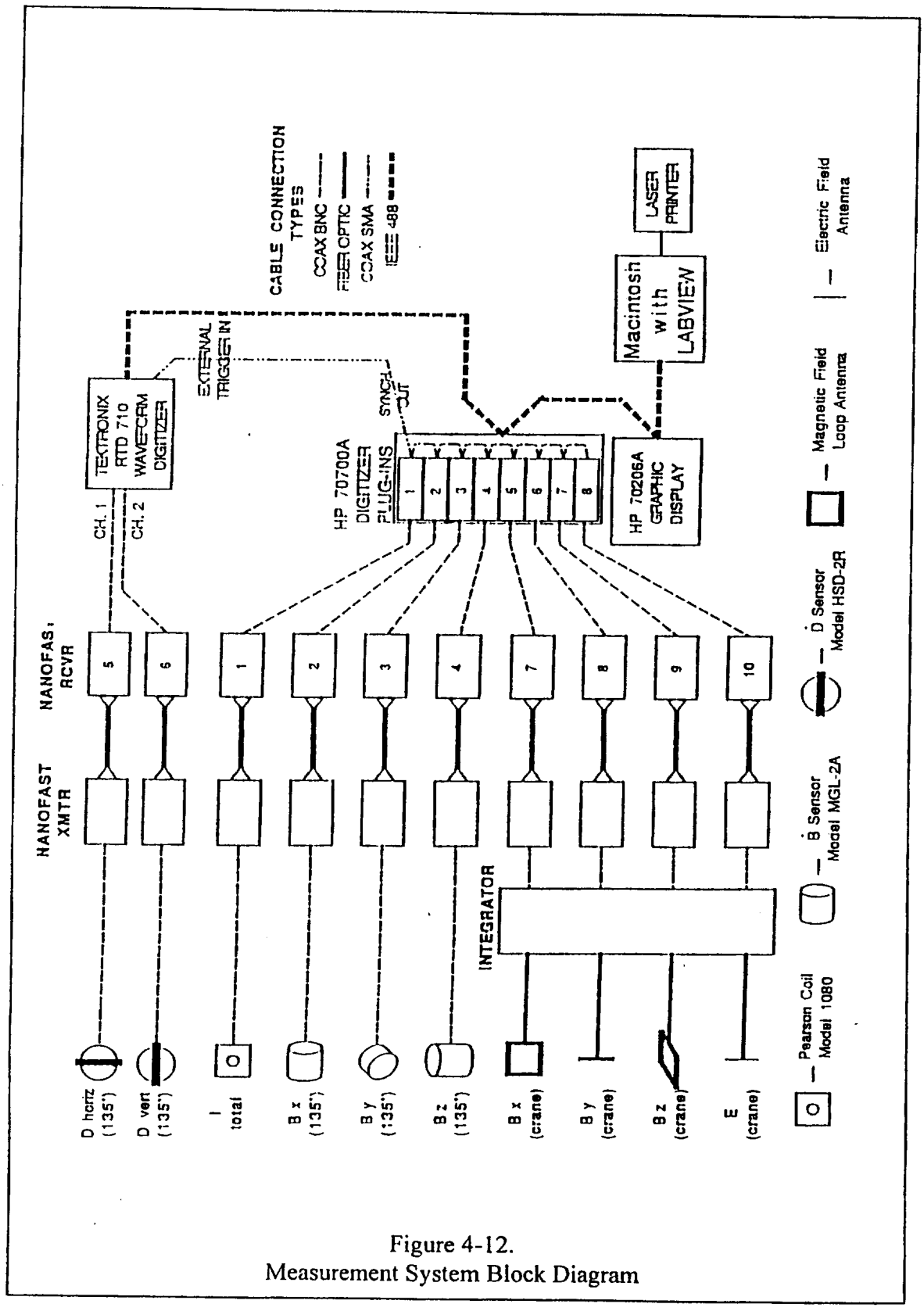

Figure 4-12.
Measurement System Block Diagram

4.3.4.3 LIVIS Data Recording

External: The two ends of each antenna were terminated in threaded twin-ax conductors; and three 124 ohm twin-ax cables were run to room 208 in the Pad Terminal Connection Room (PTCR), beneath the pad, where they interfaced through impedance matching transformers to sampling devices. The length of the cable run made it impractical to run special cables from the roof of the PCR to room 208 of the PTCR, so existing wideband

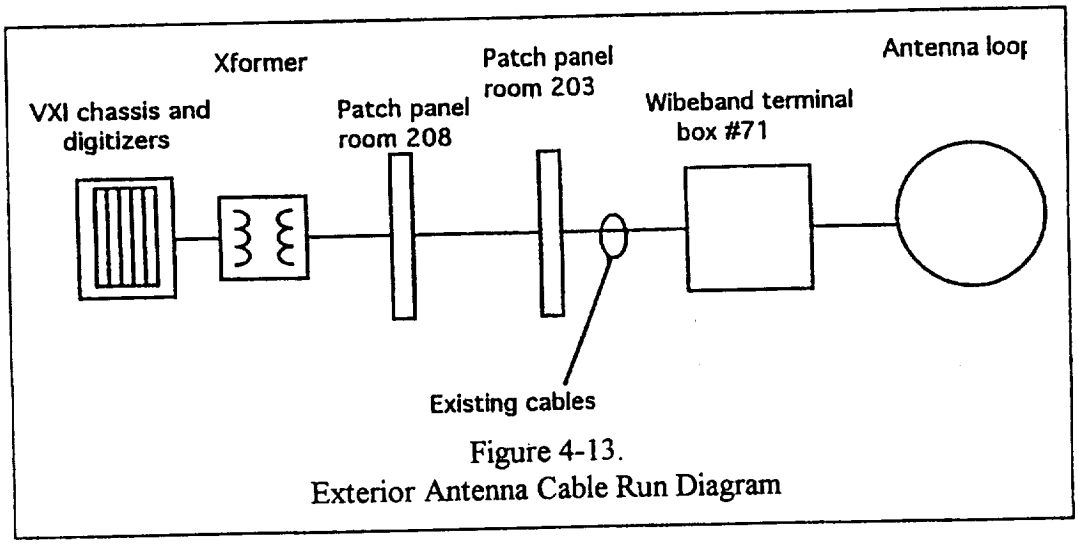

Figure 4-13.
Exterior Antenna Cable Run Diagram

cables were used. The configuration is shown in Figure 4-13.The cables labeled "Existing cables" in that figure are not the cables used previously in the permanent system.

A shorting plug (to test cable pickup) was located at the output of the antenna loop.

Internal: Initially, data were transmitted to the PTCR and processed and recorded there. Later, the processing and recording equipment was transferred to the PCR, eliminating the long line. As the PCR LIVIS hardware was now in close proximity to the test equipment, cables were merely disconnected and run through a matching transformer into the digitizers. This latter arrangement gave better results, and the results quoted herein were obtained from that configuration.

System Controller: The analog-to-digital conversion was performed by VXI Technology digitizers; these are VXI devices mounted in a VXI chassis controlled by a Hewlett Packard controller. Software for the system was written in HP BASIC.
A digitizer card contains two data acquisition channels, each possessing its own A/D converter and storage buffer. Each channel has separately configurable range and impedance controls. The sampling rates for the two channels are not independent, however.

The data acquisition trigger was provided by CWLIS. The digitizers were configured in a master-slave triggering mode whereby all digitizers began acquisition simultaneously after the master digitizer received a trigger signal from the CWLIS.

The system contained five two-channel digitizers; setup parameters for all digitizers are given in Table 4-1.

Table 4-1
Set up Parameters for Digitizers

Sampling Rate	20 MHz
Input Impedance	1 Mohm
Voltage Range	Variable (0.1,0.5. 1.2,5,10, or 50 volts)

4.4 Data

4.4.1 Catenary Wire Current

Curves from the two Pearson coils are shown in Figure 4-14.

The potential applied for the test was 4.7±0.1 MV, applied to the wire at a point 3 m above the ground. This potential proved to be a little too high, and an arc formed betwen the catenary wire (about two feet down an insulator) and ground. This arc diverted part of the generator curent away from the catenary wire. Changing the output potential would have required changing the spark gaps, a time-consuming job; so, due to time constraints, it was decided to proceed with the test, accepting the current drain and effect of the arcing on the waveform. The effect on the waveshape is shown by Figure 4-14(A), with point A indicating the time the arc formed. Prior to time A, the current shown in Figure 4-14 flowed into the catenary wire; after time A, the catenary was shorted to ground through the arc. The catenary wire current measured at the opposite (grounded) end of the catenary wires is also shown in Figure 4-14 (B) and shows the effect of some smoothing by the catenary wires. Also, the value read by the CWLIS system (B) has been found to be too high by a factor of approximately 1.9 due to the fact that it measures the reflected pulse (from a low impedance termination) superimposed on the incident pulse.

Analyses by LTI and EMA (using different methods), based on the current measurements shown in Figure 4-14 have led to the conclusion that the magnitude of the current pulse near the PCR was approximately 8 KA and had a waveform approximated by Figure 4-15.

4.4.2 I-NET and LTI Field Measurements

Data from these two systems are presented in Table 4-2, with a Summary in Table 4-3.

4.4.3 LIVIS

Data from this system are presented as waveforms and will be included in Section 4.5.

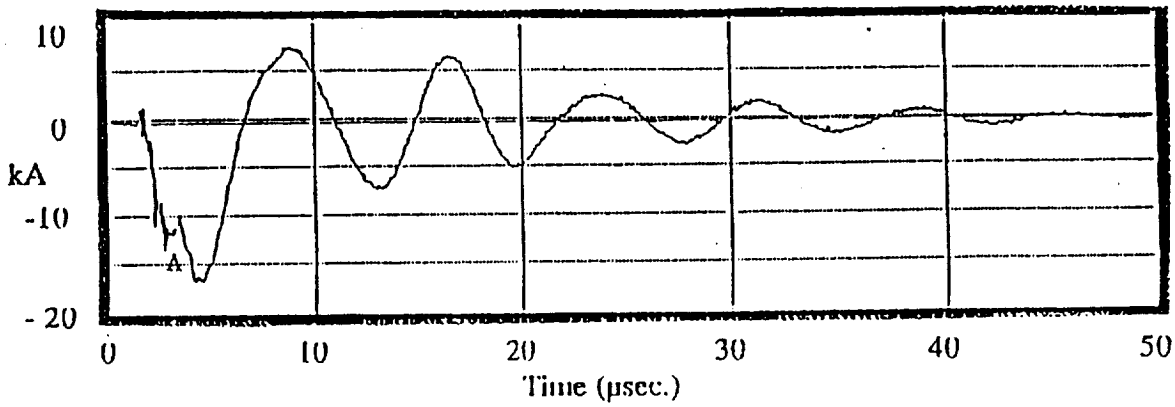

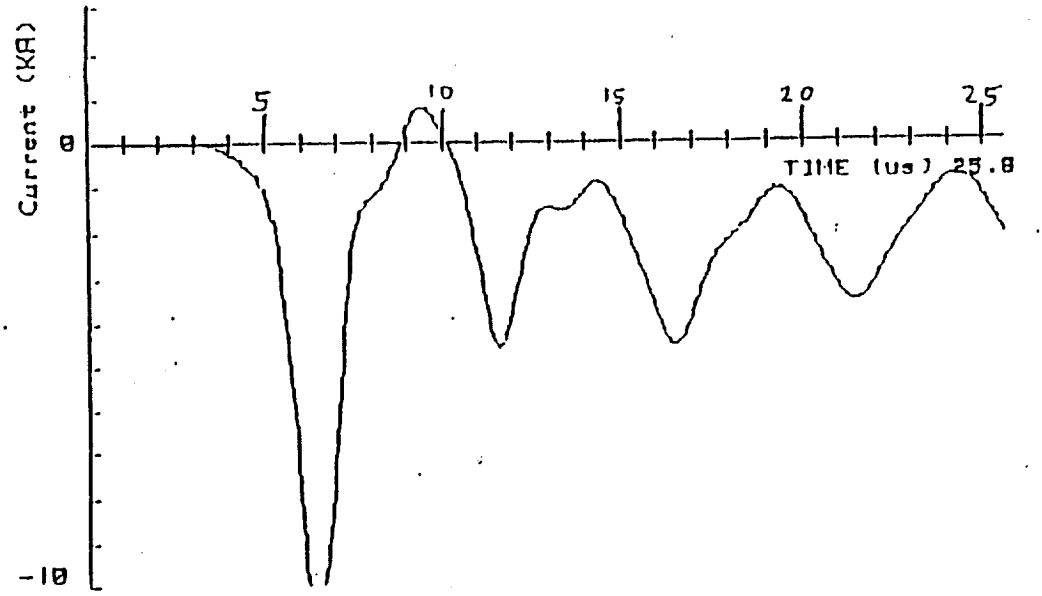

Figure 4-14 Current Waveforms
A (top): Measured at base of simulator
B (lower): Measured at opposite (grounded) end of catenary wire

4.5 Waveforms

External Fields: Typical waveforms for the external magnetic field are shown in Figure 4-16. It will be noted that these curves have the same general shape as that for the catenary wire current, that is, the oscillatory pattern of the oscillating circuit (catenary wire system) superimposed on the exponentially decaying base value representing the current decay under the influence of the catenary wire inductance. The x-component of the field, being less influenced by the pad structure, has a "cleaner" waveform than the other two components. Due to the geometric relationship with the catenary wires, it also is the component with the greatest magnitude.

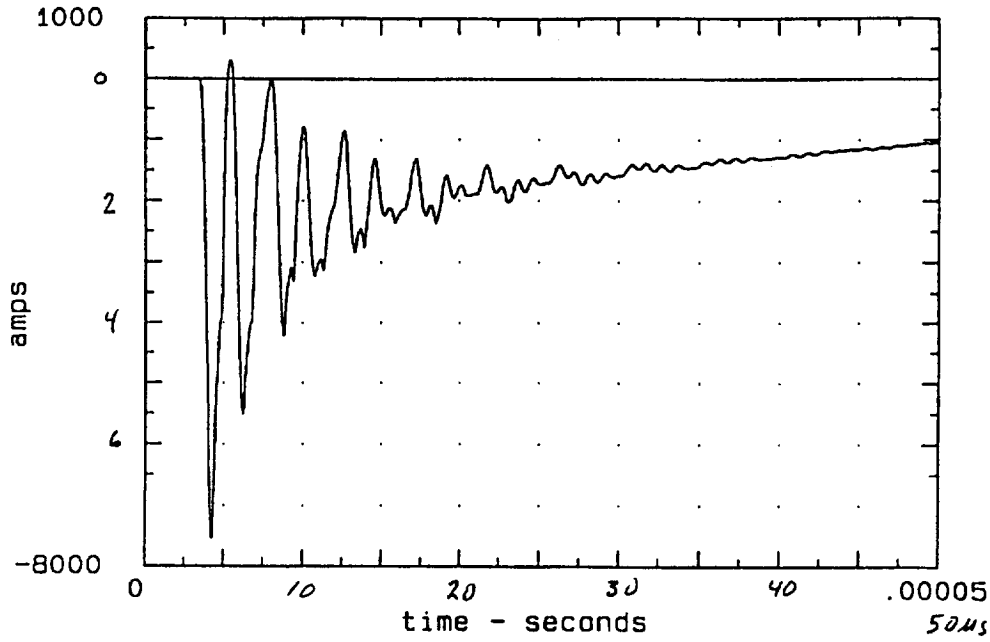

Figure 4-15
Computed Catenary Wire Current Near PCR

The magnetic field waveform observed atop the PCR, where there is minimal effect of pad structure, approximately matches those of the catenary wire current and the magnetic field outside the PCR doors. It is shown in Figure 4-17.

Pulse reflection: The H_X plot of Figure 4-16 is the case which best illustrates another interesting feature, namely that, except for the two ends of the catenary wire, the waveform is a function of position along the wire. For example, it will be noted that the peaks occur in pairs. The first peak of the first pair (A) represents the initial pulse in its first traverse of the wire. The second peak of the first pair (B) represents the reflected pulse traveling back up the wire. The sequence of pairs of pulses, then, represents later reflections traveling in the directions described above. The round trip travel time for a pulse on the catenary wire is approximately 5 μs. For different locations, the waveform will be different, as illustrated in Figure 4-18 a and b, where b applies to a location 90 m closer to the reflection point than does a. The values reported, however, are not affected appreciably, as they apply to the first part of the first pulse.

It will be noted that Figure 4-16 shows magnetic field while Figure 4-20 shows current; but the waveforms are seen to be similar.

Internal Fields: The internal fields had approximately the same shape as the external fields but smaller amplitudes (Figure 4-19).

An example of interior magnetic field data taken by the EG&G sensors is shown by Figure 4-20.

Table 4-2

Test Data

LOC'N	RUN #	I (KA)	dI/dt (KA/uS)	dE/dt (V/M/uS X	dE/dt (V/M/uS Z	E V/ X	E V/ Z	X	dH/dt (A/M/uS) Y	I-NET Z	I-NET SUM	V/M2
EXTERNAL												
U	2	7.7	10.8	7708	8161	1,618	3,124	7.65		2.83		
	5	7.5	10.6	10,864	7,862	1,769	2,820	7.66		3.01		
	6	7.5	11.3	9,402	9078	1,708	3,091	7.66	6.72	2.58	10.5	13.2
	11			9,495	13,640	1,900	3,540	7.96		4.69		
	13			10,430	10,030	1,970	3,035	7.30		2.68		
	14			9,580	9,754	1,880	3,100	7.96		4.12		
						1,808	3,118					
S	2											
135'	5											
	11											
	13											
	14											
T	21											
175'	22											
	23											
	24											
	25											
	26											
	27											
	28											
INTERNAL												
C	14	7.6	8.3									
	16	7.5	7.7									
	18	7.5	8.5									
D	24	7.6	8.5									

	25	7.7	8.4										
E	28	7.7	7.8										
A	5	7.5	7.5										
	9	7.6	8.5										
G	2	7.7	7.7										
	3	7.5	7.4										
B	10	6.8	8.0										
	11	6.8	7.8										
I	12	7.4	7.8										
	13	7.6	8.0										
J	19	7.6	7.7										
	20	7.5	7.4										
L	22	7.5	7.8										
	23	7.7	7.8										
M	26	7.6	7.8										
	27	7.6	8.2										
P	18	7.5	8.5	226	229	35.7	20.7	0.379	0.303	0.164	0.512		
	19	7.6	7.7	310	261	29.3	19.2	0.371	0.301	0.119	0.492		
				268	245	32.5	20				0.502	0.63	
Q	21			180	175	25.6	29.3	0.458	0.160	0.069	0.490		
	22			193	175	36.9	20.1	0.444	0.200	0.055	0.490		
	23			252	256	24.5	35.3	0.428	0.132	0.102	0.459		
				208	202	29	28.2				0.480	0.60	
R	24			352	186	41.5	21.7	0.315	0.116	0.111	0.354		
	25			294	196	23.4	34.3	0.313	0.105	0.083	0.340		
	27			288	183	38.1	14.4	0.225	0.126	0.091	0.273		
	28			319	274	35.9	14.3	0.343	0.099	0.133	0.381		
				313	210	34.7	21.2				0.337	0.42	
MEAN		7.5	7.9										

Table 4-2 (Cont.)

Test Data

		H (A/M)				dH/dt (V/M2)		LTI		FAST H (A/M)		
	X	Y	Z	SUM	X	Y	Z	SUM	X	Y	Z	SUM
EXTERNAL												
U	2.63		2.38									
	2.36	0.05	1.34	2.71								
	2.72	2.91	1.30	4.19								
	3.02											
	3.00											
	2.94											
				3.45								
S												
135'					4.93	0.94	1.78	5.33				
									3.59	2.57	1.59	4.69
									4.25	1.79	1.27	4.78
					4.93	2.24	0.90	5.49	4.27	1.87	1.24	4.82
								5.41				4.76
T												
175'					5.34	2.35	1.02	5.92				
					5.34	2.26	0.93	4.34				
									4.34	1.87	1.32	4.91
					5.34	2.46	1.09	4.49				
									4.47	1.99	1.40	5.09
					5:34	2.36	1.08	5.94				
									4.49	1.91	1.42	5.53
					5.62	1.22	0.35	5.76				
								5.29				5.18
INTERNAL												
C					0.22	0.082	0.19	0.30				
						0.074	0.18					
									0.095	0.024	0.070	0.120
D					0.092	0.070	0.024	0.121				

									0.09	0.048	0.015	0.103
E									.040	0.020	0.009	0.046
A					0.037	0.065	0.081	0.110				
									0.019	0.026	0.027	0.042
G					0.11	0.15	0.29	0.34				
									0	0.03	0.130	0.133
B									0.055	0.048	0.120	0.140
					0.13	0.15	0.24	0.31				
I					.10	0.060	0.093	0.149				
									0.026	0.013	0.025	0.038
J					0.057	0.085	0.076	0.127				
									0.021	0.028	0.025	0.043
L					0.086	0.064	0.061	0.123				
									0.026	0.011	0.012	0.031
M					0.040	0.085	0.021	0.096				
									0.018	0.021	0.026	0.038
P	0.0594	0.0485	0.0280	0.0816								
	0.0562	0.0480	0.0234	0.0775								
				0.0796								
Q	0.0503	0.0326	0.0238	0.0645								
	0.0436	0.0261	0.0141	0.0527								
	0.0441	0.0312	0.0320	0.0628								
				0.0600								
R	0.0308	0.0406	0.0274	0.0579								
	0.0249	0.0326	0.0270	0.0491								
	0.0331	0.0342	0.0130	0.0493								
	0.0350	0.0236	0.0295	0.0515								
				0.0504								

Table 4-2 (Cont.)

Test Data

		SLOW H (A/M)			E (V/M)	FULL SCALE H (A/M)	V/M2
	X	Y	Z	SUM			
EXTERNAL							
U						30	107
S					420	41	44
135'					360		
					190		
					110		
					290		
					270		
T					390	45	43
175'					370		
					120		
					380		
					110		
					370		
					130		
					110		
					250		
INTE	NAL						
C						1.0	2.4
					6.2		
	0.048	0.027	0.014	0.057			
D						0.9	1.0

	0.055	0.045	0.021	0.074			
E	0.016	0.014	0.062	0.066		0.6	
A					2.9	0.4	0.9
	0.018	0.011	0.006	0.022	4.5		
					3.7		
G					14.5	1.1	2.8
	0	0	0.068	0.068			
B	0.018	0.009	0.021	0.029	2.8	1.2	2.5
					2.4		
					2.6		
I					3.4	0.3	1.2
	0.017	0.006	0.006	0.019	5.8		
					4.6		
J						0.4	1.0
	0.027	0.016	0.017	0.036			
L						0.3	1.0
	0.013	0.004	0.004	0.014			
M						0.3	0.8
	0.005	0.012	0.028	0.031			
P						0.7	5.1
Q						0.5	4.9
R						0.4	3.4

LOC'N	TEST DATA			EXTRAPOLATED TO NSTS 07636 STROKE		
	H	dH/dt	E	H	dH/dt	
	A/m	V/m^2	V/m	A/m	V/m^2	
EXTERNAL						
S	4.8	4.3		62	47	135' level
T	5.2	4.2		68	45	175' level
U	3.3	19.6	3750	45		walkway outside 135' level
PCR LIVI	16.5			309		
INTERNAL TO PCR						
C	0.12	0.3	6	1.5	2.6	
D	0.1	0.1		1.4	1.1	Test pulse applied at base of catenary wire: I = 7.5 KA (equivalent to 16 KA to mast)
E	0.07			0.9		
A	0.04	0.1	4	0.6	1	dI/dt = 7.9 KA/us
G	0.13	0.3		1.7	2.9	
B	0.14	0.3	3	1.8	2.7	
I	0.04	0.2	5	0.5	1.3	
J	0.04	0.1		0.6	1.1	
L	0.03	0.1		0.5	1.1	
M	0.04	0.1		0.5	0.9	
P	0.08	0.9	47*	1.1	5.6	* 3 dimensional value based on 2 dimensional data
Q	0.06	0.9	50*	0.8	5.4	
R	5.05	0.6	50*	0.6	3.6	

Table 4-3

Summary of Test Data

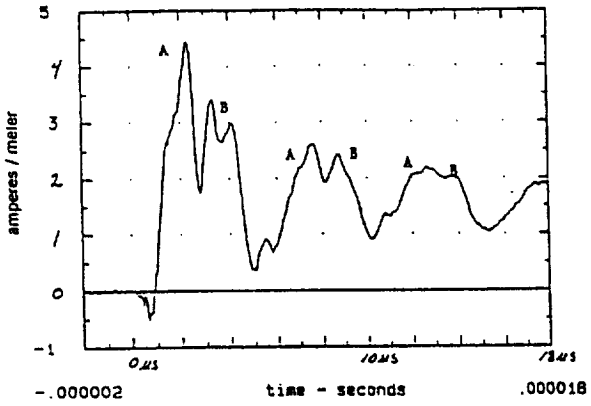

H_X (Perpendicular to PCR doors)

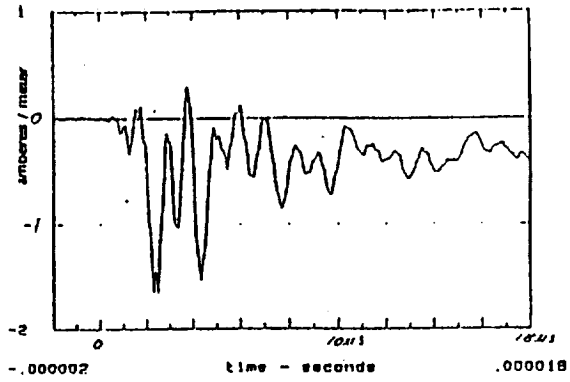

H_Y (Across PCR doors)

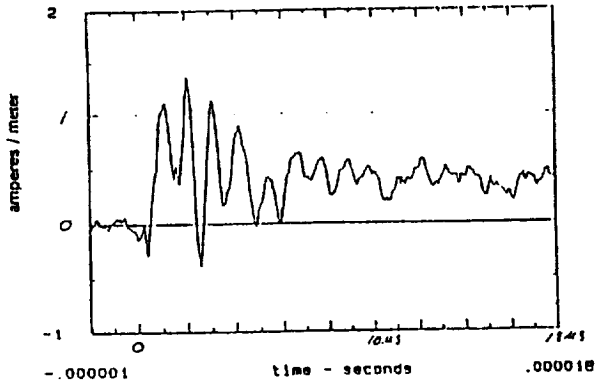

H_Z (Vertical)

Figure 4-16

Magnetic Field, H, in front of PCR doors

(LTI antennas)

It will be noted from Tables 4-2 and 4-3 that the field magnitude did not vary greatly as a function of location inside the PCR, varying from 0.03 to 0.14 A/m, with the larger values being observed near the horizontal center of the room--that is, "in front of" the door aperture.

Comparison of the magnetic field values inside the PCR to external values in front of the doors indicates a shielding effectiveness of 25-40 dB. RF measurements had shown a range of values from 30 to 50 dB [16].

Diffusion through a wall: An example of the "diffusion" of a magnetic field through a conducting wall, as discussed in Section 3.3.2, is shown by Figure 4-21.. That figure shows the underlying "slow" field components indicated by the lines drawn in. The components oriented across the doors, H_Y, and vertically, H_Z, rise rapidly to a peak and then decay to near zero at around 100 microseconds. They apparently entered the room

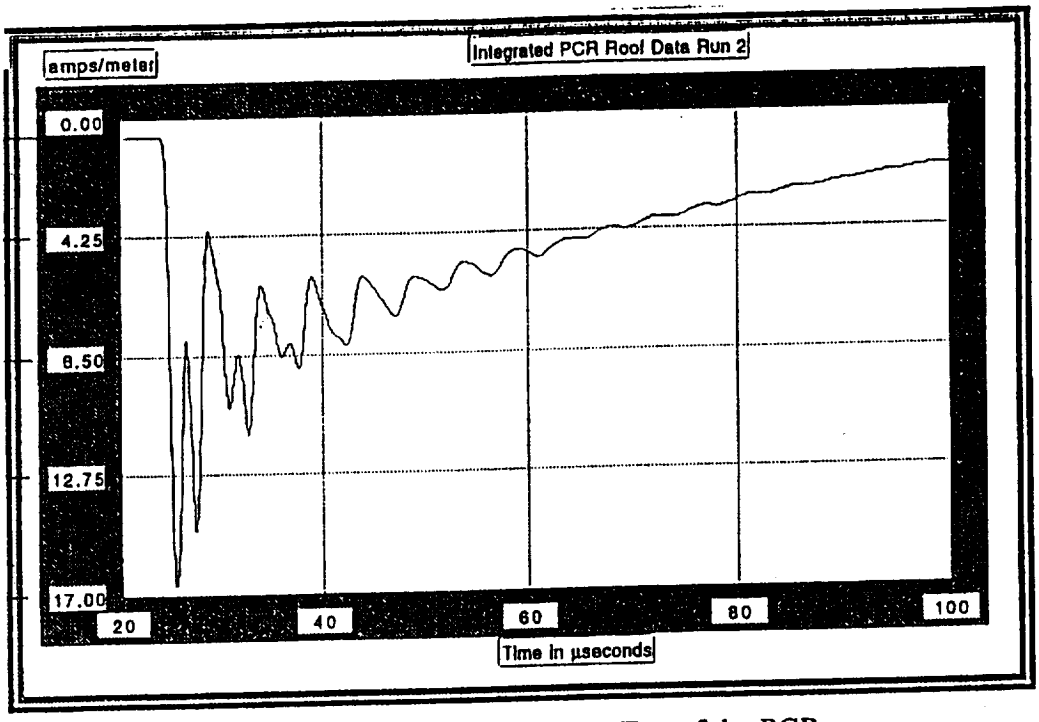

Figure 4-17. Magnetic Field on Top of the PCR

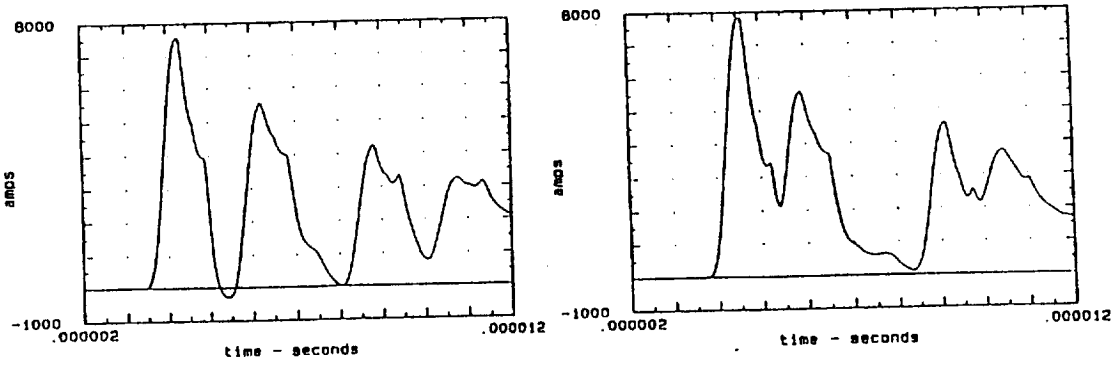

a. Current at First Location

b. Current at Second Location

Figure 4-18

via the apertures around the doors and between the two doors. The field component oriented into the door, H_X, however, takes 30 - 40 microseconds to reach its peak, after which it decays much more slowly than do the other two components. This pulse stretching , or slow build up followed by an even slower decay, is what has been meant by "diffusion."

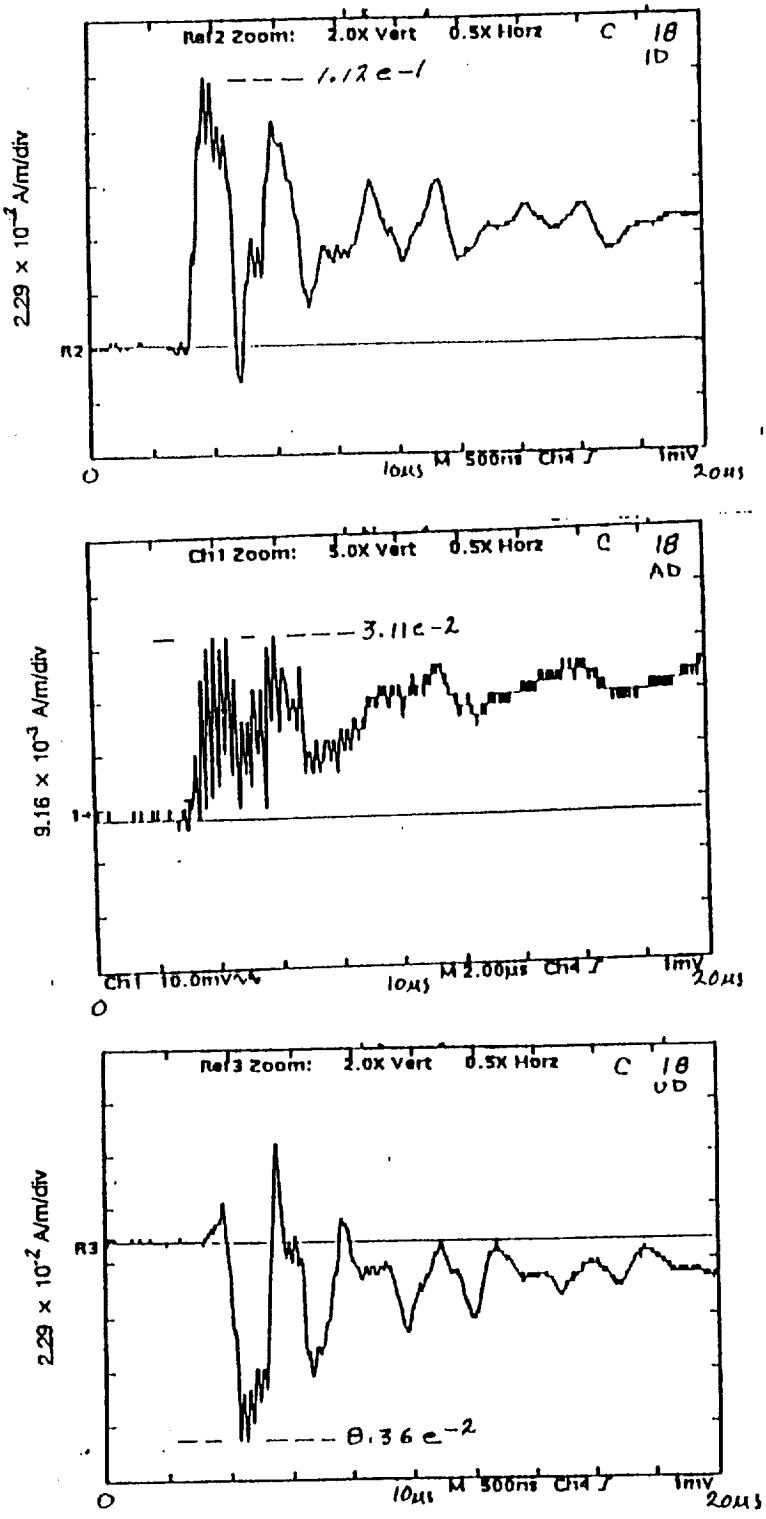

Figure 4-19. H-Field Measurements at location C
top: perpendicular to doors, H_X
center: across doors, H_Y
bottom: vertical, H_Z

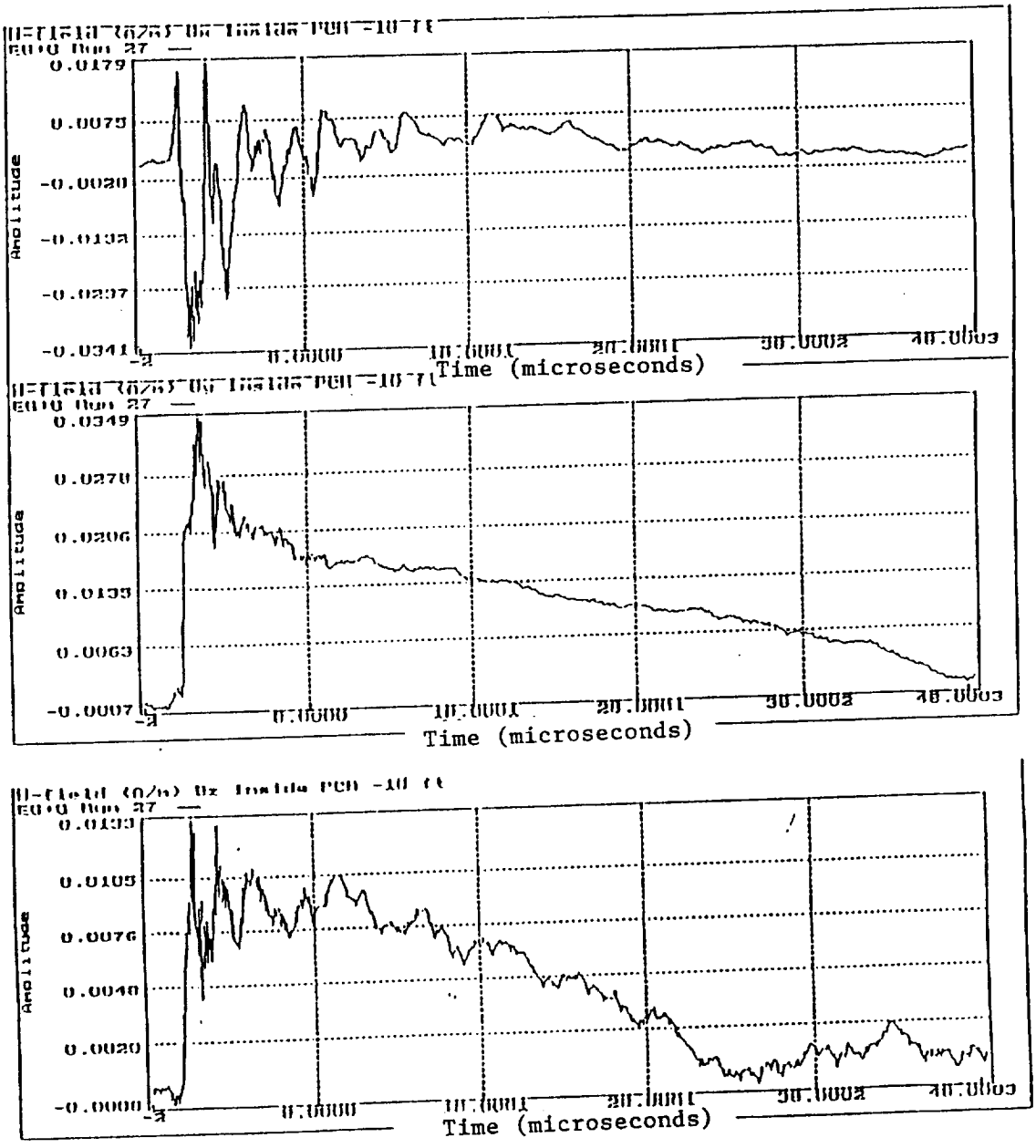

Figure 4-20
Internal Magnetic Field
Location R
EG&G Sensors

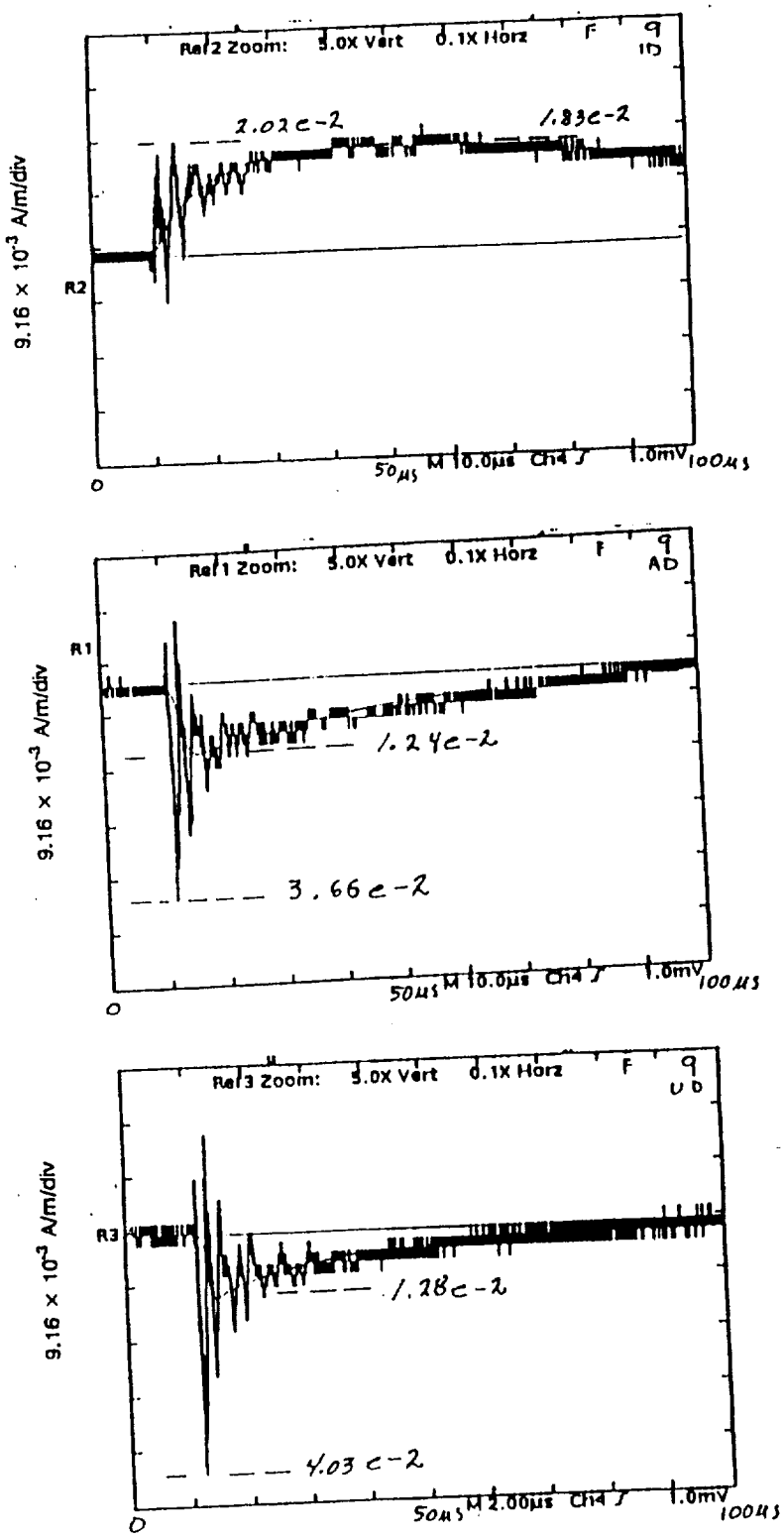

Figure 4-21.
Illustration of "diffusion": H-Field Measurements at Location F
(top: perpendicular to doors, H_X; center: across doors, H_Y; bottom: vertical, H_Z)

4.6 EMA Calculated Data

EMA calculated the magnetic field expected at the center of the doors for the conditions of the test. Those values are compared to the test results in Figure 4-22 A. Figure 4-22-B shows the computed field for a smoothed current in contrast to the "noisy" current used for Figure 4-22 A. Unexpectedly, the noisy current gives a better fit to the test data than does the smoothed current. In both cases, the maximum value is within a factor of two of the test value, but the differences in the calculated curves illustrate the importance of the input waveform.

4.7 Frequency Spectra

The frequency spectrum for the computed current is shown in Figure 4-23.

Frequency spectra for the magnetic fields have been obtained for the data collected by I-NET, that is, data from the LTI sensors suspended outside the PCR doors and the EG&G sensors at their locations outside and inside the PCR. Two of these curves are shown in Figures 4-23 and 4-24. Major frequencies from the curves are listed in Table 4-4. The 0.06 MHz peak apparently represents the first pulse. The 0.22 MHz peak corresponds approximately to the 5 μsec. round trip travel time for a pulse on the catenary wire. (That is to say, the total catenary wire length of 2145 feet is fairly close to the half wave length corresponding to th 0.22 MHz peak.) The higher frequency pulses could represent harmonics of that frequency. Also, the half wave length for the the 0.48 MHz peak is 910 feet, which matches fairly closely the 1130 foot length of the lightning-protective wire over the slide wire system. A structural match for the 700 foot half wave length associated with the 0.63 peak is not apparent. Corresponding peaks for the 0.88 and 1.12 Mhz values in the current spectrum are not apparent in the H-field spectra.

4.8 Data Summary

Significant oscillations are present in all plots of the fields. They are believed to be due to oscillations in the catenary wire current, currents induced in elements of the PCR and the launch support structure, and structural cavities which support field oscillations; but not many effective structural elements have been identified.

The consistency of the data between measurements is indicated by the following figures for the maximum deviations for the indicated data:

Current (I)	10%	Magnetic field (H)	20%
Electric field (E)	60%	dH/dt	20%

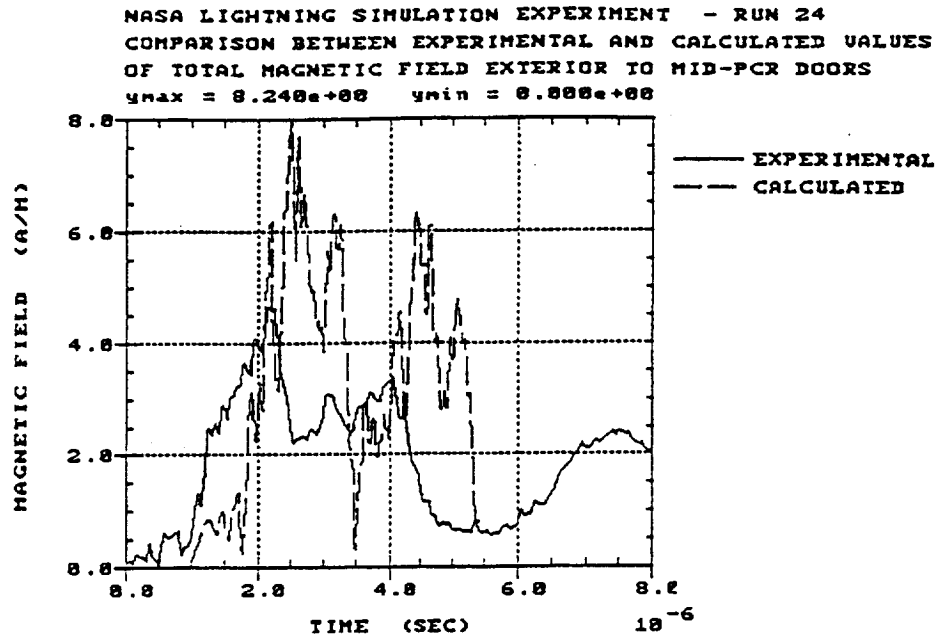

A. CALCULATED CURRENT SOURCE FROM TRANSMISSION LINE MODEL M52. EXPERIMENTAL VALUES AS THE VECTOR SUM OF D25_5.DAT, D25_6.DAT, AND D25_7.DAT

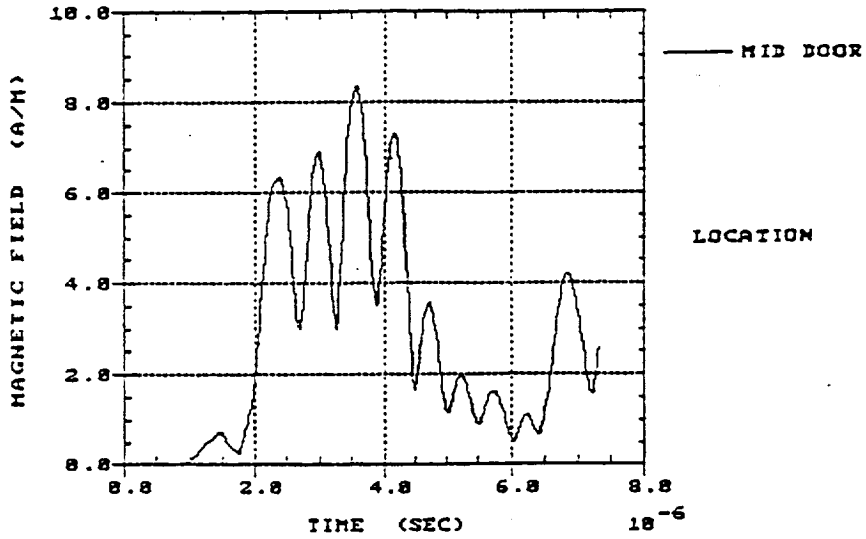

B. CURRENT SOURCE IS CALCULATED 24 POINT SMOOTHED CATENARY WIRE CURRENT - RUN 24
2 USEC ARC, 50 OHM ARC, 50 NSEC RISETIME

Figure 4-22
Total Magnetic Field Comparisons at the PCR Door Center

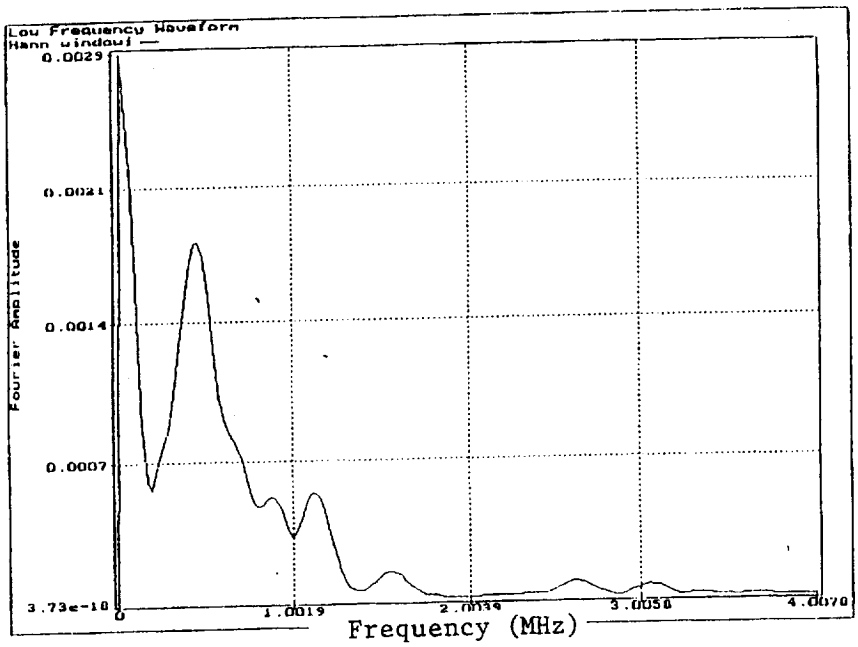

Figure 4-23
Frequency Spectrum for Computed Catenary Wire Current

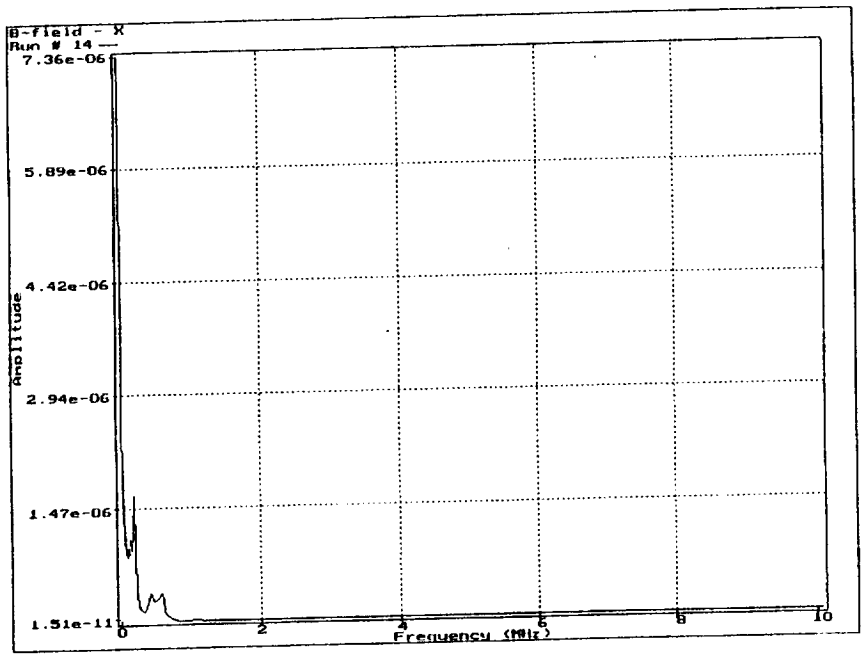

Figure 4-24.
H_X Frequency Spectrum
LTI sensors outside PCR doors, 135' level

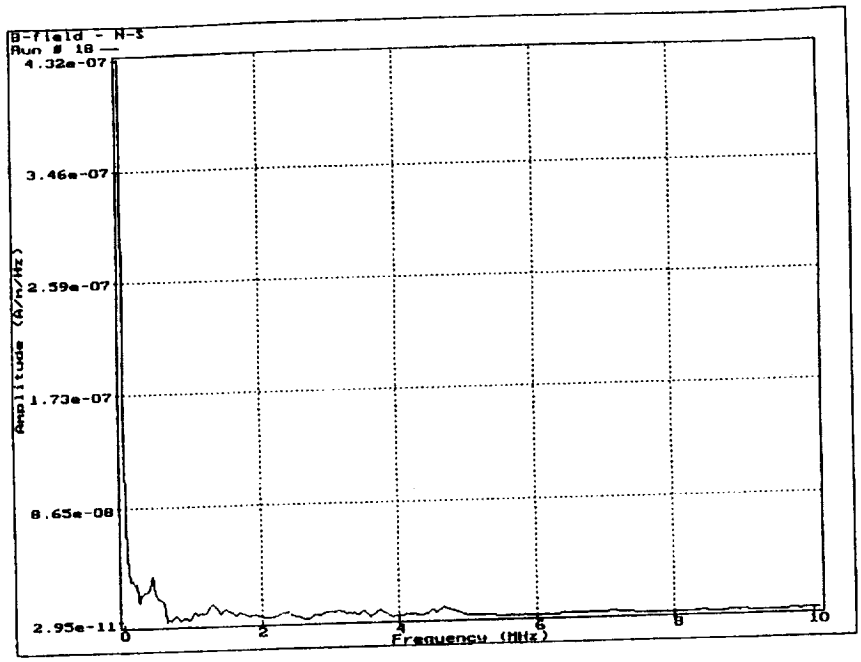

Figure 4-25.
Hx Frequency Spectrum
Location P (internal), EG&G sensors

Table 4-4. Major Spectral Components

Current	0.06 MHz		0.46 MHz		0.88 MHz	1.12 MHz
External H						
EG&G	0.07	0.22 MHz	0.48	0.63 MHz		
LTI	0.07	0.22	0.48	0.63		
Internal						
EG&G	0.07	0.22	0.48	0.63		

External Magnetic Field

H ~ 5 A/m
8% difference between 135 and 175 foot levels

Components of H:		
	H_X, into the doors	4.3 A/m
	H_Y, across the doors	1.6
	H_Z, vertical	1.3

Extrapolated to 200 kA stroke: H ~ 60-70 A/m
Extrapolation includes accounting for the difference in current and the stroke striking the mast instead of the end of the catenary wire.

dH/dt ~ 4.5 A/m/μs

Components of dH/dt:		
	$(dH/dt)_X$, Into the doors	4.0 A/m/μs
	$(dH/dt)_Y$, Across the doors	0.7
	$(dH/dt)_Z$, Vertical	1.9

External Electric Field

E ~ 3 kV/m

Components of E:		
	E_X, into doors	1.8 kV/m
	E_Z, vertical	3.1

dE/dt ~ 10 kV/m/μs

Extrapolated E (NSTS 07636 stroke)~ 45 kV/m

Internal Magnetic Field

Typical components of H:		
	H_X, perpendicular to doors	0.10 A/m
	H_Y, across doors	0.02
	H_Z, vertical	0.07

Resultant H ~ 0.03 - 0.14 A/m

Extrapolated H ~ 1 - 2 A/m

Typical components of dH/dt:		
	H_X, perpendicular to doors	0.46 A/m/μs
	H_Y, across doors	0.19
	H_Z, vertical	0.08

Resultant dH/dt ~ 0.50 A/m/μs

Extrapolated dH/dt ~ 1- 6 A/m/μs

This amounts to approximately 8 V/m^2 as the potential induced in an exposed conducting loop --probably the most important number we can supply the payload designers.

Shielding effectiveness of the PCR walls:

For E: ~ 47 dB
For H: 36 - 40 dB

The internal and external waveforms were similar, particularly as regards the first few pulses of field - the ones believed to be caused by the current pulses passing back and forth along the catenary wire. Fields of this duration are probably coupled only through the apertures around the door, and those apertures are large enough that they probably are not particularly resonant at the frequencies most associated with the magnetic fields likely to be generated by lightning. There are differences in the shape of the long duration element of the x component of the magnetic field; the long duration component external to the PCR seems to have a duration on the order of 50 microseconds, but the long duration component of the internal field often lasts much longer. In some cases, the internal field persisted even after one would have expected the external field to have completely disappeared. Effectively, the PCR acts as a low pass filter with a time constant much longer than that of the external magnetic field. This is the "diffusion" effect discussed in Sections 3.3.2 and 4.5.

For the types of magnetic field produced by lightning, the shielding effectiveness can be taken as 30-40 dB and can be taken as flat over the frequency range of most real importance.

The magnitude of magnetic field inside the PCR varies with location, from 0.04 to 0.15 A/m (test values) with the larger values being in the central portion (locations B,C,D,G -- those "looking at" the doors) and the smaller values being in the side sections (locations A, J, M, E, I, L -- those farther removed from the doors).

As seen above, the data indicate that the most significant entry for electromagnetic energy is through the door area, and apparently the primary entry areas are the rubber encased apertures around the doors and at the vertical meeting line of the two doors. The average width of this aperture is estimated at 4 cm.

5. STRIKE TO THE ROTATING SERVICE STRUCTURE

A lightning strike to the Pad B Rotating Service Structure (RSS) occurred June 25, 1994. The strike was captured on operational television (OTV), and two cameras directed approximately orthogonally show the attach point to be a top corner of the RSS. Specifically, that location is designated as main structural column 6A on corner 2/3.

There are two pieces of quantitative information on the stroke:

(1) The LLP lightning detection system operated by CCAS Weather Operations read a current value of 18 ± 2 kA.

(2) A PCR livis reading of 45 volts was measured on a cable which runs from the PCR floor to the pad apron.

The result of a survey of the location of the attach point relative to the catenary wire is shown in Figure 5-1, which shows that the attach point is well within the 1:1 "cone of protection," giving emphasis to the caveat that the "cone of protection" concept is only a rough guide.

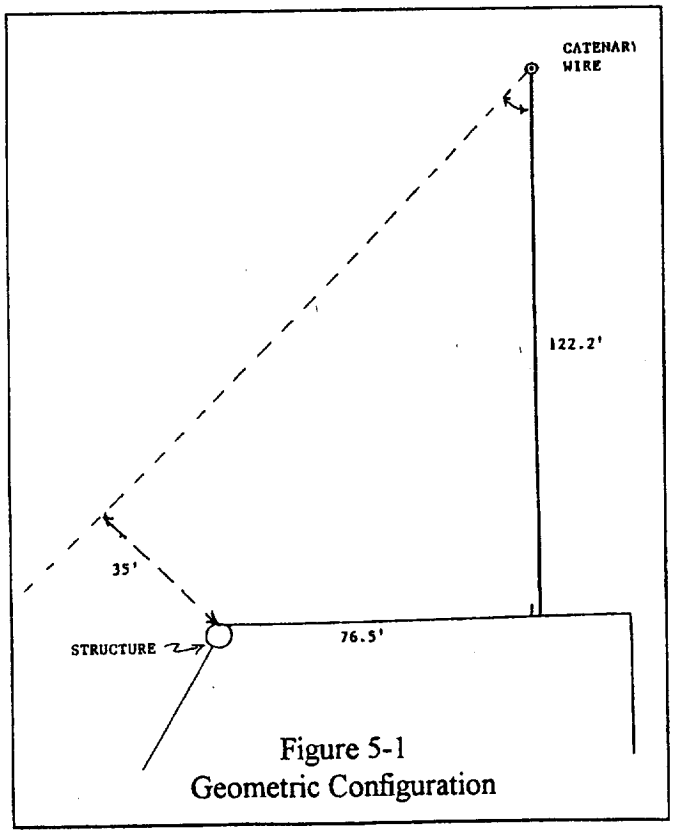

Figure 5-1
Geometric Configuration

A striking distance diagram can be used to show how a point within the "cone of protection" can receive a lightning strike. Striking distance diagrams are based on the concept that a lightning stroke will attach to the first object it approaches within a specified distance called its striking distance. This is illustrated by Figure 5-2. Such a diagram is a function of the value of the striking distance. There is no explicit relationship between stroke current and striking distance, but experimental data are available. [21] For the evaluation shown in Figure 5-2, an "approximately worst case" of 120 feet was used for the striking distance.

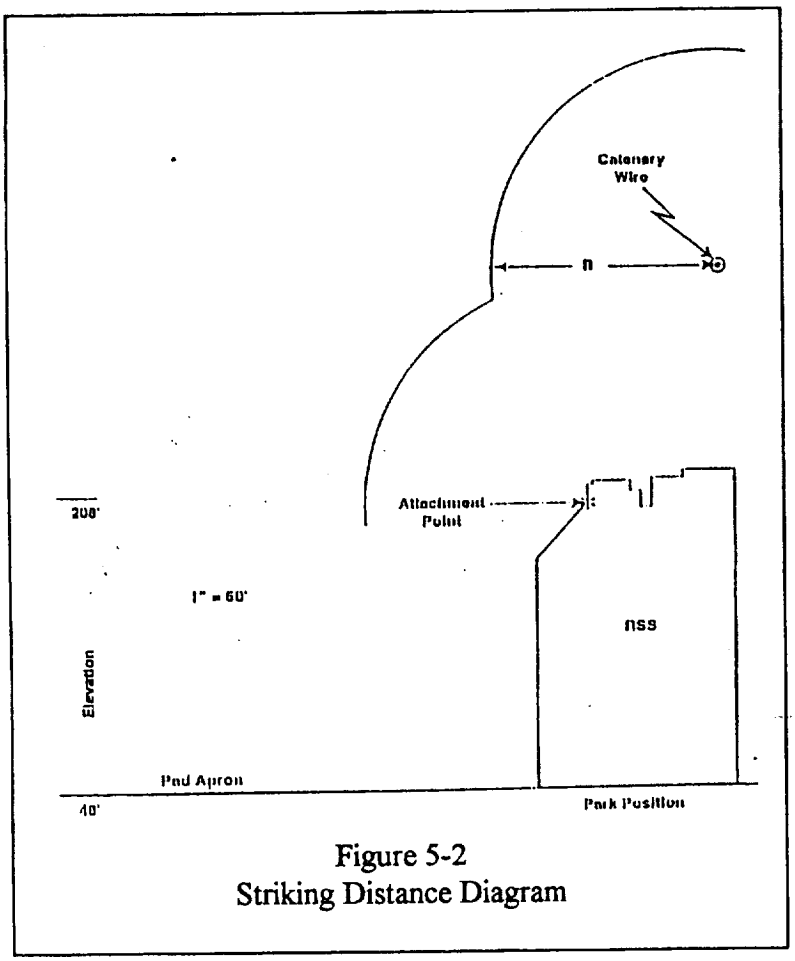

Figure 5-2
Striking Distance Diagram

(The striking distance decreases with decreasing stroke current.) The upper arc represents a cylindrical surface surrounding the catenary wire and having a radius equal to the striking distance. A stroke arriving at that surface is expected to attach to the catenary wire. The lower arc represents a spherical surface surrounding the attach point. A stroke arriving at that surface is expected to attach to the designated attach point. Thus, the location of the arrival of the stroke relative to the various surfaces determines the attach point.

In this case, television (OTV) showed that the stroke came in at an angle such that interception by the lower surface is not unreasonable and, in fact, the strike did occur to the top of the RSS. This incident shows the value of television cameras for locating attach points, as they were the only means available for that purpose in this case.

Since the stroke did not hit the catenary wire, the effect on the Catenary Wire Lightning Instrumentation System (CWLIS) was an induced effect.

The only damage found from the strike was that memory units in the control circuits for the RSS wheel drive controllers suffered some upsets. The control circuits are in metal cabinets which are in a metal room, but there are some cracks which serve as apertures. The room is located about 20 feet above the pad apron and between the two RSS legs, which serve as primary down-conductors for the lightning current.

Lightning Technologies, Inc. and Electro Magnetic Applications added this incident to their studies and found that the effect inside the PCR was approximately that of a medium-to-large stroke to the mast. The external magnetic field (in front of the PCR doors) was computed to be 22-55 A/m. Values computed by EMA are shown in Figures 5-3 to 5-5.

Two sets of curves were computed in order to bracket the case. The two sets of data are based on different waveforms for the incident lightning. The two maximum rise rates used are 180 KA/μs for data set A and 18 KA/μs for data set B. (The maximum rise rate for the NSTS 07636 stroke is l40 KA/μs.) In each of the cases, the current in each of the exterior legs is about 5 KA and about 3 KA at the pivot point. The other 5 KA goes through the FSS.

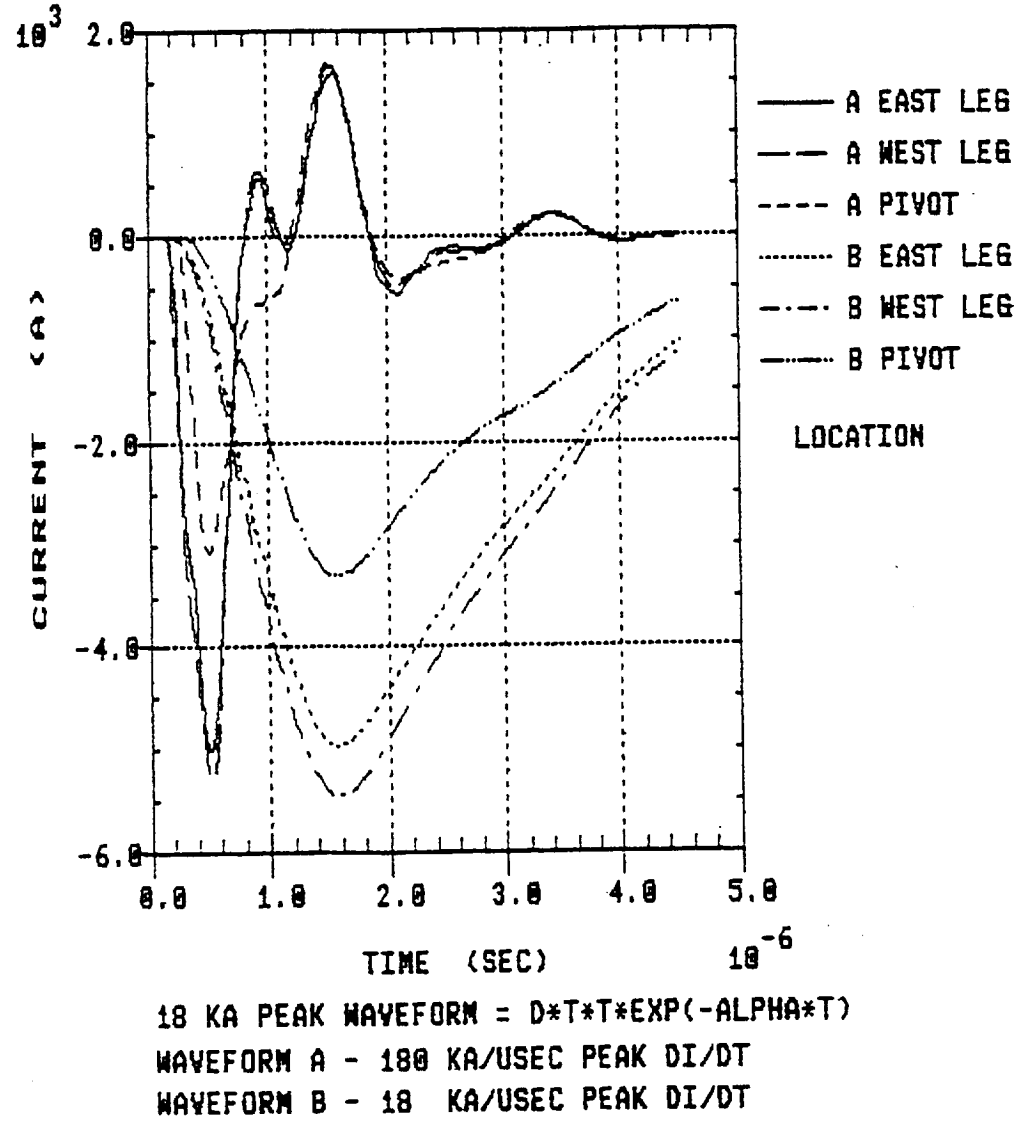

Figure 5-3
Direct Currents to Pad Apron

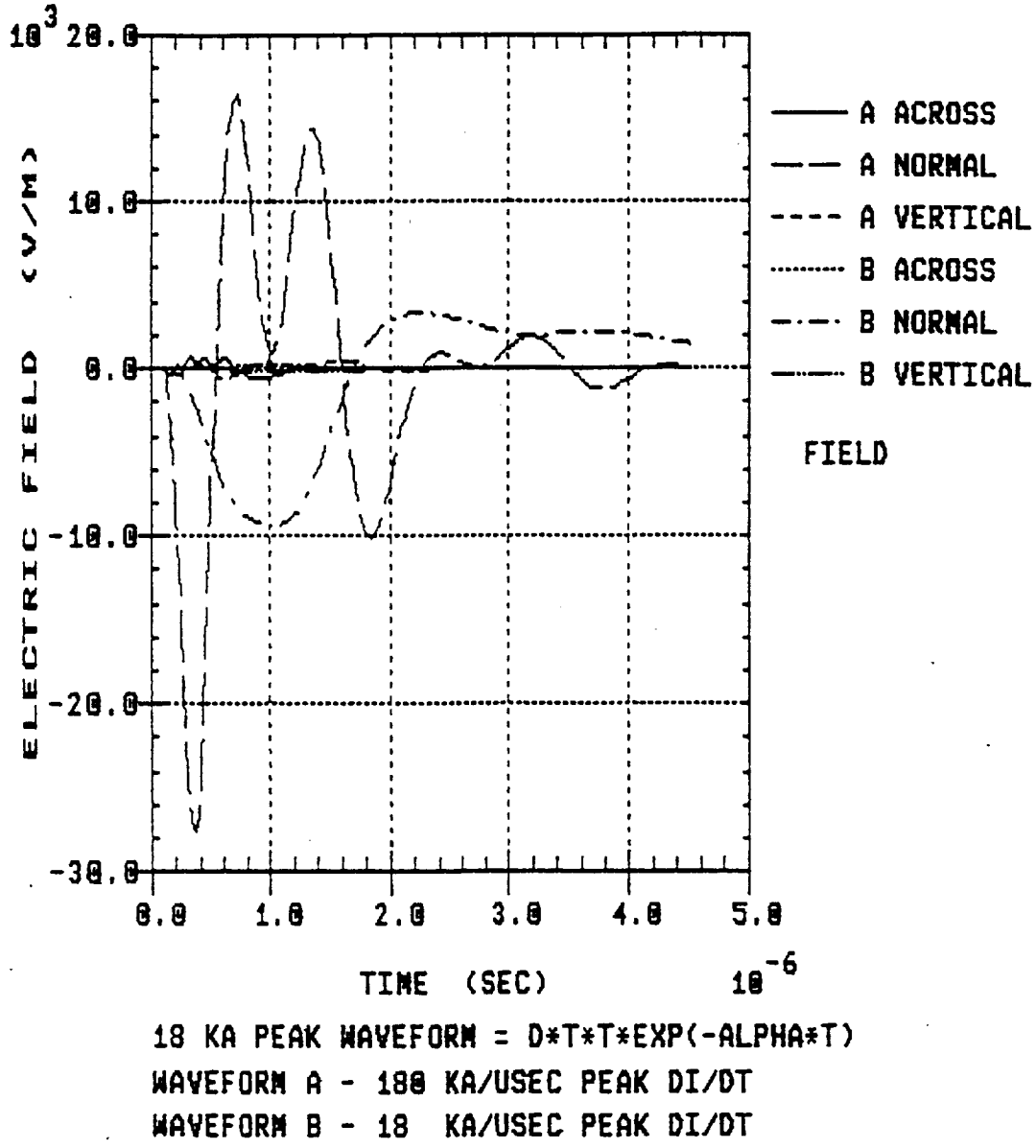

Figure 5-4
Electric Fields at PCR Door Center

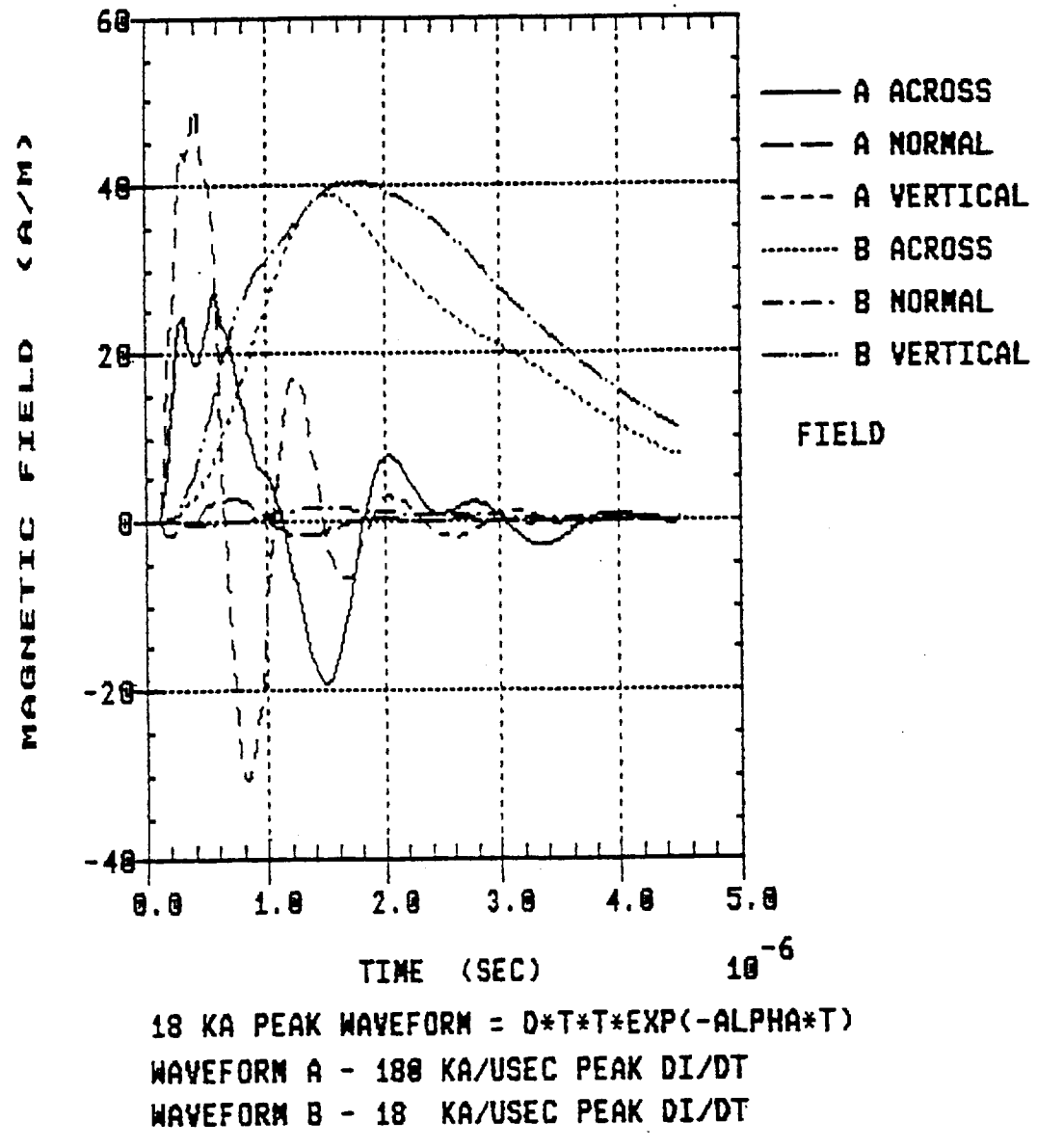

Figure 5-5
Magnetic Fields at PCR Door Center

An LTI probability analysis predicts that of 100 strokes to the pad (catenary wire), one will hit the RSS. Those would be strokes in the lower current range of lightning current distribution. The LTI calculation indicates that the currents of those strokes would be <47 KA. Other results of the LTI probabilistic analysis are given in Table 5-1.

Several possible measures to reduce the probability of a strike to the RSS have been considered, but in each case it was concluded that the gain is not worth the cost.

Results from LTI Flash Program
RSS in park position
5000 simulated strokes within a 2000' x 2000' area
1347 strikes to the catenary wire system
14 strikes to the RSS
4 strikes to the FSS

Table 5-1

6. CONCLUSIONS - PARK POSITION

6.1 Modeling

LTI conducted physical and mathematical modeling, and EMA conducted mathematical modeling. Calculated data quoted in this chapter are for a 200 KA stroke to the mast, and experimental data have been extrapolated to such a stroke.

Measurements indicate magnetic field values of 68 A/m outside and 12 A/m inside the PCR. The EMA FDTD method gave 30 A/m for the external value and an external electric field value of 6 KV/m.

Mathematical analysis by the FDTD method shows strong oscillations in both types of field, but especially in electrical fields. The validity of those oscillations is difficult to evaluate for several reasons: (1) The number and magnitude of the oscillations depend upon the shape of the applied pulse, as illustrated in Sections 3.5.3 and 3.5.5.1, (2) The method may not adequately account for energy losses by corona, and (3) Simplification must be made in the description of the physical structure.

The LTI calculations, LTI model measurements, and EMA calculations are in reasonable agreement.

Major results:

H outside PCR doors:	LTI measured	68 A/m
	EMA computed	30
H inside PCR:	LTI measured	12 A/m
E in front of doors:	EMA computed	6 kV/m
Current in structure:	LTI calculated	up to 9 kA

In an effort to determine a suitable location for a permanent magnetic field sensor in the PCR, a horizontal sense wire was placed near a wall (Figure 3-21). That loop received an induced extrapolated voltage of 30-37 volts, showing that this can be a practical means of measuring the magnetic field inside the PCR.

The location of the Payload Ground Handling Mechanism (PGHM) does not seen to have a significant effect on the magnetic field values.

Comparison of the magnetic fields due to a strike to the FSS to that due to a strike to the mast indicates that the former is 6.5 times the latter.

The nature of the waveform weighs heavily in determining the number and magnitude of oscillations observed, as mentioned above, and in determining the rate of rise of the magnetic field, which, in turn, determines the induced potential in exposed circuit loops.

The effect of the PCR-Canister grounding cables was measured for a stroke which hit the FSS. The scaled potentials were found to be 8800 volts with no leads connected and 2500 volts with four leads connected.

6.2 Testing

Test results quoted in this section are test results extrapolated to the NSTS 200 KA stroke.

The test results are considered to be the "real" results. One purpose of the modeling and analysis was to compare their results to test results and, possibly, determine ways to improve the modeling and analytical methods. They also provide some information which the test does not.

Fields outside the PCR are high enough to be a hazard for sensitive equipment: $H \cong 45$ A/m and $dH/dt \cong 43$ volts induced in a loop of 1 m^2 area. However, this is not a problem under normal conditions, as no sensitive equipment is normally present in that region.

The magnetic field inside the PCR is low enough that it will not be a concern for most payload users; however, they need to be aware of the values so they can evaluate the situation with respect to their payloads. Except for locations near the door apertures, the field values do not change radically with location inside the room (0.3 - 1.2 A/m).

The rate of change of magnetic field inside the room is high enough that payload designers need to ensure that unshielded loops are not present in their payloads (0.8 - 5.1 V/m^2).

A more complete tabulation of these data is given in Table 4-3.

A comparison of data from the models with date from the test follows:

	Test	LTI Measured	EMA Calculated
H outside PCR doors	41-45 A/m	68 A/m	140 A/m
H inside PCR	0.3 - 1.2	12	0.5-1.6

Comparison of the magnetic field measured by the LIVIS loops on the PCR roof with the values measured at locations B and C show that the field at the center of the PCR is approximately 1/123 (42 dB) that on the roof for a stroke to the mast. PCR LIVIS loops on the roof can, then, be used to provide a measure of the field inside the PCR.

CWLIS readings, also, can give approximate estimates of values inside the PCR for a strike to the mast:

$H\ (A/m) \cong 0.0083 \times I$ where I = total CWLIS current I kA

V (potential induced in an unshielded conducting loop, in volts/m^2 of loop area) = $0.057 \times dI/dt$ where dI/dt = kA/μs as read by CWLIS

$E(V/m) = 9.5 \times dI/dt$

7. ANALYSIS OF THE CASE WITH THE VEHICLE PRESENT

7.1 Introduction

Except for the LTI modeling discussed in Section 7.2, the material in this chapter applies to the configuration with the RSS in the mate position and the payload bay and PCR doors open.

To the payload owner, conditions in the Orbiter payload bay are as important as those in the PCR; but since circumstances did not permit simulator testing with the vehicle present, the alternative was to evaluate that situation by analysis. The method that seemed most appropriate is the FDTD method described in Section 3.5.1. Results obtained by that method, presented in Sections 3.5.2 and 3.5.3, and a "blind test" to compare results with the simulator test results (Table 7-1) have provided acceptable confidence in this method. Figure 7-1 shows the segments into which the system is divided for this analysis.

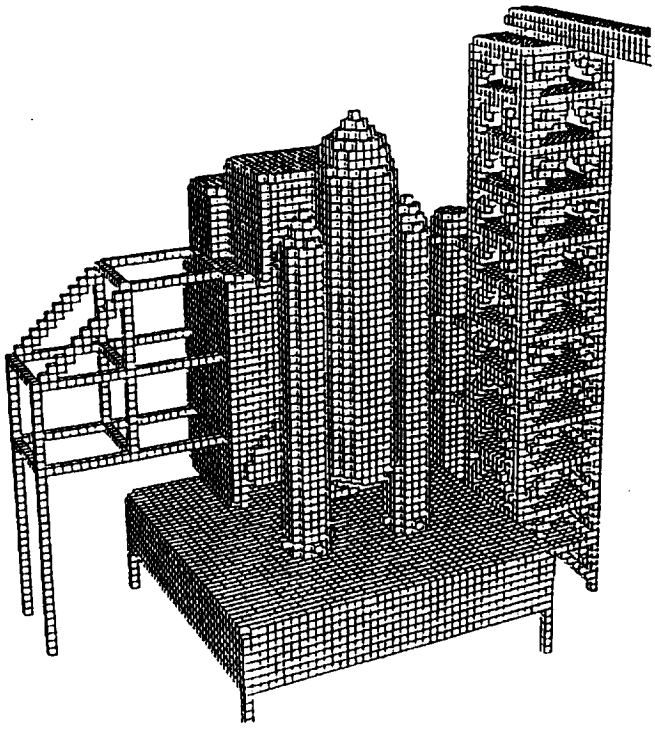

Figure 7-1
Configuration Analyzed

A 200 kA/m stroke having the Component A waveform of the NSTS design stroke is applied to the mast

More details of this analysis method are given in [7].

7.2 Potentials and Currents

There are four "ground straps" used to electrically bond the Orbiter to the PCR, two at the top of the doors and two at the bottom. Currents in these four straps and a drag-on cable, when present, have magnitudes of the order of a few hundred amperes. LTI modeling shows 700 amperes with all four straps connected and 2000 amperes with only one strap - a lower one - connected. The currents appear to be roughly shared between the ground straps and the drag-on cable; disconnecting the drag-on cable slightly increases the ground strap currents.

	LOCN	MEASMT	EG&G	LTI	EMA	EMA/TEST
EXTERNAL						
	U	H	3-4 A/m		6-8 A/m	2
		dH/dt	11-12 A/m/μs		10-100 A/m/μs	1-8
		E	4,700-6,000 V/m		4,000-11,000 V/m	1-2
	S	H		4-6 A/m	5-9 A/m	1-2

Table 7-1
Blind Test Results

LTI modeling found that with all four ground straps in place,potential between the PCR and the Orbiter was 800 volts. Connecting only the top straps gives 3,200 volts, and connecting only the bottom straps gives 900 volts. Removing all four straps gives 20 kV. (Figure 7-2)

EMA analysis found the potential between the PCR and the Orbiter, with the ground straps in place, to be of the order of 10 kV and have a strong oscillating component, as seen in .Figure 7-3. The magnitude is a function of the rise time of the lightning current waveform, as discussed in Section 3.5.2.

7.3 Fields

Figure 7-4 indicates external magnetic fields of 180 A/m on the PCR roof and 140 A/m near the PCR door on the RSS side.

Figure 7-5 indicates that the magnetic field at the PCR-Orbiter interface gap (seal) varies significantly, in magnitude and polarity with location around the seal, varying in magnitude from 20 to 60 A/m.

Inside the PCR, the magnetic field varies significantly from location to location, ranging from about 10 A/m at a point midway between the Orbiter payload and the interior PCR service structure (Figure 7-6), increasing to gap values for locations near the gap. The interior field shows only a weakly oscillating component.

The field varies significantly with position inside the payload bay, also, as seen by Figure 7-7. In this case, there are no drag-on cables. The four ground straps are in place. A "dummy" payload is simulated as a cylinder filling about 2/3 of the aft interior space of the payload bay. Points A, B, D, and E lie on a vertical line which lies just outside the payload cylinder toward the interior of the PCR. Point C lies in the middle of the empty portion of the payload bay. Values of the field at those points are listed on the figure.

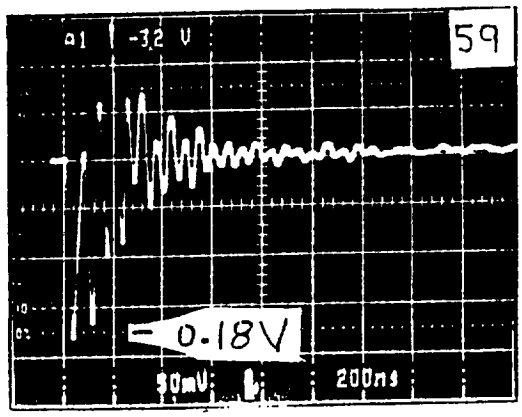

All Straps Connected

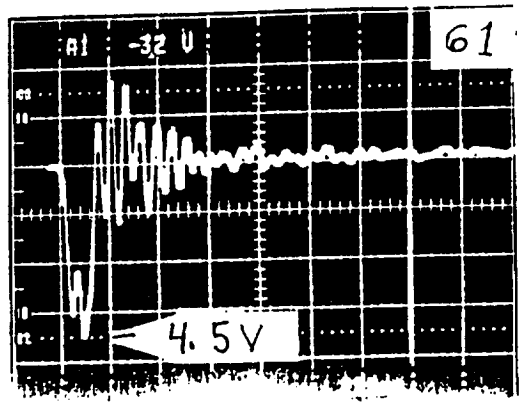

No Straps Connected

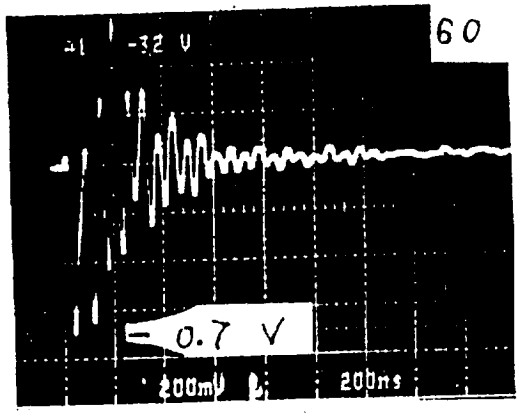

Top Straps Connected

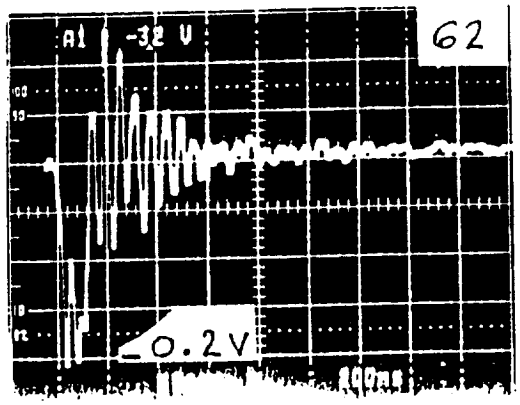

Bottom Straps Connected

Figure 7-2
Effect of Strap Connections on Model (LTI)

Significant entrances for electromagnetic coupling are (1) the environmental seal (~10"), (2) the payload bay hinge line (~ 1.75"), and (3) a gap at the floor of the PCR (~ 3' x 7:"), as shown on Figure 7-8.

7.4 White Room - Orbiter Interface

PCR Not Present

An analysis was made of the interface between the Orbiter and the White Room on the Orbiter Access Arm. There is a "grounding" cable across that interface until the beginning of the hatch-closing process.

With the PCR removed and the grounding cable connected, the potential between the White Room and the Orbiter is calculated to be 20 kV. When the cable is removed, that

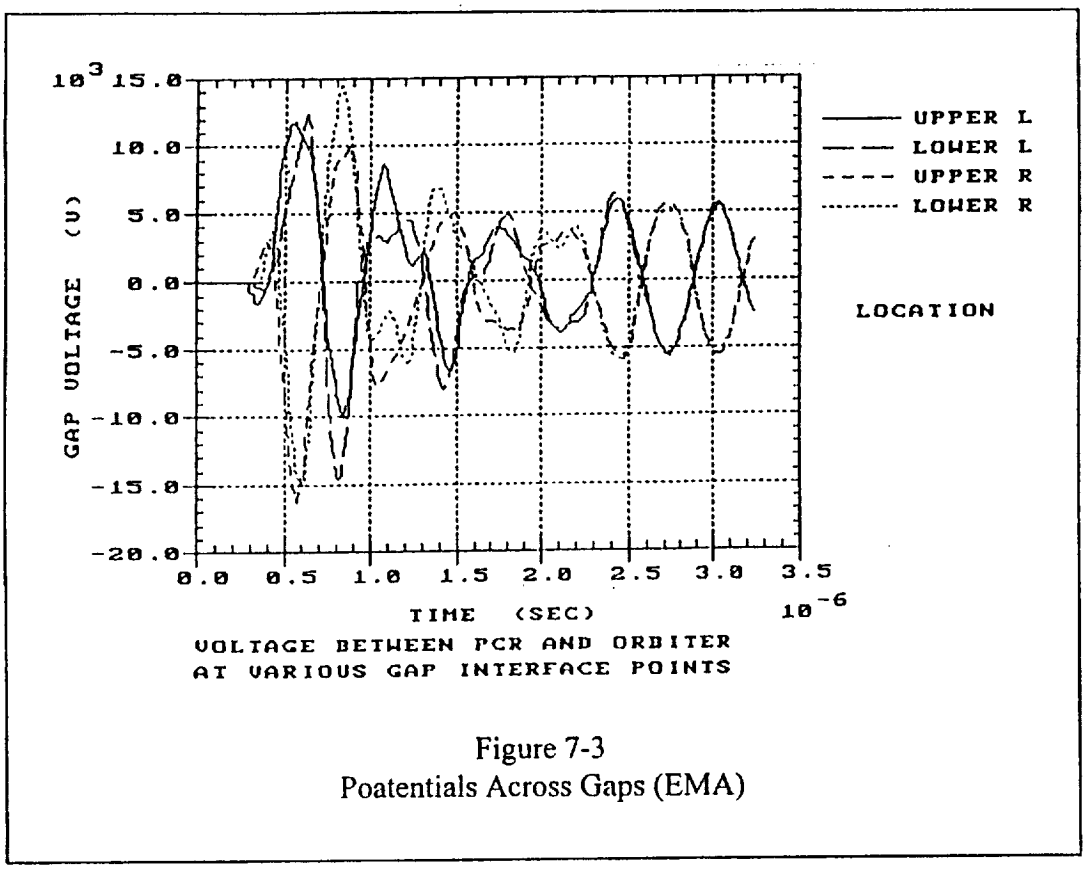

Figure 7-3
Poatentials Across Gaps (EMA)

potential becomes 100 kV (Figure 7-9). This could represent a hazard to equipment in the Orbiter as well as personnel making contact across the interface.

Shortening the cable from its present three meters to two meters would provide a one third reduction of potential. (Figure 7-10)

The metal bridge across the interface is, in its present configuration, not effective in reducing the lightning hazard, as both ends are insulated from their respective structures. Grounding those two ends to their structures would reduce the potential to 4 kV (with the existing ground cable also in place). (Figure 7-11)

Currents in the grounding cable for the three cases discussed above are shown in Figure 7-12.

7.5 Summary

This analysis indicates that for the mate configuration, the fields inside the PCR and the Orbiter payload bay will be considerably higher than were indicated for the inside of the

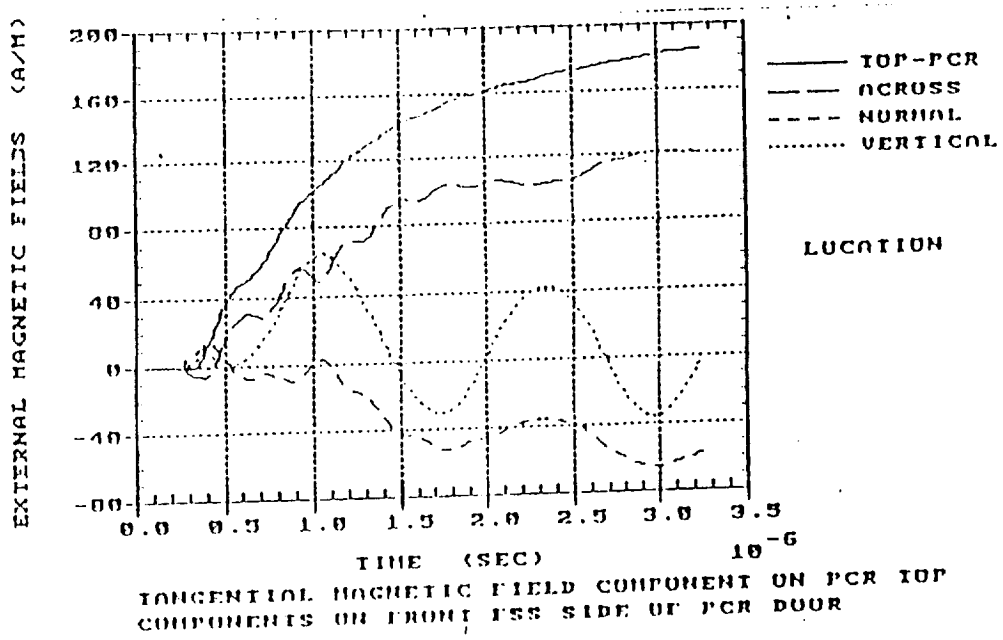

Figure 7-4
External H

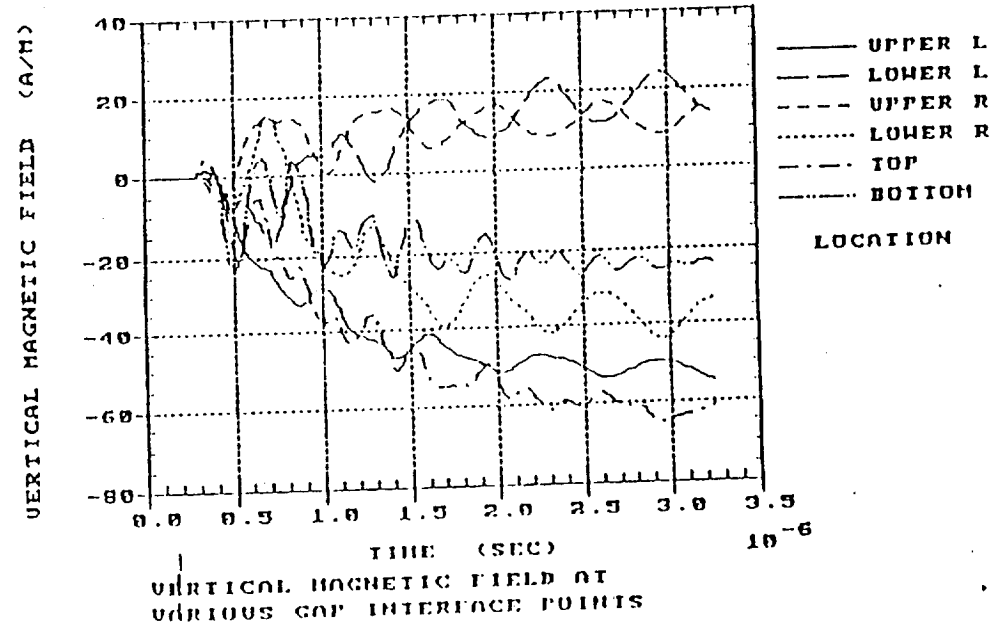

Figure 7-5
H at Gaps

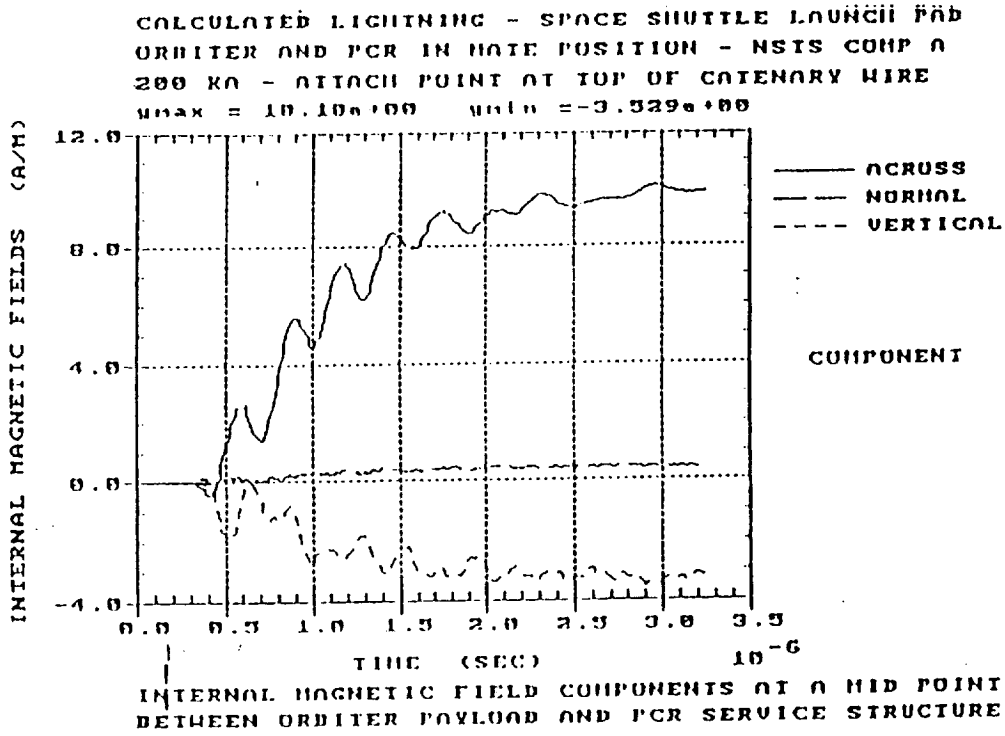

Figure 7-6
H Between Payload Bay and PCR

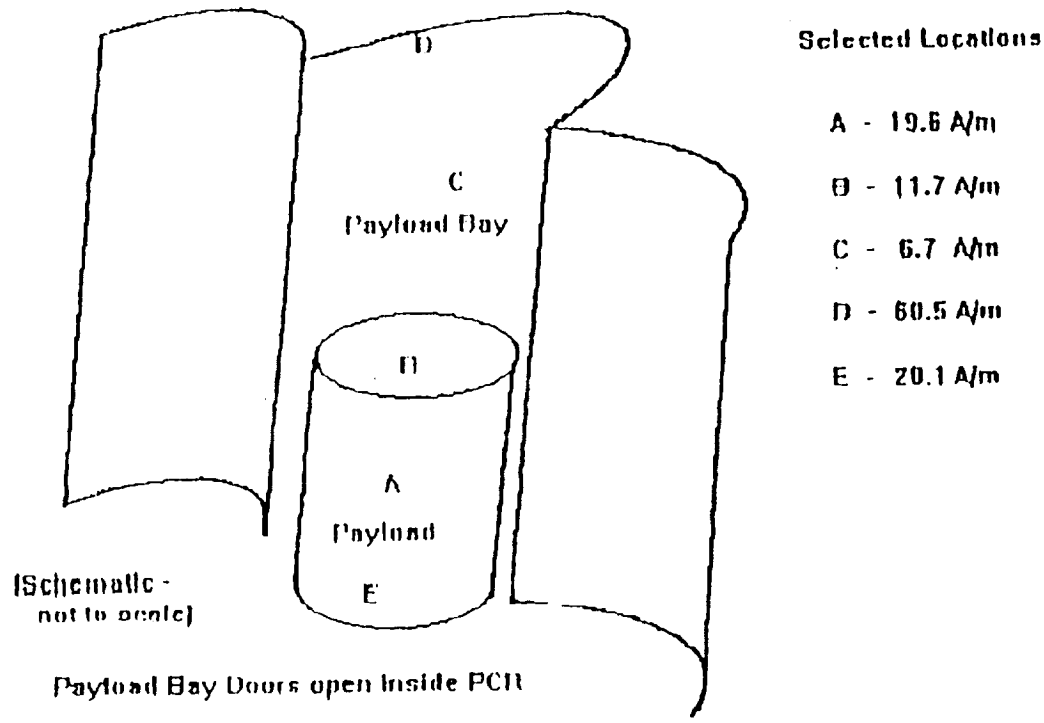

Figure 7-7
H Inside the Payload Bay

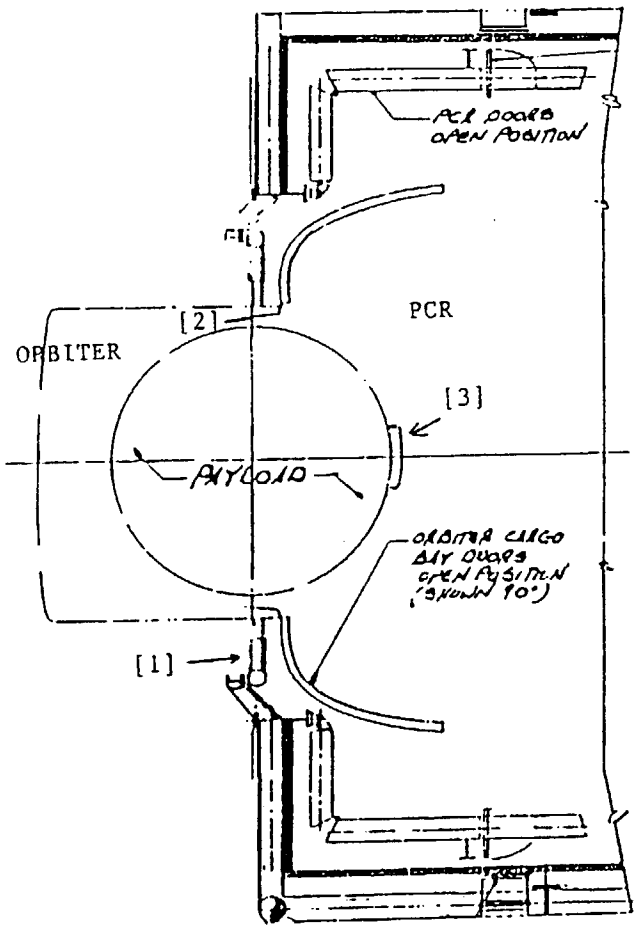

Figure 7-8
Electromagnetic Apertures

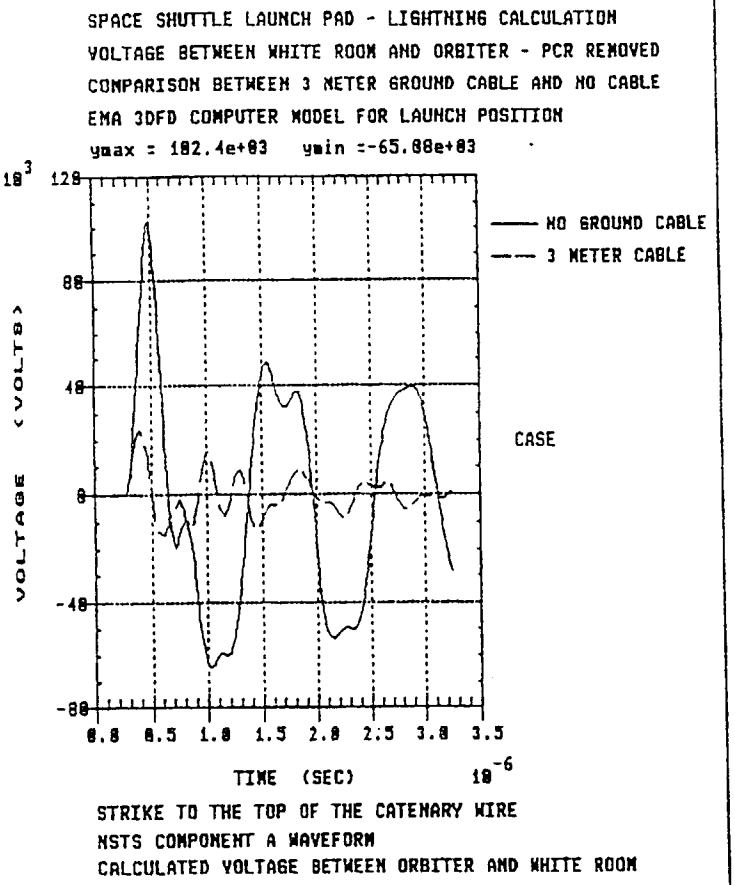

Figure 7-9
Effect of Grounding Cable

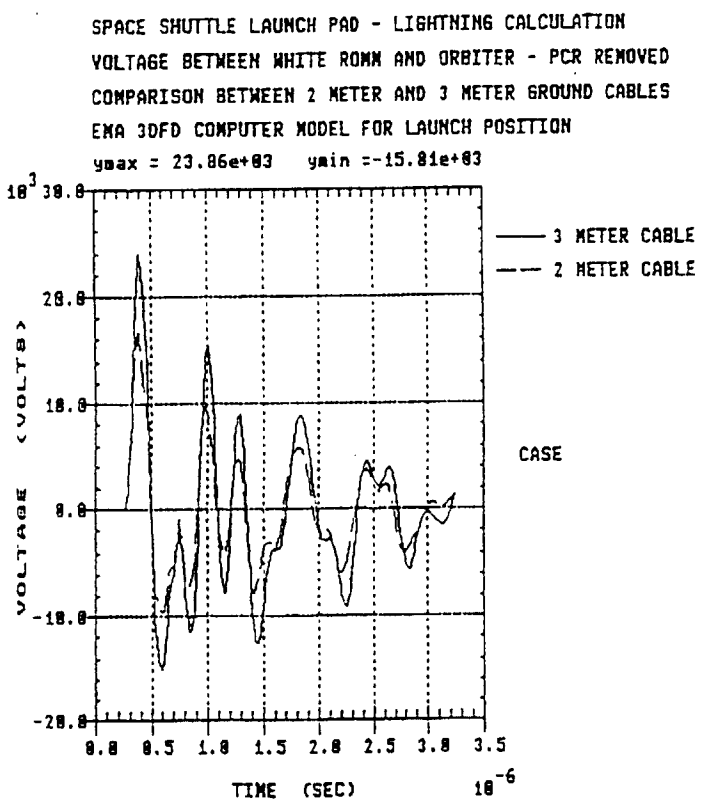

Figure 7-10
Effect of Grounding Cable Length

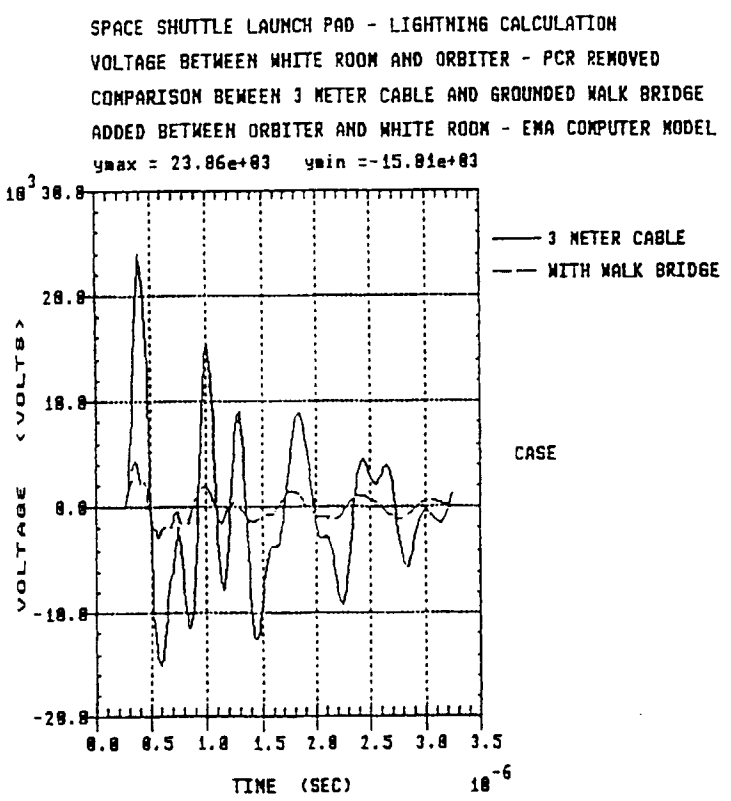

Figure 7-11
Effect of Grounding Bridge

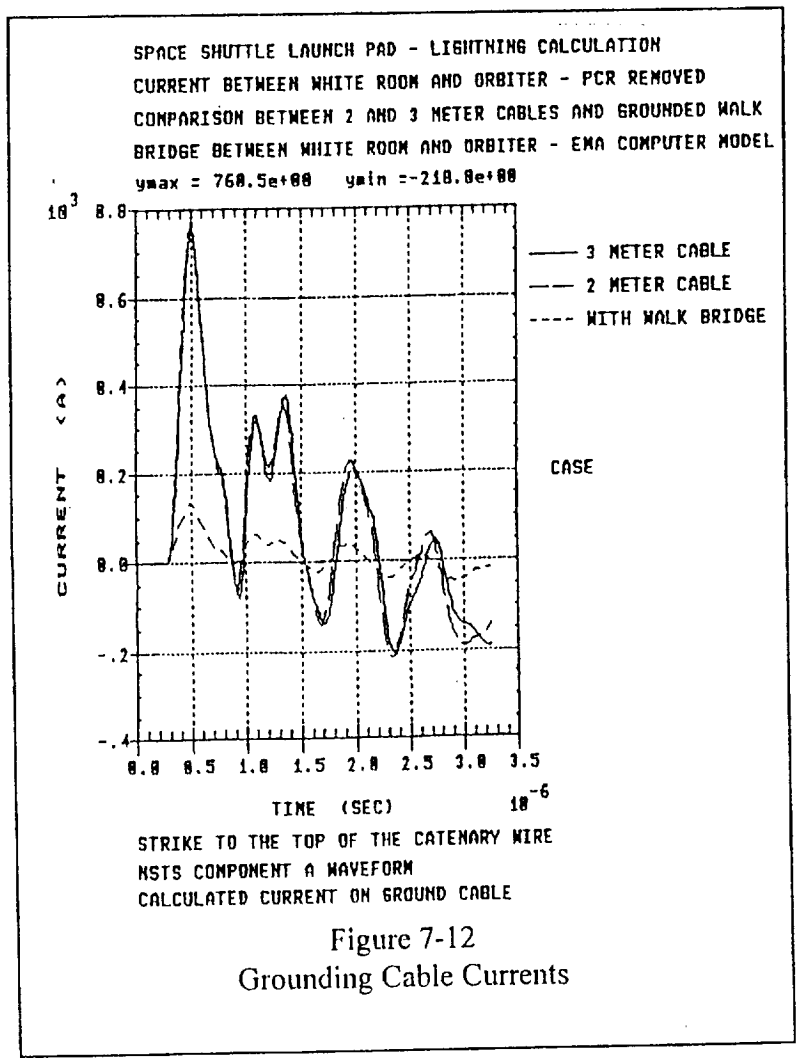

Figure 7-12
Grounding Cable Currents

PCR by the test data for the park position. This may be due in part to differences between the test and the analysis, but it is believed to be due primarily to leakage through the PCR - Orbiter apertures. A value of 10 A/m for the midpoint between the Orbiter payloads and the PCR PGHM indicates an increase of a factor of perhaps 5 for payload locations in the PCR. That is, fields of about 5 A/m may be seen in the PCR and higher in the payload bay (Figure 7-7) when the two are open to each other. Induced voltages would be expected to increase similarly. That situation could be improved by placing a metallic screen across the gap at the PCR floor.

Both methods (LTI modeling and EMA analysis) show that the "ground" straps between the PCR and the Orbiter are effective in reducing the potential between those two structures, although the two methods give substantially different numbers.

The "ground" cable between the White Room and the Orbiter is effective, and its effectiveness could be increased by reducing its length by one-third. (In most lightning considerations, the voltage drop across a conductor is due to the inductance of the conductor ($E = -L\ dI/dt$), and the inductance of a single conductor is approximately proportional to its length.) The "grounding" effectiveness across that interface can be increased significantly by arranging for the two ends of the bridge to make electrical contact with their structures.

A means should be found to connect the ground cable to the Orbiter when the hatch is in the process of being closed, or that operation should not be performed during phase two lightning conditions.

The relatively large values computed for the magnetic field in the payload bay when it is opened to the PCR are consistent with experience: Of the four instances of payload problems possibly related to lightning (2 apparently due to lightning and two uncertain), all four occurred when the payloads were in the payload bay with the doors open to the PCR.

As a continuation of the effort to obtain good data on fields inside the payload bay, particularly, and also the PCR, a self-contained device to measure the magnetic fields produced by natural lightning has been developed by I-NET. It records maximum current, maximum rate of change of current, and waveform. At the time of this report preparation, no strikes to a pad have occurred since this instrument (2 units) has been in place. It is sometimes referred to as a "shoe box" because of its size (about two shoe boxes).

8 SUMMARY

8 1 Introduction

Discussion in this summary will be restricted to cases in which the NASA design stroke is assumed to have struck the catenary wire system, specifically, the mast That protective system is effective but not perfect, over the fifteen years of shuttle usage, the pads have received 113 flashes to the catenary wire system and two which attached to structure beneath the catenary wire system, one to the RSS structure near the PCR and one to the oxygen vent cap in the raised position The 18 kA stroke to the RSS had an effect in the PCR comparable to a medium sized stroke to the mast Instrumentation was not available to measure the effect in the PCR of the stroke to the vent cap, but a similar case was investigated in the physical modeling phase and is discussed in [13], with some results given in Table 1 (Case 2)

It will be noted that more attention is given in this report to magnetic fields than electric fields, that is because electric fields are more easily shielded and, therefore, do not present as serious a problem as do magnetic fields

8 2 Physical Modeling and Analysis

Results from the physical modeling and analysis are discussed in Chapter 3 They have been useful in providing basic information, bounding the problem, providing a comparison of physical modeling and analysis with a full scale experiment, evaluating analytical methods, suggesting improvements to those methods, and adding to confidence in the test results

The FILAMENT program predicted currents and magnetic fields around the model reasonably well It is useful in predicting the magnetic field outside the PCR but is not well adapted to determining the field internal to a shielded room such as the PCR

The FDTD program, when considering the configuration corresponding to the LTI Case 1, gave results consistent with the measured values and the FILAMENT values

8 3 RSS in Park Position

8 3 1 The Simulator Test

Significant oscillations are present in all plots of the fields They are believed to be due to oscillations in the catenary wire current, currents induced in elements of the PCR and the launch support structure, and structural cavities which support field oscillations, but not many effective structural elements have been identified

Field magnitudes:

External (outside PCR doors): $H \cong 43$ A/m
$dH/dt \cong 85$ A/m/μs
$E \cong 100$ kV/m
$dE/dt \cong 400$ kV/m/μs

Internal: $H \cong 1.2$ A/m
$dH/dt \cong 1.8$ A/m/μs
This amounts to approximately 2 V/m^2 as the potential induced in an exposed conducting loop -- probably the most important number we can supply payload designers.

The variation of magnetic field with location inside the PCR ranges from 0.3 to 1.2 A/m, with the larger values being in the central sector (locations B, C, D, G -- those "looking at" the doors) and the smaller values being in the side sections (locations A, J. M, E, I, L) -- those farther removed from the doors. The data thus indicate that the most significant entry is through the door area, and we believe the primary entry region to be through the rubber encased apertures around the doors and at the vertical meeting line of the two doors. The average width of the the center line aperture is estimated at 4 cm.

The internal and external waveforms were similar, particularly as regards the first few pulses of field - the ones believed to be caused by the current pulses passing back and forth along the catenary wire. Fields of this duration are probably coupled only through the apertures around the door, and those apertures are large enough that they probably are not particularly resonant at the frequencies most associated with the magnetic fields likely to be generated by lightning. There are differences in the shape of the long duration element of the x-component of the magnetic field; the long duration component external to the PCR seems to have a duration of the order of 50 μs, but the long duration component of the internal field often is much greater. In some cases, the internal field persisted even after one would have expected the external field to have completely disappeared. Effectively, the PCR acts as a low pass filter with a time constant much longer than that of the external magnetic field. This is the "diffusion" effect discussed in Sections 3.3.2 and 4.5.

Shielding effectiveness of the PCR walls:

For E: ~ 47 dB
For H: ~ 36-40 dB

One would expect greater shielding effectiveness for electric fields than for magnetic fields. Perhaps the internal electric fields are more the result of the changing internal magnetic fields than the result of direct leakage of electric fields from the outside.

8.4 Vehicle Present, RSS in Mate Position

No testing was done for this case, so the data presented here result from FDTD analysis for the configuration in which the PCR doors and the payload bay doors are open. The analysis indicates that for the mate configuration, the magnetic fields inside the PCR and the Orbiter payload bay will be considerably higher than were indicated for the inside of the PCR by the test data for the park position. This may be due in part to differences in results between the test and analysis; but it is believed to be due primarily to leakage through the PCR - Orbiter apertures, which are considerably larger than the apertures for the PCR doors when closed. Values of 10 - 20 A/m are calculated for points just outside the payload cylinder in the payload bay toward the interior of the PCR. Induced voltages would be expected to increase similarly.

8.5 White Room - Orbiter Interface

An analysis was made of the interface between the Orbiter and the White Room on the Orbiter Access Arm for the time when the PCR is not present. There is a "grounding" cable across that interface until the beginning of the hatch-closing process.

With the grounding cable connected, the potential between the White Room and the Orbiter is calculated to be 20 kV; and the current in the grounding cable is calculated to be 9 kA. When the cable is removed, the potential becomes 100 kV -- a potential hazard to equipment in the Orbiter as well as personnel making contact across the interface.

The metal bridge across the interface is, in its present configuration, not effective in reducing the lightning hazard, as both ends are insulated from their respective structures. Grounding those two ends to their structures would reduce the potential to 4 kV (with the existing ground cable also in place).

8.6 CWLIS Values

Results from the simulator test raised a question regarding the accuracy of the current values obtained by the Catenary Wire Lightning Instrumentation System (CWLIS). The data from that system seemed high by an undetermined amount. Data from subsequent testing by TE-ISD-3 and I-NET, using low level pulses and observing the patterns at the catenary wire terminations, verified that this is the case, the error being that addition of the reflected pulses was not accounted for in calibration of the system. Since the round trip transit time between terminals is 5 μs, several pulses occur within a waveform as measured by CWLIS. Data obtained from the low level pulse measurements indicate that the correction factor is approximately 1.9 and the characteristic impedance of the catenary wire system as seen at the termination is approximately 400 ohms.

8.7 Natural Lightning

As mentioned in Section 7.5, experience indicates that the most lightning-vulnerable situation for payloads is in the payload bay with both sets of doors open. The analytical results described in Chapter 7 confirm this and give some estimates of the field values, but there are no experimental data on those fields. In response to this deficiency, I-NET has developed a self-contained portable magnetic field sensor which is suitable for use in the payload bay during ground operations. The instrument measures maximum magnetic field, maximum rate of rise of the field, and the waveform and stores the data for up to ten strokes. The data can then be read by a laptop computer. The dimensions of the instrument are 6" x 12" x 13", and the weight is 12 pounds. It has two sensitivity ranges: 0-2 and 0-20 A/m. It can be used at most any location where portability is desired. Two units have been constructed and placed in the PCRs and, when the two sets of doors are open, on a PGHM platform at a location over the PCR-Orbiter interface. At the time of this report preparation, no data have been obtained, as there has not been a strike to a pad since the units were placed there. This instrument is expected to be valuable in defining conditions in the payload bay and other locations, with the advantage that it records data on natural lightning. The dependence upon natural lightning, however, means that the rate of obtaining data will be low.

8.8 Oscillations

The FDTD method may well be the lightning protection analytical method of the future. It has performed well in this study (cf. Sections 3.5.5 and 7.1) and has been used to provide the only information presently available on fields in the Orbiter payload bay. But it is still in a stage in which its results need verification to provide confidence. One feature of the results which is questionable is the presence of oscillations with magnitudes which are not otherwise observed or predicted. Examples are seen in Figures 3-33, 5-5, 7-3, 7-4 and 7-9 to 7-12. Oscillations are normal phenomena in responses to lightning waveforms, but they normally are not observed of the magnitude predicted here. The question needing an answer is whether these oscillations are real or strictly a mathematical result. It must be kept in mind that the calculated oscillations are strongly dependent upon the shape of the input waveform. It has been suggested that perhaps some energy losses have not been adequately accounted for, perhaps corona losses, although corona losses have been included in the analysis. Data from the tests show oscillations in the frequency range predicted but not of the magnitude predicted. This could be due to reduced sensitivity at the higher frequencies of the detecting and recording equipment, but the characteristics quoted for the EG&G sensors indicate adequate sensitivity in that range.

It has been pointed out that the pad structure is an unusual facility because of its size, and the large dimensions of the structure do suggest the possibility of resonances in the frequency range predicted. The pulse reflections observed on the catenary wire system suggest that reflections may occur also on the principal pad structure and that the resulting

reflected pulses may be a source of magnetic field oscillations. There arre tentative plans to insert small pulses to the pad structure and look for pulse reflections in the structural elements.

The portable sensor described in the above section is capable of recording frequencies up to 3.5 MHz, which includes most of the significant oscillations predicted by the FDTD analysis, so it should be useful in evaluating the reality of those oscillations for natural lightning (keeping in mind that the oscillations are a function of the waveform and that the waveform is affected by the interaction of the lightning pulse with the structure.)

It is anticipated that data from the portable sensor can be used to develop transfer functions relating fields at various locations on the pad structure and vehicle.

8.9 Recommendations

1. The feasibility of temporarily inserting a metal grate across the Orbiter - PCR floor gap should be considered.

2. PCR - Canister, PCR - Orbiter, and access arm White Room - Orbiter grounding cables should be shortened to the extent practicable.

3. All drag-on cables (PCR - payload bay) should be shielded, with the shields grounded at both ends.

4. The feasibility of connecting a cable between the access arm White Room and the Orbiter during closeout of the Orbiter hatch should be evaluated. If such a cable is found to be impractical, personnel should not work on that hatch during Phase 2 conditions.

5. A means should be found to ground the White Room - Orbiter bridge at both ends.

6. The five foot personnel standoff distance from the PCR - payload bay interface during Phase 2 conditions should be continued. When operations permit, payloads should be inside the PCR or the payload bay -- not at the interface -- during Phase 2 conditions.

7. Payload designers should be advised of potential fields and rise rates in the PCR and payload bay and should be advised to avoid unshielded conducting loops.

8. The PCR LIVIS system should be up-graded.

9. Any electronic equipment on the pad structure in a location external to the PCR and the Orbiter should be well shielded.

10. When it is time to replace the environmental seal, it would be desirable to consider the feasibility of adding a conducting fabric.

11. The portable field sensors should be used in continuing programs to:
    (1) Evaluate the reality of predicted oscillations in field values and
    (2) Develop transfer functions to relate fields in various locations on the structure and in the PCR and payload bay.

REFERENCES

[1] Franklin H. Branin
Computer Aided Design
Electronics, Jan. 9, 1967, pp. 88-103

[2] Franklin H. Branin
Computer Methods of Network Analysis
Proc. IEEE, Vol. 55a, pp. 1787 - 1801, Nov., 1967

[3] Leon O. Chua and Pen-Min lin
Computer Aided Analysis of Electronic Circuits
Prentice-Hall, Englewood Cliffs, New Jersey

[4] R. S. Collier, F. J. Eriksen, and R. A. Perala
Lightning Threat Analysis for the Space Shuttle Launch Pad and the Payload Changeout Room Using Finite Difference Methods
EMA-94-R-007, 1994

[5] Richard S. Collier and Franklin A. Fisher
Lightning Induced Electromagnetic Environment of the Space Shuttle Payload Changeout Room - Modeling
16th International Aerospace and Ground Conference on Lightning and Static Electricity
Mannheim, Germany, 1994

[6] Richard S. Collier and Garland L. Thomas
Finite Difference Calculations of Lightning Effects at the Space Shuttle Launch Pad
1995 International Conference on Lightning and Static Electricity
Williamsburg, Virginia

[7] Richard S. Collier
EMA-94-R-007
Lightning Threat Analysis for the Space Shuttle Launch Pad and the Payload Changeout Room Using Finite Difference Methods

[8] R. A. Dalke
EMA-87-R-11
Parameterization of HEMP Coupling through Apertures in Nested Enclosures as a Function of Aperture Size, Incident Polarization, and Enclosure Size
March, 1988

[9] H. W. Dommel
Digital Computer Solution of Electromagnetic Transients in Single and Multiphase Networks; IEEE Trans., Vol. PAS-88, pp. 388-399, April, 1969

[10] H. W. Dommell and W. S. Meyer
Computation of Electromagnetic Transients
Proc. IEEE, Vol. 62, pp. 983-993, July, l974

[11] A. Eckhoff, F. A. Fisher, P. Medelius, C. Nguyen, and G. Thomas
Lightning Induced Electromagnetic Environment of the Space Shuttle Payload Changeout Room - Measuring
16th International Aerospace and Ground Conference on Lightning and Static Electricity, 1994

[12] F. A. Fisher, J. A. Plumer, and R. A. Perala
Aircraft Lightning Protection Handbook
Federal Aviation Administration, USA,1989

[13] Franklin A. Fisher
FILAMENT - A Program for Transient Analysis of Interconnected Wires
15th International Aerospace and Ground Conference on Lightning and Static Electricity, pp.10-1 --10-12
Atlantic City, NJ, USA, 1992

[14] Franklin A. Fisher
Study of Lightning Effects at the Payload Changeout Room (PCR)
Report No. LT-92-831, 1992

[15] F. A. Fisher
Simulated Lightning Tests at the Payload Changeout Room (PCR) (Final)
LT-94-1025, 1994

[16] KSC
Shielding Effectiveness Measurements of Launch Complex 39B Payload Changeout Room Doors
Test Report MDSSC-F482-53150-92, NAS-10-11400, 1992

[17] D. E. Merewether and R. Fisher
Finite Difference Solution of Maxwell's Equations for EMP Applications
EMA-79-R-4, 1982

[18] G. Mur
Absorbing Boundary Conditions for the Finite Difference Approximations of the Time Domain Electromagnetic Field Equations
IEEE Trans. EMS-23-4, pp. 377-382, Nov., 1981

[19] NASA
Space Shuttle Lightning Protection, Test and Analysis Requirements
NSTS 07636

[20] Mark Nurge and Steven Santuro (TE-CID-32)
Lightning Simulation Test Summary Report, 1993

[21] Martin A. Uman
The Lightning Discharge, p. 101
Academic Press, 1987